Metabolic Determinants of Hepatic Lipotoxicity

by

Robert Anthony Egnatchik

Dissertation

Submitted to the Faculty of the

Graduate School of Vanderbilt University

in partial fulfillment of the requirements

for the degree of

DOCTOR OF PHILOSOPHY

in

Chemical and Biomolecular Engineering

May, 2014

Nashville, Tennessee

Approved:

Jamey D. Young, Ph.D.

G. Kane Jennings, Ph.D.

Matthew J. Lang, Ph.D.

Alyssa H. Hasty, Ph.D.

ACKNOWLEDGEMENTS

My time at Vanderbilt has been an exciting period in my life. Over the past four years, I had the privilege to be constantly engaged in translational research which satisfied my desire to be creative in a field which bridges engineering and biology. For this, I am grateful for the guidance of Jamey D. Young, who provided the perfect research environment for me. I am thankful for his patience to listen to my concerns about experimental design and analysis. I respect his endurance to sit through many hours and read too many words of my outside the box hypotheses and postulations about all things lipotoxicity. Additionally, I am thankful for his honesty when my theories became too outlandish or *ahem* "hokey".

I also thank G. Kane Jennings, Matthew J. Lang, and Alyssa H. Hasty, who provided insight and constructive criticism over the years as my thesis committee. I am also thankful for my collaborators Masa Shiota, David Jacobson, and Josh Fessel. From Masa, I learned everything I know about *in vivo* liver metabolism. I appreciate David Jacobson opening his lab to me and providing me with the tools to study intracellular calcium. Lastly, I am grateful for the unique opportunity Josh Fessel provided me to study metabolic disorders in pulmonary hypertension. Funding for most of my time at Vanderbilt was supported by a National Science Foundation Graduate Research Fellowship.

Without the excellent caliber of students in the Young Lab, learning new methods would have been a more difficult, tedious, and less fun process. I appreciate the many conversations I have had over the years with Taylor Murphy, Neil Templeton, Casey Duckwall, Alison McAtee, Adeola Adebiyi, Martha Wall, Young Mi Whang, and Irina Trenary. I am thankful for the many discussions about molecular modeling and error propagation that Lara Jazmin and I had over the years. Lastly, I am truly appreciative for my lab partner and friend, Alexandra K. Leamy. The

past four years would have been a long slog without her tenacious approach to uncover the mechanisms of lipotoxicity.

Lastly, I am eternally grateful my family. As a child, my parents John and Lynn Egnatchik fostered a desire for learning about the natural world in me. They always believed in me and urged me to continue my academic pursuits and pursue my goals at every stage. Finally, without the constant support of my wife, Hali Egnatchik, none of this would have been possible. I cherish the miles we have run throughout Nashville to escape from our respective laboratories and Ph.D. projects for a few hours. I apologize for all the times I randomly started talking gibberish about glutamine metabolism as we walked the dog or were at the grocery store. You didn't have to love me like you did, but you did, and I thank you.

TABLE OF CONTENTS

Page

CHAPTER 6

LIST OF FIGURES

CHAPTER 4

CHAPTER 5

CHAPTER 6

CHAPTER 7

LIST OF ABBREVIATIONS

General: *AOA,* aminooxyacetic acid; *BAPTA,* N,N'-[1,2-ethanediylbis(oxy-2,1-phenylene)]bis[N-[2-[(acetyloxy)methoxy]-2-oxoethyl]]-, bis[(acetyloxy)methyl] ester; ;*BSA,* bovine serum albumin; *CAC*, citric acid cycle; *ETOX*, etomoxir; *FFA*, free fatty acid; *GC-MS*, gas chromatography-mass spectrometry; *H₂DCFDA*, 2'-7'-dichlorodihydrofluorescein diacetate; *mPMVEC*, mouse pulmonary microvascular endothelial cells; *MFA,* metabolic flux analysis; *MUFA,* monounsaturated fatty acid; *NAC;* n-acetyl cysteine; *NAFLD,* non-alcoholic fatty liver disease; *NASH,* non-alcoholic steatohepatitis; *OA,* oleate; *PAH,* pulmonary arterial hypertension; *PHEN;* phenformin; *PA,* palmitate; *PI;* propidium iodide; *ROS,* reactive oxygen species; *SFA;* saturated fatty acid.

Metabolites and enzymes: *AcCoA*, acetyl-CoA; *αKG*, alpha-ketoglutarate; *Asp,* aspartate; *Cit*, citrate; *Fum*, fumarate; *Glc*, glucose; *Glu*, glutamate; *Gln*, glutamine; *Lac*, lactate; *Mal*, malate; *Net Glyc*, net glycolysis; PEP, phosphoenolpyruvate; *Pyr*, pyruvate; *Suc*, succinate; *ADH*, alpha-ketoglutarate dehydrogenase; *CS*, citrate synthase; *FUS,* fumarase; *GLN/GLS*, glutaminase; *Glud1/GDH*, glutamate dehydrogenase *GOT,* glutamate oxaloacetate transaminase; *ME*, malic enzyme; *PC*, pyruvate carboxylase; *PEPCK*, phosphoenolpyruvate carboxykinase.

CHAPTER 1

INTRODUCTION

The underlying theme of this dissertation is the application of ^{13}C metabolic flux analysis (MFA) to uncover the molecular mechanisms and metabolic phenotypes of disease. As a major tool in the metabolic engineering arsenal, MFA is used to define the intracellular fluxes, or flow of material, in biological systems. Since the metabolic fluxes of a system are ultimately the result of genetic alterations, protein signaling, and environmental effects, flux calculations reflect functional output of multiple levels of systemic regulation. With an understanding between upstream signaling pathways and metabolic flux, therapeutic targets can be selected to alter the course of pathology. The majority of this dissertation applies ^{13}C MFA and traditional biochemical techniques to define mechanisms of how elevated lipids promote cellular dysfunction in obesity. Additionally, the metabolic phenotype of a model of pulmonary arterial hyptertension driven by mutations in the bone morphogenic protein receptor 2 is characterized using ^{13}C MFA.

Obesity is associated with elevated plasma free fatty acids and dysregulated lipid trafficking resulting in the ectopic, non-adipose deposition of fat. In the liver this accumulation of lipid results in fatty liver and can progress to the more aggressive non-alcoholic steatohepatitis (NASH). Because the liver is a central regulator of amino acid, lipid, and glucose metabolism, these pathologies are associated with impairments in gluconeogenesis, mitochondrial anaplerosis, and lipoprotein export.   These disorders are marked by increases in stress signaling pathways, oxidative stress, apoptosis, and possibly liver failure but often lack non-invasive methods to diagnose the disease. Collectively, these phenotypes are termed hepatic lipotoxicity.

1

Traditionally, experimental models in lipoxicity depended on the measurement of signaling pathways and lipid concentrations. Recently *in vitro* and *in vivo* studies have employed the use of stably labeled isotope tracers to provide dynamic information on the flow of material through metabolic pathways, or flux. Although these studies indicated that elevated hepatic lipids and liptoxicity are associated with altered CAC anaplerosis, no biochemical mechanism exists connecting lipid accumulation with these metabolic alterations. Lack of unifying mechanism hinders the development of novel therapeutic targets.

Pulmonary arterial hypertension was studied in addition to lipotoxicity. Caused by mutations in the bone morphogenic protein receptor, there is currently little understanding how alterations in this receptor's function promote disease. Therefore a pilot study was performed on a model of pulmonary hypertension to define how the mutations reprogram metabolism. Armed with this knowledge, methods to exploit the metabolic phenotype for therapeutic and diagnostic purposes can be pursued.

The use of ^{13}C MFA to develop molecular mechanisms of disease in this dissertation is divided into the following chapters:

Chapter 2 reviews previous studies detailing the general hepatic phenotype of fatty liver and NASH and the experimental models employed *in vivo* and *in vitro*. Also, reviewed is metabolic flux analysis (MFA), a novel method employed in the subsequent chapters to calculate how fluxes are altered in the context of lipotoxicity and pulmonary hypertension.

Chapter 3 characterizes mitochondrial metabolism and oxidative stress in hepatic cells undergoing lipotoxicity *in vitro*. Antioxidants and mitochondrial inhibitors were combined with

MFA to test the hypothesis that elevated saturated fatty acids disrupt normal mitochondrial metabolism leading to oxidative stress and apoptosis. Through the use of stable isotope tracers, it was found that fatty acid oxidation does not fuel these mitochondrial abnormalities. Instead lipotoxicity is characterized by increased glutamine anaplerosis, which fuels enhanced CAC flux. However the mechanism by which palmitate initiates mitochondrial dysfunction was still unclear. The main mechanistic findings of Chapter 3 are summarized in Figure 1.1.
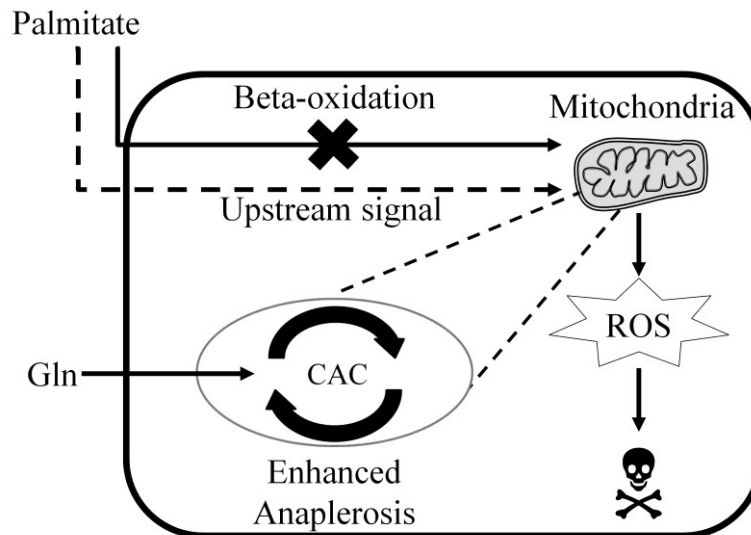
Figure 1.1: Mechanism of lipotoxicity tested and developed in Chapter 3. In Chapter 3, the hypothesis that palmitate induces oxidative stress by altering mitochondrial metabolism was tested. Through the use of antioxidants, mitochondrial inhibitors, ^{13}C tracers, and mathematical modeling it was found that fatty acid beta-oxidation does not fuel the overactive mitochondrial phenotype. Instead glutamine anaplerosis provided carbon for the enahced flux. Since beta-oxidation does not fuel mitochondrial dysfunction, a putative 'upstream signal' must exist to connect palmitate overload and oxidative stress.

Chapter 4 defines a role for calcium signaling in lipotoxicity. Elevated saturated fatty acids were associated with a redistribution in intracellular calcium from the endoplasmic reticulum to the mitochondria. We hyphothesized this redistribution in intracellular calcium is the unknown

upstream signal linking palmitate overload and the metabolic phenotype defined in Chapter 3.

^{13}C MFA studies revealed that chelation of free intracellular calcium attenuated the glutamine anaplerosis characteristic of lipotoxicity. Additionally, other hallmarks of lipotoxicity such as oxidative stress and apoptosis were reduced in the presence of the calcium chelator. This finding links endoplasmic reticulum (ER) stress to oxidative stress in lipotoxicity (Figure 1.2).
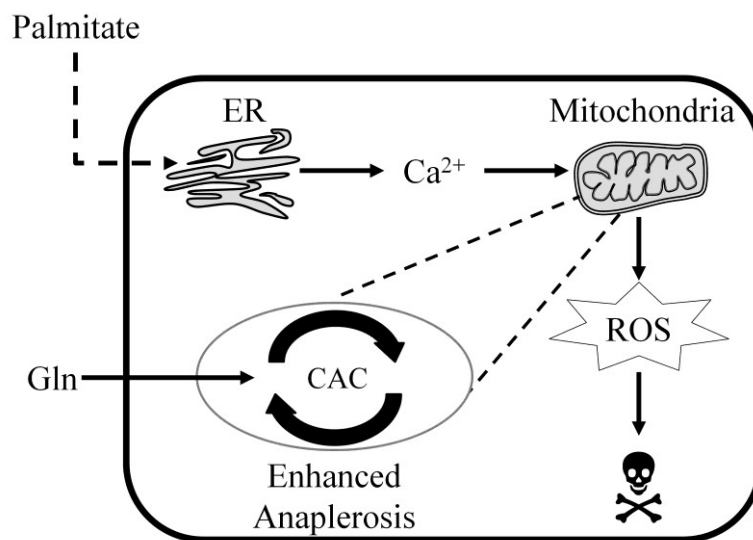
Figure 1.2: Summary of calcium-dependent lipotoxicity mechanism tested in Chapter 4. In Chapter 4, the hypothesis that intracellular calcium flux stimulates overactive mithondrial metabolism in palmitate lipotoxicity was tested. Chelation of intracellular calcium mitigated the palmitate-induced metabolic phenotype and reduced apoptosis and oxidative stress.

Chapter 5 tests the hypothesis that extracellular glutamine combined with lipotoxic concentrations of palmitate increases hepatic dysfunction. Substitution of extracellular glutamine with glutamate under lipotoxic conditions resulted in equivalent amounts of cell death in hepatic cell lines, indicating these two amino acids were functionally equivalent in promoting lipotoixicty. Pharmacological inhibitors and RNAi mediated knockdown of glutamate anaplerosis were applied to dissect whether glutamate dehydrogenase or glumatate oxaloacetate

transaminase (GOT) provided α-ketoglutarate for CAC anaplerosis (Figure 1.3). It was found

that mitochondrial glumatate oxaloacetate transaminase (GOT2) activity is the primary pathway

used for citric acid cycle anaplerosis, and inhibiting this pathway can reduce palmitate

lipotoxicity. Additionally the hypothesis that GOT metabolism fuels lipotoxicity in primary

hepatocytes was tested. Replacing extracellular glutamine with glutamate, it was found that

primary hepatocyte lipotoxicity was increased. This result was exacerbated when the equivalent

output of GOT metabolism was substitued (α-ketoglutarate and aspartate).
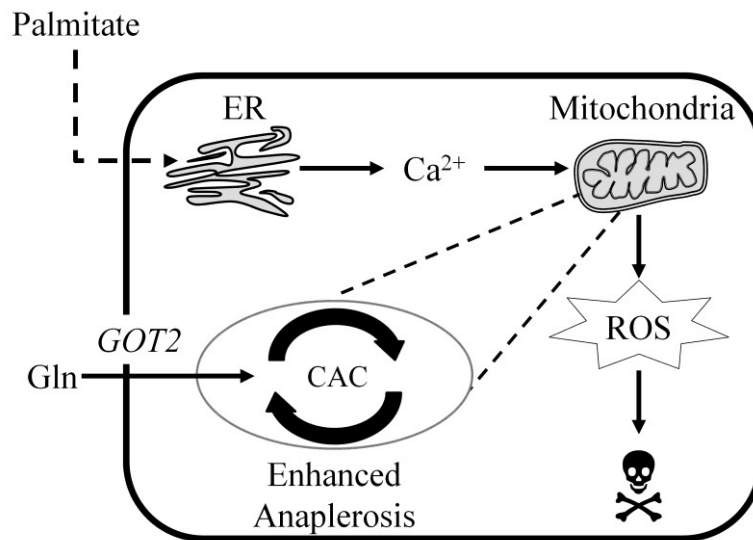
Figure 1.3: Mechanism of lipotoxicity developed in Chapter 5. In Chapter 5, the
hypothesis that extracellular glutamine synergizes with palmitate overload to enhance
lipotoxicity was tested. It was found that GOT2 metabolism was the main method of
anaplerosis in hepatic lipotoxicity.

Chapter 6 examines anaplerosis in the context of BMPR2 mutation driven pulmonary arterial

hypertension. ^{13}C MFA was applied to study how an *in vitro* model of pulmonary hypertension

relies upon glutamine anaplerosis to sustain CAC flux.

Chapter 7 summarizes the main findings of the dissertation and presents an experimental

platform for future studies.

CHAPTER 2

BACKGROUND AND SIGNIFICANCE

NAFLD and NASH: The hepatic manifestation of the metabolic syndrome

The host of obesity associated pathologies spanning insulin resistance, cardiac disease, hypertension, and dyslipidemia is termed the metabolic syndrome. The hepatic manifestations of metabolic syndrome are fatty liver and non-alcoholic steatohepatitis (NASH). Both of these diseases are characterized by the dysregulated accumulation of hepatic lipids. Fatty liver is present in approximately 30% of the adult American population and is difficult to non-invasively detect (1). Of the population with fatty liver, a small portion of patients with fatty liver will progress to NASH, characterized by apoptosis and inflammation (2). While many different facets of the disease such as risk factors of insulin resistance or poor diet or the biomarkers (ER stress, plasma aminotransferases) have been studied in detail, the biochemical mechanisms which influence the progression and severity from fatty liver to NASH are not well understood. Therefore, a critical need exists to define pathological mechanisms to enable development of novel pharmacologic or nutritional interventions for persons with NASH (3).

NASH models and the role of fatty acids

Identifying persons with NASH for experimental studies and clinical trials relies on biopsies and plasma samples as markers of disease severity. Using liver biopsies, NASH progression is based upon the NAFLD Activity Score (NAS) and fibrosis. NAS was designed by the Pathology Committee of the NASH Clinical Research Network (4) as a scoring system of 14

histological features, including lobular inflammation, the level of steatosis, and hepatocellular ballooning, which is used as a guideline for differentiating severity of NAFLD (NAS ≥5 diagnosed as "NASH", ≤3 "Not NASH"). Plasma indicators of acute liver injury include elevated levels of alanine aminotransferase and aspartate aminotransferase. Although these enzymes are reliable biomarkers of liver injury, their presence is not specific to NASH. Therefore, they remain somewhat equivocal when used as the sole metric for assessing the state of NAFLD progression.

Due to the lack of definitive biomarkers for non-invasive monitoring of NAFLD in humans, as well as the limited scope of interventions that can be applied in clinical studies, animal models provide an important research tool that enables mechanistic studies of NASH development. There are many different diet-induced and genetic models of steatosis/steatohepatitis, each having its own advantages, disadvantages, and idiosyncrasies. (Larter et. al (5) have provided an excellent review on the various animal models in steatohepatitis.) For example, common genetically obese mouse models such as the leptin resistant db/db or leptin deficient ob/ob do not spontaneously develop NASH despite pronounced hepatic lipid accumulation (6,7). In order to model NASH in these animals it is necessary to provide a seconday 'hit' or insult to initiate liver inflammation and fibrosis. In *ob/ob* models, it is possible to use lipopolysaccharide to initiate acute liver damage (8). Alternatively, it is possible to model NASH in *db/db* mice by feeding a methionine and choline deficient (MCD) diet (9). Even wild-type animals fed a MCD diet will rapidly develop hepatic steatosis, inflammation, and liver fibrosis (10-12). Additionally, the liver damage in non-genetically obese mice occurs independently of insulin resistance, providing a model that is free from the confounding effects of dysregulated insulin signaling (13). This model of NAFLD/NASH may

prove to be particularly important in light of recent data which indicate a disconnection between hepatic lipid accumulation and insulin resistance in studies on hypobetalipoproteinaemic human patients (14,15). However, because of obvious differences in etiology between MCD-diet-induced NASH and human NASH, questions still remain as to whether the MCD mouse model provides a relevant *in vivo* recapitulation of human disease (16). Instead of the MCD diet, rats and mice fed high-fat diets (HFD) may provide a more accurate model of human steatohepatitis since these models mimic the overnutrition that is typical of obesity. In fact, analysis of liver tissues from both high-fat fed mice and human NAFLD patients reveal similar trends of lipid alterations and histological changes (17).

As an alternative to human and animal studies, *in vitro* experiments using hepatic cell lines and primary hepatocytes have provided detailed insight into the molecular mechanisms that regulate lipotoxicity under conditions that mimic the *in vivo* disease state. In particular, obesity and insulin resistance are associated with elevated plasma levels of free fatty acids and triglycerides (TGs) (18). *In vitro* experiments in a diverse range of cell types have demonstrated that saturated fatty acid (SFA) overexposure promotes the expression of pro-inflammatory cytokines, impairs insulin signaling, and stimulates apoptosis characterized by both ER impairments and oxidative stress (19-23). In contrast, monounsaturated fatty acids induce significant steatotic triglyceride formation but do not initiate apoptosis (18,21). However, an accepted mechanism explaining how SFAs trigger apoptotic signaling or promote the progression from NAFLD to NASH has yet to be determined conclusively (24). Several putative signaling mechanisms including the accumulation of reactive oxygen species (ROS), endoplasmic reticulum (ER) stress, and increased ceramide synthesis have been hypothesized to explain how SFAs initiate apoptosis in hepatic cells. In particular, ceramide signaling has been

9

hypothesized as an initiator of hepatic lipoapoptosis due to the fact that ceramides are synthesized *de novo* from palmitate and serine and have been shown to promote apoptosis in myocytes (25). However, studies using both pharmacologic and genetic interventions have revealed that SFAs can induce apoptosis independently of ceramide synthesis in a variety of cell types including CHO (26,27), breast cancer cells (19), and H4IIEC3 hepatomas (28), suggesting that other mechanisms involving ER stress and ROS accumulation may predominate in these tissues.

ROS accumulation and oxidative stress

An elevated level of ROS, or oxidative stress, has been proposed as a possible companion to ER stress in promoting NASH development. Although normally present at low levels, ROS accumulate in response to cellular stress, mitochondrial dysfunction, or decreased antioxidant defenses. The electrons lost from Complexes I and III of the electron transport chain combine with oxygen to generate ROS, which includes superoxide ions, hydroxyl radicals, and hydrogen peroxide (29). In addition to their role in mediating signaling pathways, some ROS can be powerful oxidizing agents and indiscriminately damage many important components of the cell including DNA, lipid membranes, and proteins (30). Evidence for oxidative stress in NASH patients and animal models includes the accumulation of oxidized lipids such as malodialdehyde (31). NASH-associated oxidative stress has also been attributed to a variety of mechanisms including upregulated levels of cytochrome P450 2E1 (32), NADPH oxidase (33), and changes in mitochondrial function such as increased beta-oxidation (34-36).

Although hepatic oxidation of free fatty acids, as measured by positron emission tomography, is elevated in obese individuals (37), the role of beta-oxidation in promoting

lipotoxic ROS accumulation is unclear. *In vitro* studies using H4IIEC3 rat hepatoma cells appear to be in disagreement on this point. One study used etomoxir, a specific inhibitor of the rate-limiting enzyme carnitine palmitoyltransferase-1 (38), to prevent the transport of fatty acyl CoAs into the mitochondria. After combined treatment with palmitate and etomoxir, the authors measured a decrease in ROS levels in comparison to treatment with palmitate alone (34). Conversely, another study also in the same cell line found ROS accumulation to be independent of beta-oxidation (39). While both studies concluded that palmitate exerts toxic effects through ROS accumulation, only one indicated that beta-oxidation may be the source of increased ROS production. Alternatively, a recent *in vivo* study demonstrated that increased beta-oxidation may actually protect against NASH by enhancing lipid disposal. Administering PPAR-α agonists to mice on a MCD diet resulted in attenuated scores of liver damage while simultaneously increasing peroxisomal beta-oxidation (40). Recent studies in pancreatic β-cells (41) and breast cancer cells (19) agree with these results. Both studies used etomoxir to reduce beta-oxidation. Reducing beta-oxidation had no positive effect on palmitate-induced apoptosis and even increased cell death in response to excessive SFA treatment (19,41). Taken together, these studies indicate that lipids may play a more complex role in promoting hepatic ROS accumulation other than simply providing fuel substrates for increased oxidative metabolism. This could involve indirect effects to dysregulate normal mitochondrial function.

ER Stress

The ER is a specialized organelle that is integral in many cellular functions, particularly disulfide bond formation, proper protein folding, and synthesis and secretion of several critical biomolecules including steroids, cholesterol, and lipids (42). The ER also is the most important

regulator of intracellular calcium as a result of its large Ca^{2+} stores and Ca^{2+} ATPases, which are necessary for proper functioning of Ca^{2+}-dependent chaperones that stabilize protein folding. Very small changes in cellular redox state (43) or abnormal accumulation of unfolded proteins and/or toxic lipid species (44) can result in activation of compensatory response pathways, which comprise the unfolded protein response (UPR) (42,45,46). In models of lipotoxicity and fatty liver, increased lipid membrane saturation is associated with ER stress as marked by the pro-apoptotic ER stress protein CHOP and loss of ER calcium (47-50). Knockdown of CHOP did not prevent lipotoxicity (48). Although it appears that CHOP does not contribute significantly to lipoxicitiy, the role of depleted ER calcium is unclear.

JNK stress signaling

Stimulation of the c-Jun N-terminal kinase (JNK) pathways has been hypothesized as a concurrent pro-apoptotic mechanism in NASH and lipotoxicity. JNK stress signaling pathways are stimulated by the same factors that have been demonstrated to contribute to NASH, including inflammation, oxidative stress, and ER stress. JNK activation has been observed in NASH patients as well as murine models of steatohepatitis (51,52). Unlike the ER stress produced CHOP, pharmacological inhibition of JNK attenuated SFA-dependent apoptosis in both hepatic cell lines and primary mouse hepatocytes (53). Additionally, JNK activation appears to be a common component in both ER stress and oxidative stress signaling. In a model of lipid-induced ER stress, JNK activation was observed rapidly after exposure to lysophosphatidylcholine (54). At high levels, ROS are known to activate pro-apoptotic pathways through JNK-dependent signaling, and studies using *in vitro* models have confirmed that SFA-induced oxidative stress is associated with JNK activation. Murine models of NASH display increased lipid peroxidation products as well as JNK activation (55) and elevated hepatic apoptosis. It has also been shown

that co-treating hepatic cells with antioxidants reduces palmitate-induced JNK phosphorylation (34). These observations demonstrate that JNK signaling is involved in mediating stress responses and promoting apoptosis in SFA-treated liver cell models.

The two liver-specific isoforms of JNK, JNK1 and JNK2, are both associated with obesity-related liver injury (56). In particular, JNK1 activity is associated with elevated steatohepatitis and apoptosis (57). This is due to JNK1's unique ability to phosphorylate c-Jun, which can then be integrated into the activator protein-1 (AP-1) complex, a pro-apoptotic transcription factor (58,59). Knockdown of JNK1 in both murine models and primary hepatocytes resulted in reduced markers of steatohepatitis and lipotoxicity (52). JNK1-null mice fed a high-fat diet exhibited less steatosis, liver inflammation, and fewer apoptotic cells in comparison to wild-type controls. This same study found that antisense oligonucleotide knockdown of JNK1 in high-fat fed wild-type mice resulted in the attenuation of continued liver damage and a reduction in apoptotic cells. Similarly, it has been shown that palmitate stimulates the expression of p53 upregulated modulator of apoptosis through a JNK1-dependent mechanism (58).

While JNK1 activation appears to be directly related to increased apoptosis and liver injury, the role of JNK2 is less clear. One *in vitro* study using primary hepatocytes isolated from JNK2$^{-/-}$ mice demonstrated decreased apoptosis in the presence of saturated fatty acids (53). In this model of lipotoxicity, JNK phosphorylation was associated with elevated Bim-dependent Bax activation. Conversely, a separate study indicated that JNK2 had no effect on apoptosis and liver injury, as JNK2$^{-/-}$ mice had similar inflammation grades and increased apoptosis as compared to wild-type mice on the same high-fat diet (52). Bim over expression was also associated with JNK2 deficiency with this model, suggesting JNK2 regulates apoptosis possibly

through the repression of BIM. A separate study also found *jnk2 -/-* mice had no change in histology compared to control animals on a MCD diet and no change in serum ALT levels(57). These studies demonstrate JNK2 may be involved in lipid toxicity, but seems unlikely to contribute NASH.

NASH is associated with dysregulated mitochondrial metabolism and anaplerosis

Several recent studies highlight a role of accelerated mitochondrial metabolism in lipotoxicity and NAFLD. For example, $[U-^{13}C_3]$ propionate and D_2O isotope tracers were administered to patients with high and low levels of intrahepatic triglyceride content to study the impact of liver fat levels on *in vivo* mitochondrial metabolism (60). Examination of ^{13}C incorporation patterns in blood glucose revealed that mitochondrial oxidative metabolism was approximately 2-fold greater in NAFLD patients. This significant increase in mitochondrial activity in NAFLD patients coincided with elevation of both systemic lipolysis and gluconeogenesis by 50% and 30%, respectively. It was hypothesized that increased mitochondrial CAC activity satisfied the energy demand for elevated gluconeogenesis. However, the increase in gluconeogenic flux alone is unlikely to account for the almost two-fold increase in the rate of mitochondrial metabolism, suggesting that alternative endergonic mechanisms are active in the presence of excess lipids. The investigators proposed that the correlation between high levels of intrahepatic triglycerides, FFA delivery to the liver, and elevated CAC fluxes could explain the induction of oxidative stress in NAFLD patients. Similar experiments using $[U-^{13}C_3]$ propionate and D_2O isotope tracers performed in mice revealed that animals fed a high fat diet had higher rates of CAC flux (61). After 32 weeks of HFD feeding, mice exhibited elevated superoxide dismutase activity. It was hypothesized that these enzymes were elevated to

counteract ROS accumulation due to heightened mitochondrial activity and increased anaplerosis from pyruvate carboxylase. These two *in vivo* isotope labeling studies reveal that activated hepatic mitochondrial metabolism is a common characteristic of NAFLD in both human subjects and animal models.

Alternatively, stable isotope-based metabolic flux analysis (MFA) has been performed to study how elevated SFAs impact central metabolism of hepatic cells cultured *in vitro* (39). Detailed flux mapping with $[U-^{13}C_5]$glutamine revealed that palmitate treatment strongly increased CAC fluxes relative to glycolytic fluxes in H4IIEC3 cells. Changes in intracellular metabolic fluxes coincided with the onset of ROS accumulation and preceded the appearance of apoptotic markers such as caspase 3/7 activation and DNA laddering. Glycolytic fluxes including glucose uptake and lactate secretion were significantly inhibited by palmitate, whereas CAC and anaplerotic fluxes were significantly upregulated. The timing of these events suggests that palmitate-stimulated metabolic flux alterations were responsible for generating ROS and triggering apoptosis. Interestingly, increased glutamine anaplerosis, rather than fatty acid beta-oxidation, was reported to fuel the observed increase in CAC. Additionally, by varying the concentration of various amino acids in the cell culture medium it was possible to modify the metabolic phenotype of palmitate-treated H4IIEC3 cells. These alterations were also reflected in changes to ROS accumulation and cell viability. Overall, these studies suggest that mitochondrial dysfunction arising from increased FFA availability plays a key role in both *in vitro* and *in vivo* lipotoxicity mechanisms. The ability of amino acids to simultaneously modulate mitochondrial metabolism and lipotoxic outcomes implies that nutritional interventions may provide one possible strategy to control NAFLD progression. However, the regulatory

connections linking FFAs to altered mitochondrial function and fuel source selection are still undefined.

While these studies support a role for accelerated mitochondrial metabolism in NASH and lipotoxicity, other studies provide conflicting evidence. For example, liver biopsies from NASH patients demonstrated decreased activity of the mitochondrial respiratory chain (62). Similarly, mitochondria isolated from C57BL/6 mice with HFD induced NASH had decreased state 3 respiration compared to control (63). *Ob/ob* mice also demonstrated depressed ETC activity possibly as a function of increased tyrosine nitration of these key mitochondrial proteins (64). Decreased ATP levels have also been reported in livers isolated from MCD diet fed rats as function of impared ETC activity (65). These conflicting hypotheses on the role of mitochondria in NASH models warrant further study with comprehensive, systems biology techniques. A summary of the broad phenotypes of NASH is presented in Figure 2.1.
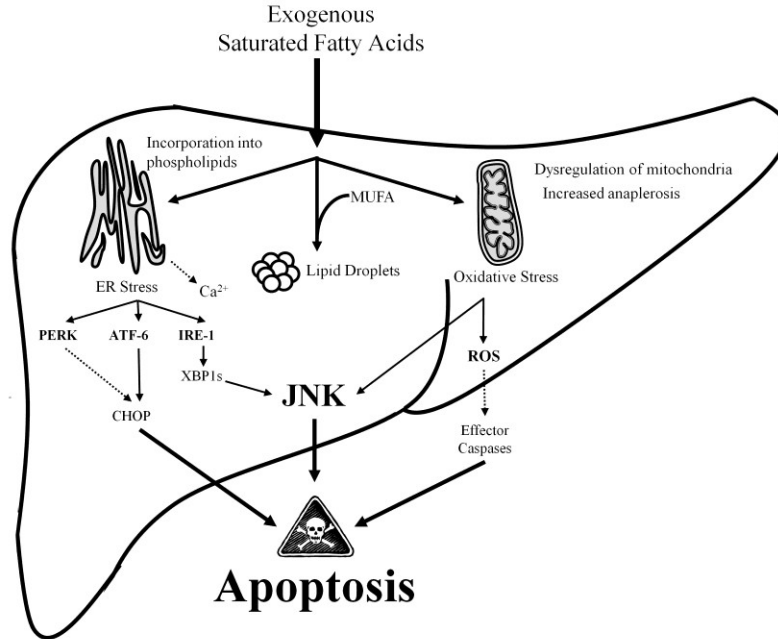
Figure 2.1: General phenotypes associated with NASH and lipotoxicity *in vitro* and *in vivo*. Elevations in exogenous plasma FFA cause liver disorders characterized by ER and mitochondrial impairments. Excess saturated fatty acids promote pro-apoptotic phenotypes while monounsaturated fatty acids induce protective triglyceride formation. The pro-apoptotic arm of lipotoxicity is marked by aberrant saturated phospholipid metabolism which induces ER stress marked by the induction of the PERK, ATF-6, and IRE-1 pathways. CHOP expression is common to many lipotoxic models although it has been shown simply be an indicator of disorder and not functionally contribute to disease progression. In addition to ER stress, mitochondrial metabolism is overactive in both cell culture models and animal models of lipotoxicity. This overactice metabolic state leads to oxidative stress which can activate JNK stress pathways and initiate apoptosis. In this dissertation a hypothetical mechanistic link between saturated fatty acid overload, ER calcium efflux, and oxidative stress is tested.

Metabolic Flux and Isotopomer Analysis

Metabolism is the phenotypic accumulation of gene transcription and protein regulation. Traditional biochemical approaches to studying metabolism involved perturbing single, specific metabolic pathways using inhibitors or genetic modification, and measuring the altered accumulation or production of the pathway metabolites. However, metabolic pathways are not simply defined by one or two reactions and the flux through these pathways does not always

17

correlate to enzyme expression due to allosteric control and post-translational modification. Instead, metabolic pathways are highly connected networks where individual reactions can influence the overall metabolic phenotype of the cell. Therefore, concentrations of individual metabolites do not provide the best insight into the overall metabolic phenotype. To fully understand how stimuli, genetic manipulation, or inhibitors truly affect the overall metabolic phenotype of the cell, it is necessary to integrate the metabolic network's response. This approach necessitates accurate calculation of the metabolic network reaction rates, or fluxes. Calculating these fluxes provide metabolic "maps" which describe the overall state of metabolism.

^{13}C metabolic flux analysis (MFA) is the ideal method for calculating intracellular fluxes in a metabolic network. Early approaches in metabolic flux analysis relied solely on the stoichiometry of the reaction network constraints to calculate net fluxes. This approach is most successful in determining the flow of material through linear or branched pathways. However, intracellular metabolism is not just a system of linear pathways. Instead many steps of central carbon metabolism include reversible, parallel, and cyclical pathways. While the balancing of cofactors such as ATP and NADH can help resolve some of these pathways using stoichiometric analysis, it assumes these constraints are balanced internally which may not hold true for all situations (66).

The addition of stable labeled isotope tracers to the experimental system addresses the shortcomings of stoichiometric MFA by providing additional information to constrain reaction network models. In ^{13}C MFA, carbon substrates are labeled and fed to cells until metabolic steady state is reached (70). As cells metabolize the ^{13}C labeled substrate, the tracer will be incorporated into downstream metabolites with specific labeling patterns. Therefore, the

labeling patterns of these ^{13}C isotope isomers, or isotopomers, represent the relative contributions of different metabolic pathways to the metabolite pool as well as the associated carbon transitions. Isotopomer data is collected by allowing the cell's to metabolize the tracer until isotopic steady state is reached, quenching intracellular metabolism, and extracting the intracellular metabolites.

Isotopomers are primarily analyzed in two ways: nuclear magnetic resonance (NMR) or gas chromatography-mass spectrometry (GC-MS). Unlike NMR analysis, GC-MS analysis of ^{13}C labeled metabolites requires a derivatization step to make samples volatile. NMR provides detailed positional analysis, such as which carbon is isotopically labeled and whether adjacent carbons are similarly labeled. GC-MS provides mass isotopomer information, offers greater sensitivity, and is more applicable for small quantities. The mass isotopomer distribution ranges from M0 (no ^{13}C tracer) to M+n where n is the total number of carbons which can be labeled. GC-MS also often provides multiple ion fragments specific to a parent metabolite. These ion fragments may contain all or a subset of the atoms of the parent. Therefore to identify positional labeling, compositional knowledge of these subsets of atoms for each parent ion must be known as well as the MID for the fragment. These fragment ions greatly aid in the calculation of intracellular fluxes, particulary when the EMU method is used (described below). A summary of GC-MS mass isotopomer analysis is presented in (Figure 2.2).
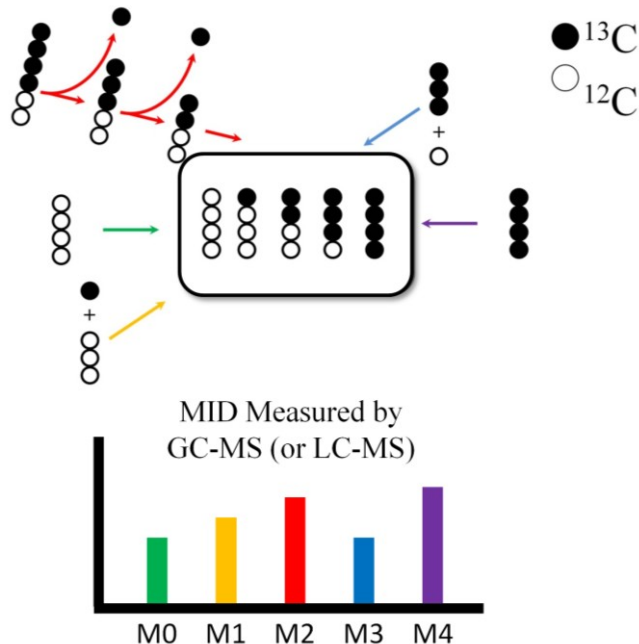
Figure 2.2: Mass isotopomer distribution (MID) provided by GC-MS analysis. Feeding cells ^{13}C tracer in culture produces unique ^{13}C enrichment patterns in downstream metabolites. These enrichment patterns reflect pathways (marked by arrows in the figure) which use the isotope tracer relative to unlabeled carbon sources. GC-MS allows for the measurement of mass isotopomers, that is metabolic fragments which differ in mass due to the differeing incorporation of [13]C. We denote these as M0, M1, M2, etc. in order of increasing mass (up to M4 in the presented figure).

Steady State ^{13}C MFA

In the following equations for ^{13}C MFA, it is assumed that experimental system is at metabolic and isotopic steady state. This assumption designates that production rates are balanced with consumption rates and no net material accumulates within the system. In the steady state experiment, the total reactions of the metabolic network and corresponding fluxes can be represented as the following mass balance equation on the metabolites:

$$S \cdot v = 0$$

where S denotes the stoichiometric matrix from the reaction network and v designates the flux vector for all reaction fluxes. In a system with J fluxes and K metabolites, the degrees of

freedom, F, is given by J-K. When F fluxes can be measured, the experimental system is exactly

determined, and it is possible to solve for the unknown fluxes directly. However when less than

F fluxes can be measured, the system is underdetermined. In this situation, additional constraints

must be added to the metabolic model to solve for fluxes. It is in these underdetermined

situations that ^{13}C isotope tracers become critical to solving fluxes within a reaction network.

The addition of ^{13}C measurements creates an overdetermined system, often with redundant

measurements. In this situation, a least squares approach is taken to calculate intracellular fluxes

by minimizing the lack of fit between the observed ^{13}C metabolite labeling patterns and the

simulated measurements. Mass isotopomer distributions are simulated by adding isotopomer

balances to the metabolic model.

Elementary Metabolite Units

Previous methods to simulate the MID of a metabolite solved for all possible isotopomers

(69). A recently developed approach to simulating the MID for isotopomers is the elementary

metabolite unite (EMU) method. The EMU is critical in the ^{13}C steady state MFA approach

taken in this dissertation. An EMU of a metabolite is simply any subset of the atoms that form

the structure of the compound (67). EMU reactions simultaneously improve upon stoichiometric

MFA by taking into account atom transitions associated with metabolite pathways and the

subsets of EMU fragments for each metabolite. This process greatly reduces the number of

variables necessary to simulate the isotopomer distribution for a given set of fluxes. For

example, to simulate the labeling in aspartate in the simple network in Figure 2.3, one needs to

know the reaction stoichiometry and associated carbon atom transitions as well as the fragments

that need to be simulated. Additionally, if we know the source of the labeling (in this model

Glu) and dilution (AcCoA) we can develop a minimal number of sub reaction networks to simulate the labeling in aspartate. This process ensures that strictly the minimal number of metabolite fragments is simulated to describe the isotopomer of interest.

Metabolic Reaction Network
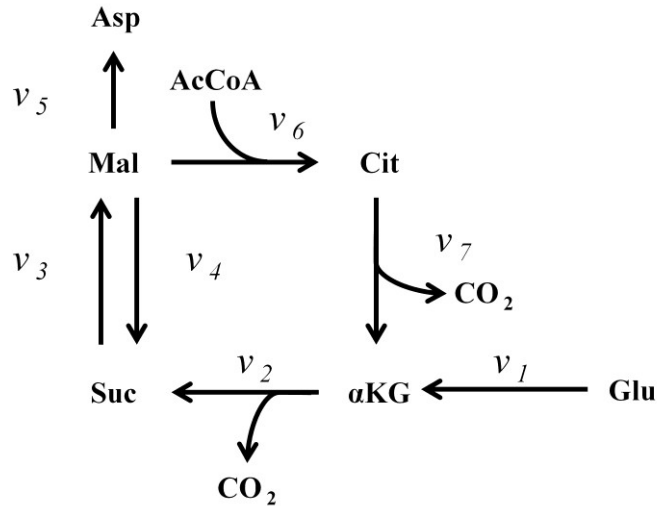
Reaction Number	Stoichiometry	Carbon atom transition
1	Glu → αKG	abcde → abcde
2	αKG → Suc + CO_2	abcde → bcde + a
3	Suc → Mal	abcd → abcd
4	Mal → Suc	abcd → abcd
5	Mal → Asp	abcd → abcd
6	AcCoA + Mal → Cit	ab + cdef → fedbac
7	Cit → αKG + CO_2	abcdef → abcde + f

Figure 2.3: Metabolic network used for simple EMU example of CAC anaplerosis. In the above reaction network fully labeled glutamate (Glu) enters the CAC as α-ketoglutarate (αKG) is metabolized through succinate (Suc), malate (Mal), and citrate (Cit) with production of aspartate (Asp) leaving the cycle. Additionally, acetyl coenzyme A (AcCoA) can enter the cycle to dilute the tracer from glutamate. The associated carbon transitions for the metabolic network are given in the table. For the purpose of this example, reactions have been condensed and atom symmetry has been neglected, although the EMU approach can easily handle these situations.

Size 4 EMU Reaction Network   *Size 2 EMU Reaction Network*
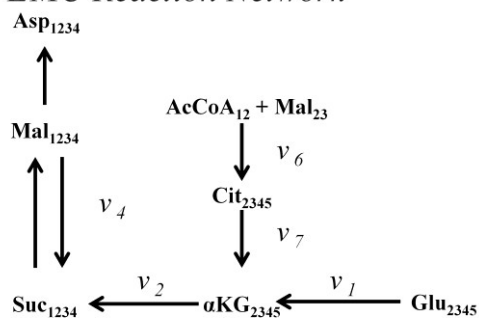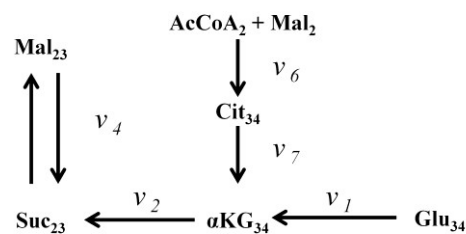
Size 1 EMU Reaction Network
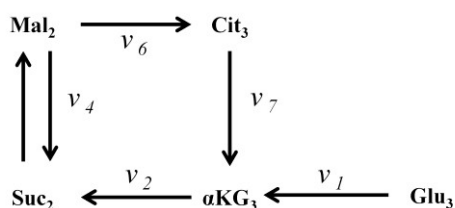
Figure 2.4: EMU reaction networks needed to simulate the labeling in aspartate (Asp). In this figure, subscripts indicate the metabolite carbons involved in the network. To simulate the labeling in Asp_{1234} (i.e. all four Asp carbons) from Figure 2.3 using the EMU method, one first designates the reactions that are involved in the formation of the metabolite until a reaction involving metabolites of a smaller EMU size is involved. In the Size 4 EMU network, the process yields a reaction (v_6) which consumes two independent two carbon fragments to produce a 4 carbon citrate. Therefore the next EMU size network is of size 2 and the Size 3 EMU network is not considered to simulate Asp_{1234}.

In order to convert the metabolic reaction network into EMU notation, mass balances are set around the EMUs of the metabolites similar to normal isotopomer/metabolite balancing. This process will give rise to multiple reaction networks balanced around EMUs of equal size (i.e. size 1, size 2, … size n). The example this results in balances around size 1, 2, and 4 networks. The multiple decoupled EMU balances are represented by the following equations:

$$0 = A_{1,k}X_{1,k} + B_{1,k}Y_{1,k}$$

$$0 = A_{2,k}X_{2,k} + B_{2,k}Y_{2,k}$$

$$\dots$$

$$0 = A_{n,k}X_{n,k} + B_{n,k}Y_{n,k}$$

Where

$$A_{n,k} = \begin{cases} -sum\ of\ fluxes\ consuming\ jth\ EMU\ in\ X_n\ j = k \\ flux\ to\ the\ jth\ EMU\ in\ X_n\ from\ the\ kth\ EMU\ in\ X_n\ j \neq k \end{cases}$$

$$B_{n,k} = flux\ to\ the\ jth\ EMU\ in\ X_n\ from\ the\ kth\ EMU\ in\ Y_n$$

Additionally, X_n and Y_n are matrices which respectively refer to the unknown and known MIDs (experimental GC-MS measurements) of the EMUs of the nth size. For the example, the known MIDs are the network substrates Glu and AcCoA.

Calculating the final fluxes of the metabolic network involves the minimization between simulated MIDs and fluxes versus observed (experimental) MIDs (68) and fluxes:

$$\min \varphi = (x(u) - x^{obs})^T \cdot \sum_x{}^{-1} \cdot (x(u) - x^{obs})$$

$$s.t.\ N \cdot u \geq 0$$

Where the objective function to minimized, φ, is the covariance-weighted sum of squared residuals (SSR). $x(u)$ denotes the vector of simulated measurements and conversely x^{obs} is a vector of observed labeling and flux measurements. $\sum_x$ designates the measurement covariance

matrix and N is the null space vector of the stoichiometric matrix S. Levenberg-Marquardt

nonlinear least-squares solution methods can then be used to minimize the SSR by modulating

free fluxes (u). These free fluxes are identified by:

$$v = N \cdot u$$

In summary, EMU decomposition of metabolites in a network model predicts the

isotopomer MID for a metabolite for a given set of fluxes. Absolute fluxes are then calculated

by solving the inverse problem, minimizing the lack of fit between similuated MIDs and

observed experimental MIDs using an optimization function (Figure 2.5).
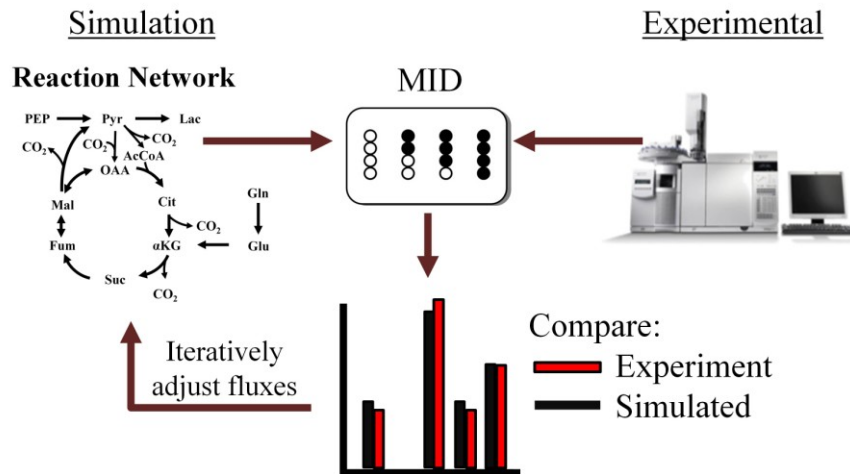
Figure 2.5: General protocol for ^{13}C MFA. MFA involves the estimation of intracellular fluxes by minimizing the difference between experimental, GC-MS derived MIDs and simulated MIDs to characterize the movement of material through metabolic pathways. This requires the development of a reaction network that defines the metabolic reactions and their associated carbon transitions to simulate a MID for a set of fluxes. Experimentally measured extracellular fluxes can also be used to constrain the reaction network. Fluxes are iteratively adjusted until convergence is achieved.

Conclusion

Fatty liver and NASH are metabolic disorders which disrupt normal hepatic function and lead to liver failure. ^{13}C metabolic flux analysis using EMU decomposition is an ideal way to calculate fluxes to describe the metabolic phenotype of a cell in response to lipid perturbation. In the rest of this disseration, the application of ^{13}C MFA (and GC-MS isotope tracer analysis) to dissect metabolic pathways associated with a hepatic cell model of lipotoxicity will be discussed in more detail.

References

1. Barshop, N. J., Sirlin, C. B., Schwimmer, J. B., and Lavine, J. E. (2008) Review article: epidemiology, pathogenesis and potential treatments of paediatric non-alcoholic fatty liver disease. *Alimentary Pharmacology & Therapeutics* **28**, 13-24

2. Reddy, J. K., and Rao, M. S. (2006) Lipid metabolism and liver inflammation. II. Fatty liver disease and fatty acid oxidation. *American Journal of Physiology-Gastrointestinal and Liver Physiology* **290**, G852-G858

3. Feldstein, A., and Gores, G. J. (2004) Steatohepatitis and apoptosis: Therapeutic implications. *American Journal of Gastroenterology* **99**, 1718-1719

4. Kleiner, D. E., Brunt, E. M., Van Natta, M., Behling, C., Contos, M. J., Cummings, O. W., Ferrell, L. D., Liu, Y. C., Torbenson, M. S., Unalp-Arida, A., Yeh, M., McCullough, A. J., Sanyal, A. J., and Nonalcoholic Steatohepatitis, C. (2005) Design and validation of a histological scoring system for nonalcoholic fatty liver disease. *Hepatology* **41**, 1313-1321

5.   Larter, C. Z., and Yeh, M. M. (2008) Animal models of NASH: Getting both pathology and metabolic context right. *Journal of Gastroenterology and Hepatology* **23**, 1635-1648

6.   Leclercq, I. A., Farrell, G. C., Schriemer, R., and Robertson, G. R. (2002) Leptin is essential for the hepatic fibrogenic response to chronic liver injury. *Journal of Hepatology* **37**, 206-213

7.   Sahai, A., Malladi, P., Pan, X. M., Paul, R., Melin-Aldana, H., Green, R. M., and Whitington, P. F. (2004) Obese and diabetic db/db mice develop marked liver fibrosis in a model of nonalcoholic steatohepatitis: role of short-form leptin receptors and osteopontin. *American Journal of Physiology-Gastrointestinal and Liver Physiology* **287**, G1035-G1043

8.   Yang, S. Q., Lin, H. Z., Lane, M. D., Clemens, M., and Diehl, A. M. (1997) Obesity increases sensitivity to endotoxin liver injury: Implications for the pathogenesis of steatohepatitis. *Proceedings of the National Academy of Sciences of the United States of America* **94**, 2557-2562

9.   Sahai, A., Malladi, P., Green, R. M., and Whitington, P. F. (2003) Steatohepatitis and liver fibrosis associated with upregulated osteopontin expression in diabetic/insulin-resistant db/db mice fed a methionine and choline deficient diet. *Hepatology* **38**, 497A-497A

10.   Dela Pena, A., Leclercq, I., Field, J., George, J., Jones, B., and Farrell, G. (2005) NF-kappa B activation, rather than TNF, mediates hepatic inflammation in a murine dietary model of steatohepatitis. *Gastroenterology* **129**, 1663-1674

11.   Weltman, M. D., Farrell, G. C., and Liddle, C. (1996) Increased hepatocyte CYP2E1
        expression in a rat nutritional model of hepatic steatosis with inflammation.
        Gastroenterology **111**, 1645-1653

12.   Koteish, A., and Diehl, A. M. (2001) Animal models of steatosis. *Seminars in Liver
        Disease* **21**, 89-104

13.   Rinella, M. E., and Green, R. M. (2004) The methionine-choline deficient dietary model
        of steatohepatitis does not exhibit insulin resistance. *Journal of Hepatology* **40**, 47-51

14.   Visser, M. E., Lammers, N. M., Nederveen, A. J., van der Graaf, M., Heerschap, A.,
        Ackermans, M. T., Sauerwein, H. P., Stroes, E. S., and Serlie, M. J. (2011) Hepatic
        steatosis does not cause insulin resistance in people with familial
        hypobetalipoproteinaemia. *Diabetologia* **54**, 2113-2121

15.   Amaro, A., Fabbrini, E., Kars, M., Yue, P., Schechtman, K., Schonfeld, G., and Klein, S.
        (2010) Dissociation Between Intrahepatic Triglyceride Content and Insulin Resistance in
        Familial Hypobetalipoproteinemia. *Gastroenterology* **139**

16.   Larter, C. Z. (2007) Not all models of fatty liver are created equal: Understanding
        mechanisms of steatosis development is important. *Journal of Gastroenterology and
        Hepatology* **22**, 1353-1354

17.   Gorden, D. L., Ivanova, P. T., Myers, D. S., McIntyre, J. O., VanSaun, M. N., Wright, J.
        K., Matrisian, L. M., and Brown, H. A. (2011) Increased Diacylglycerols Characterize
        Hepatic Lipid Changes in Progression of Human Nonalcoholic Fatty Liver Disease;
        Comparison to a Murine Model. *Plos One* **6**

18.   Listenberger, L., Han, X., Lewis, S., Cases, S., Farese, R., Ory, D., and Schaffer, J.
        (2003) Triglyceride accumulation protects against fatty acid-induced lipotoxicity.

Proceedings of the National Academy of Sciences of the United States of America **100**, 3077-3082

19.   Hardy, S., El-Assaad, W., Przybytkowski, E., Joly, E., Prentki, M., and Langelier, Y. (2003) Saturated fatty acid-induced apoptosis in MDA-MB-231 breast cancer cells - A role for cardiolipin. *Journal of Biological Chemistry* **278**, 31861-31870

20.   Turpin, S., Lancaster, G., Darby, I., Febbraio, M., and Watt, M. (2006) Apoptosis in skeletal muscle myotubes is induced by ceramides and is positively related to insulin resistance. *American Journal of Physiology-Endocrinology and Metabolism* **291**, E1341-E1350

21.   Okere, I., Chandler, M., McElfresh, T., Rennison, J., Sharov, V., Sabbah, H., Tserng, K., Hoit, B., Ernsberger, P., Young, M., and Stanley, W. (2006) Differential effects of saturated and unsaturated fatty acid diets on cardiomyocyte apoptosis, adipose distribution, and serum leptin. *American Journal of Physiology-Heart and Circulatory Physiology* **291**, H38-H44

22.   Srivastava, S., and Chan, C. (2008) Application of metabolic flux analysis to identify the mechanisms of free fatty acid toxicity to human hepatoma cell line. *Biotechnology and Bioengineering* **99**, 399-410

23.   Pagliassotti, M., Wei, Y., and Wang, D. (2005) Saturated fatty acids induce cytotoxicity in hepatocytes via effects on the endoplasmic reticulum. *Obesity Research* **13**, A31-A31

24.   Malhi, H., and Gores, G. J. (2008) Molecular Mechanisms of Lipotoxicity in Nonalcoholic Fatty Liver Disease. *Seminars in Liver Disease* **28**, 360-369

25.   Turpin, S. M., Lancaster, G. I., Darby, I., Febbraio, M. A., and Watt, M. J. (2006) Apoptosis in skeletal muscle myotubes is induced by ceramides and is positively related

to insulin resistance. *American Journal of Physiology-Endocrinology and Metabolism* **291**, E1341-E1350

26.   Listenberger, L. L., Ory, D. S., and Schaffer, J. E. (2001) Palmitate-induced apoptosis can occur through a ceramide-independent pathway. *Journal of Biological Chemistry* **276**, 14890-14895

27.   Listenberger, L. L., Han, X. L., Lewis, S. E., Cases, S., Farese, R. V., Ory, D. S., and Schaffer, J. E. (2003) Triglyceride accumulation protects against fatty acid-induced lipotoxicity. *Proceedings of the National Academy of Sciences of the United States of America* **100**, 3077-3082

28.   Noguchi, Y., Young, J. D., Aleman, J. O., Hansen, M. E., Kelleher, J. K., and Stephanopoulos, G. (2009) Effect of Anaplerotic Fluxes and Amino Acid Availability on Hepatic Lipoapoptosis. *Journal of Biological Chemistry* **284**, 33425-33436

29.   Adam-Vizi, V., and Chinopoulos, C. (2006) Bioenergetics and the formation of mitochondrial reactive oxygen species. *Trends in Pharmacological Sciences* **27**, 639-645

30.   Brookes, P. S., Yoon, Y. S., Robotham, J. L., Anders, M. W., and Sheu, S. S. (2004) Calcium, ATP, and ROS: a mitochondrial love-hate triangle. *American Journal of Physiology-Cell Physiology* **287**, C817-C833

31.   Chalasani, N., Deeg, M. A., and Crabb, D. W. (2004) Systemic levels of lipid peroxidation and its metabolic and dietary correlates in patients with nonalcoholic steatohepatitis. *American Journal of Gastroenterology* **99**, 1497-1502

32.   Weltman, M. D., Farrell, G. C., Hall, P., Ingelman-Sundberg, M., and Liddle, C. (1998) Hepatic cytochrome p450 2E1 is increased in patients with nonalcoholic steatohepatitis. *Hepatology* **27**, 128-133

33.   Lambertucci, R. H., Hirabara, S. M., Silveira, L. D. R., Levada-Pires, A. C., Curi, R., and Pithon-Curi, T. C. (2008) Palmitate increases superoxide production through mitochondrial electron transport chain and NADPH oxidase activity in skeletal muscle cells. *Journal of Cellular Physiology* **216**, 796-804

34.   Nakamura, S., Takamura, T., Matsuzawa-Nagata, N., Takayama, H., Misu, H., Noda, H., Nabemoto, S., Kurita, S., Ota, T., Ando, H., Miyamoto, K., and Kaneko, S. (2009) Palmitate Induces Insulin Resistance in H4IIEC3 Hepatocytes through Reactive Oxygen Species Produced by Mitochondria. *Journal of Biological Chemistry* **284**, 14809-14818

35.   Sanyal, A. J., Morowitz, C., Clore, J., Shiffman, M. L., Luketic, V. A., Sterling, R., and Ghatak, N. (1999) Nonalcoholic steatohepatitis (NASH) is associated with insulin resistance and mitochondrial structural abnormalities. *Gastroenterology* **116**, A1271-A1271

36.   Sanyal, A. J., Campbell-Sargent, C., Mirshahi, F., Rizzo, W. B., Contos, M. J., Sterling, R. K., Luketic, V. A., Shiffman, M. L., and Clore, J. N. (2001) Nonalcoholic steatohepatitis: Association of insulin resistance and mitochondrial abnormalities. *Gastroenterology* **120**, 1183-1192

37.   Iozzo, P., Bucci, M., Roivainen, A., Nagren, K., Jaervisalo, M. J., Kiss, J., Guiducci, L., Fielding, B., Naum, A. G., Borra, R., Virtanen, K., Savunen, T., Salvadori, P. A., Ferrannini, E., Knuuti, J., and Nuutila, P. (2010) Fatty Acid Metabolism in the Liver, Measured by Positron Emission Tomography, Is Increased in Obese Individuals. *Gastroenterology* **139**, 846-U203

38.   Weis, B. C., Cowan, A. T., Brown, N., Foster, D. W., and McGarry, J. D. (1994) Use of a selective inhibitor of liver carnitine palmitoyltransferase-I (CPT-I) allows quantification

if its contribution to total CPT-1 activity in rat-heat - Evidence that the dominant cardiac CPT-1 isoform is identical to the skeletal muscle enzyme. *Journal of Biological Chemistry* **269**, 26443-26448

39.   Noguchi, Y., Young, J., Aleman, J., Hansen, M., Kelleher, J., and Stephanopoulos, G. (2009) Effect of Anaplerotic Fluxes and Amino Acid Availability on Hepatic Lipoapoptosis. *Journal of Biological Chemistry* **284**, 33425-33436

40.   Ip, E., Farrell, G. C., Robertson, G., Hall, P., Kirsch, R., and Leclercq, I. (2003) Central role of PPAR alpha-dependent hepatic lipid turnover in dietary steatohepatitis in mice. *Hepatology* **38**, 123-132

41.   Choi, S.-E., Jung, I.-R., Lee, Y.-J., Lee, S.-J., Lee, J.-H., Kim, Y., Jun, H.-S., Lee, K.-W., Park, C. B., and Kang, Y. (2011) Stimulation of Lipogenesis as Well as Fatty Acid Oxidation Protects against Palmitate-Induced INS-1 beta-Cell Death. *Endocrinology* **152**, 816-827

42.   Kaufman, R. J. (2002) Orchestrating the unfolded protein response in health and disease. *Journal of Clinical Investigation* **110**, 1389-1398

43.   Scorrano, L., Oakes, S. A., Opferman, J. T., Cheng, E. H., Sorcinelli, M. D., Pozzan, T., and Korsmeyer, S. J. (2003) BAX and BAK regulation of endoplasmic reticulum Ca2+: A control point for apoptosis. *Science* **300**, 135-139

44.   Wek, R. C., and Anthony, T. G. (2010) Obesity: stressing about unfolded proteins. *Nature Medicine* **16**, 374-376

45.   Ron, D., and Walter, P. (2007) Signal integration in the endoplasmic reticulum unfolded protein response. *Nature Reviews Molecular Cell Biology* **8**, 519-529

46.   Zhang, K. Z., and Kaufman, R. J. (2006) The unfolded protein response - A stress signaling pathway critical for health and disease. *Neurology* **66**, S102-S109

47.   Ozcan, U., Cao, Q., Yilmaz, E., Lee, A., Iwakoshi, N., Ozdelen, E., Tuncman, G., Gorgun, C., Glimcher, L., and Hotamisligil, G. (2004) Endoplasmic reticulum stress links obesity, insulin action, and type 2 diabetes. *Science* **306**, 457-461

48.   Pfaffenbach, K., Gentile, C., Nivala, A., Wang, D., Wei, Y., and Pagliassotti, M. (2010) Linking endoplasmic reticulum stress to cell death in hepatocytes: roles of C/EBP homologous protein and chemical chaperones in palmitate-mediated cell death. *American Journal of Physiology-Endocrinology and Metabolism* **298**, E1027-E1035

49.   Wei, Y., Wang, D., Gentile, C., and Pagliassotti, M. (2009) Reduced endoplasmic reticulum luminal calcium links saturated fatty acid-mediated endoplasmic reticulum stress and cell death in liver cells. *Molecular and Cellular Biochemistry* **331**, 31-40

50.   Fu, S., Yang, L., Li, P., Hofmann, O., Dicker, L., Hide, W., Lin, X., Watkins, S. M., Ivanov, A. R., and Hotamisligil, G. S. (2011) Aberrant lipid metabolism disrupts calcium homeostasis causing liver endoplasmic reticulum stress in obesity. *Nature* **473**, 528-531

51.   Puri, P., Mirshahi, F., Cheung, O., Natarajan, R., Maher, J. W., Kellum, J. M., and Sanyal, A. J. (2008) Activation and Dysregulation of the Unfolded Protein Response in Nonalcoholic Fatty Liver Disease. *Gastroenterology* **134**, 568-576

52.   Singh, R., Wang, Y., Xiang, Y., Tanaka, K. E., Gaarde, W. A., and Czaja, M. J. (2009) Differential Effects of JNK1 and JNK2 Inhibition on Murine Steatohepatitis and Insulin Resistance. *Hepatology* **49**, 87-96

53. Malhi, H., Bronk, S. F., Werneburg, N. W., and Gores, G. J. (2006) Free fatty acids induce JNK-dependent hepatocyte lipoapoptosis. *Journal of Biological Chemistry* **281**, 12093-12101

54. Kakisaka, K., Cazanave, S. C., Fingas, C. D., Guicciardi, M. E., Bronk, S. F., Werneburg, N. W., Mott, J. L., and Gores, G. J. (2012) Mechanisms of lysophosphatidylcholine-induced hepatocyte lipoapoptosis. *American Journal of Physiology-Gastrointestinal and Liver Physiology* **302**, G77-G84

55. Wang, Y., Ausman, L. M., Russell, R. M., Greenberg, A. S., and Wang, X.-D. (2008) Increased apoptosis in high-fat diet-induced nonalcoholic steatohepatitis in rats is associated with c-Jun NH2-terminal kinase activation and elevated proapoptotic Bax. *Journal of Nutrition* **138**, 1866-1871

56. Davis, R. J. (2000) Signal transduction by the JNK group of MAP kinases. *Cell* **103**, 239-252

57. Schattenberg, J. M., Singh, R., Wang, Y. J., Lefkowitch, J. H., Rigoli, R. M., Scherer, P. E., and Czaja, M. J. (2006) JNK1 but not JNK2 promotes the development of steatohepatitis in mice. *Hepatology* **43**, 163-172

58. Cazanave, S. C., Mott, J. L., Elmi, N. A., Bronk, S. F., Werneburg, N. W., Akazawa, Y., Kahraman, A., Garrison, S. P., Zambetti, G. P., Charlton, M. R., and Gores, G. J. (2009) JNK1-dependent PUMA Expression Contributes to Hepatocyte Lipoapoptosis. *Journal of Biological Chemistry* **284**, 26591-26602

59. Sabapathy, K., Hochedlinger, K., Nam, S. Y., Bauer, A., Karin, M., and Wagner, E. F. (2004) Distinct roles for JNK1 and JNK2 in regulating JNK activity and c-Jun-dependent cell proliferation. *Molecular Cell* **15**, 713-725

60.   Sunny, N. E., Parks, E. J., Browning, J. D., and Burgess, S. C. (2011) Excessive Hepatic Mitochondrial TCA Cycle and Gluconeogenesis in Humans with Nonalcoholic Fatty Liver Disease. *Cell Metab* **14**, 804-810

61.   Satapati, S., Sunny, N. E., Kucejova, B., Fu, X. R., He, T. T., Mendez-Lucas, A., Shelton, J. M., Perales, J. C., Browning, J. D., and Burgess, S. C. (2012) Elevated TCA cycle function in the pathology of diet-induced hepatic insulin resistance and fatty liver. *Journal of Lipid Research* **53**, 1080-1092

62.   Perez-Carreras, M., Del Hoyo, P., Martin, M. A., Rubio, J. C., Martin, A., Castellano, G., Colina, F., Arenas, J., and Solis-Herruzo, J. A. (2003) Defective hepatic mitochondrial respiratory chain in patients with nonalcoholic steatohepatitis. *Hepatology* **38**

63.   Mantena, S. K., Vaughn, D. P., Jr., Andringa, K. K., Eccleston, H. B., King, A. L., Abrams, G. A., Doeller, J. E., Kraus, D. W., Darley-Usmar, V. M., and Bailey, S. M. (2009) High fat diet induces dysregulation of hepatic oxygen gradients and mitochondrial function in vivo. *Biochemical Journal* **417**

64.   Garcia-Ruiz, I., Rodriguez-Juan, C., Diaz-Sanjuan, T., del Hoyo, P., Colina, F., Munoz-Yague, T., and Solis-Herruzo, J. A. (2006) Uric acid and anti-TNF antibody improve mitochondrial dysfunction in ob/ob mice. *Hepatology* **44**

65.   Serviddio, G., Bellanti, F., Tamborra, R., Rollo, T., Romano, A. D., Giudetti, A. M., Capitanio, N., Petrella, A., Vendemiale, G., and Altomare, E. (2008) Alterations of hepatic ATP homeostasis and respiratory chain during development of non-alcoholic steatohepatitis in a rodent model. *European Journal of Clinical Investigation* **38**

66. Petersen, S., de Graaf, A. A., Eggeling, L., Möllney, M., Wiechert, W., and Sahm, H. (2000) In vivo quantification of parallel and bidirectional fluxes in the anaplerosis of Corynebacterium glutamicum. *J Biol Chem* **275**, 35932-35941

67. Antoniewicz, M. R., Kelleher, J. K., and Stephanopoulos, G. (2007) Elementary metabolite units (EMU): A novel framework for modeling isotopic distributions. *Metabolic Engineering* **9**, 68-86

68. Antoniewicz, M. R., Kelleher, J. K., and Stephanopoulos, G. (2006) Determination of confidence intervals of metabolic fluxes estimated from stable isotope measurements. *Metabolic Engineering* **8**, 324-337

69. Schmidt, K., Carlsen, M., Nielson, J., Villadsen, J. (1997) Modeling isotopomer distributions in biochemical networks using isotopomer mapping matrices. *Biotechnology and Bioengineering* **55**, 831-840.

70. Zamboni, N., Fendt S.M., Ruhl, M., Sauer, U. (2009) 13C-based metabolic flux analysis. *Nature Protocols* **4**, 878-892.

CHAPTER 3

PALMITATE-INDUCED ACTIVATION OF MITOCHONDRIAL METABOLISM
PROMOTES OXIDATIVE STRESS AND APOPTOSIS IN H4IIEC3 RAT HEPATOCYTES

Abstract

Hepatic lipotoxicity is characterized by reactive oxygen species (ROS) accumulation, mitochondrial dysfunction, and excessive apoptosis, but the precise sequence of biochemical events leading to oxidative damage and cell death remain unclear. The goal of this study was to delineate the role of mitochondrial metabolism in mediating hepatocyte lipotoxicity. We treated H4IIEC3 rat hepatoma cells with free fatty acids in combination with antioxidants and mitochondrial inhibitors designed to block key events in the progression toward apoptosis. We then applied ^{13}C metabolic flux analysis (MFA) to quantify mitochondrial pathway alterations associated with these treatments. Treatment with palmitate alone led to a doubling in oxygen uptake rate and in most mitochondrial fluxes. Supplementing culture media with the antioxidant N-acetyl-cysteine (NAC) reduced ROS accumulation and caspase activation and partially restored cell viability. However, ^{13}C MFA revealed that treatment with NAC did not normalize palmitate-induced metabolic alterations, indicating that neither elevated ROS nor downstream apoptotic events contributed to mitochondrial activation. To directly limit mitochondrial metabolism, the complex I inhibitor phenformin was added to cells treated with palmitate. Phenformin addition eliminated abnormal ROS accumulation, prevented the appearance of apoptotic markers, and normalized mitochondrial carbon flow. Further studies revealed that

glutamine provided the primary fuel for elevated mitochondrial metabolism in the presence of palmitate, rather than fatty acid beta-oxidation, and that glutamine consumption could be reduced through co-treatment with phenformin but not NAC. Our results indicate that ROS accumulation in palmitate-treated H4IIEC3 cells occurs downstream of altered mitochondrial oxidative metabolism, which is independent of beta-oxidation and precedes apoptosis initiation.

Introduction

There are currently two competing views on the role of lipid beta-oxidation in the development of non-alcoholic fatty liver disease (NAFLD) (2,3). One view holds that impaired or incomplete beta-oxidation leads to hepatic steatosis and accumulation of lipid intermediates that inhibit insulin signaling (4,5). The other view holds that increased supply of free fatty acids (FFAs) to liver results in excessive beta-oxidation that fuels reactive oxygen species (ROS) accumulation and inflammation (6-8). Recently, isotope tracers and nuclear magnetic resonance (NMR) were applied to determine *in vivo* metabolic fluxes in human subjects with either high or low intrahepatic triglyceride content (3). It was found that citric acid cycle (CAC) flux was approximately 2-fold greater in NAFLD patients. This increase in mitochondrial activity was associated with a 50% higher rate of systemic lipolysis and a 50% higher rate of hepatic anaplerotic flux, demonstrating that elevated lipid levels strongly impact mitochondrial function in NAFLD patients. Similar metabolic alterations were measured in high-fat diet (HFD) fed mice, which were associated with elevated oxidative stress markers (2). The authors hypothesized that citric acid cycle (CAC) activation is required to meet energetic demands in the face of reduced respiratory efficiency resulting from mitochondrial oxidative damage. In this contribution, we explore an alternative hypothesis, which is the possibility that FFAs can

enhance mitochondrial metabolism independently of beta-oxidation through a mechanism that precedes the onset of oxidative damage.

This study builds upon an extensive literature that uses hepatic cell lines to mimic the effects of obesity, NAFLD, and non-alcoholic steatohepatitis (NASH) in culture (9-13). Studying the effects of lipid oversupply in cultured cells is useful because it enables complete control of the cellular environment to examine basic biochemical mechanisms of hepatic lipotoxicity. In this context, saturated fatty acid (SFA) treatments lead to acute lipotoxicity that is associated with increased ROS and endoplasmic reticulum (ER) stress but is independent of ceramide synthesis (10,14,15). Furthermore, the response to SFA treatment is altogether different from that of monounsaturated fatty acid (MUFA) treatment, which induces steatotic triglyceride formation without initiating ROS accumulation or apoptosis (16). Therefore, modulating the FFA composition of the culture medium can be used to achieve varied outcomes ranging from progressive lipotoxicity to benign steatosis.

Prior *in vitro* experiments have attributed the onset of SFA-induced oxidative stress to activation of NADPH oxidases (17) or increased fatty acid beta-oxidation (9). In the mitochondria, loss of electrons from complexes I and III of the electron transport chain (ETC) can combine with oxygen to generate ROS, which include superoxide ions, hydroxyl radicals, and hydrogen peroxide (18). ROS are powerful oxidizing agents that indiscriminately damage many important components of the cell including DNA, lipid membranes, and proteins (19). At high levels, ROS are known to activate pro-apoptotic pathways, thus initiating programmed cell death. ROS accumulation can trigger apoptosis through c-Jun N-terminal kinase (JNK) stress signaling pathways (20). Antioxidant co-treatments have been shown to prevent JNK phosphorylation and JNK-mediated insulin resistance in SFA-treated H4IIEC3 cells (9). Co-

treatment with a radical scavenger also prevented HepG2 human hepatoma cell death in the presence of elevated palmitate (21). These prior studies indicate that ROS accumulation is potentially a committed step in the lipotoxicity mechanism, and that JNK activation may be one mechanism by which ROS accumulation initiates apoptosis (9,11). However, the role of specific metabolic pathways in promoting ROS accumulation, as well as the mechanism of their dysregulation by palmitate, remains largely undefined.

Stable isotope-based metabolic flux analysis (MFA) has been previously applied to study how elevated SFAs impact central metabolism in hepatic cells (10). Detailed flux mapping with [U-^{13}C$_5$]glutamine revealed that palmitate treatment strongly increased CAC fluxes relative to glycolytic fluxes in H4IIEC3 cells. Changes in intracellular metabolic fluxes coincided with the onset of ROS accumulation and preceded the appearance of apoptotic markers such as caspase 3/7 activation and DNA laddering. The same study showed that oleate co-treatment led to a reversal of the palmitate-induced metabolic phenotype and completely rescued H4IIEC3 cells from apoptosis, which was likely a result of enhanced partitioning of palmitate into triglyceride stores. Together with the previously described human and mouse data, these studies suggest that mitochondrial dysregulation arising from increased FFA availability plays a key role in both *in vitro* and *in vivo* lipotoxicity mechanisms, but they do not directly assess whether enhanced mitochondrial metabolism is a cause or a consequence of other lipotoxic effects such as oxidative stress or apoptosis initiation. Furthermore, they do not conclusively define whether FFAs are acting primarily as a fuel substrate to activate CAC flux.

To address these questions, we applied ^{13}C MFA in combination with treatments designed to alter ROS accumulation and mitochondrial metabolism in H4IIEC3 rat hepatoma cells fed lipotoxic concentrations of the SFA palmitate. These studies revealed that palmitate

40

increased oxygen consumption and CAC fluxes independently of fatty acid beta-oxidation. Glutamine, rather than lipid, was the preferred substrate used to fuel palmitate-induced increases in mitochondrial metabolism. Co-treating cells with the antioxidant N-acetyl cysteine (NAC) prevented ROS accumulation and caspase activation in the presence of palmitate but did not reverse the palmitate-associated metabolic phenotype. On the other hand, direct inhibition of mitochondrial metabolism with the complex I antagonist phenformin abolished palmitate-associated flux alterations while reversing other lipotoxicity markers. The results indicate that palmitate-induced dysregulation of mitochondrial oxidative metabolism is the primary cause of ROS accumulation and apoptosis in H4IIEC3 cells. Interestingly, these metabolic alterations are independent of fatty acid beta-oxidation and precede the onset of oxidative damage or apoptosis initiation.

Materials and Methods

Materials-

Palmitate, oleate, bovine serum albumin, phenformin, N-acetyl cysteine, low glucose Dulbecco's modified Eagle's medium (DMEM), and etomoxir were purchased from Sigma (St. Louis, MO, USA). AICAR was purchased from Cayman Chemicals (Ann Arbor, MI, USA). Propidium iodide (PI) and 2',7'-dichlorodihydrofluorescein diacetate (H$_2$DCFDA) were purchased from Invitrogen (Carlsbad, CA, USA).

Cell culture-

41

The H4IIEC3 rat hepatoma cell line (American Type Culture Collection, Manassas, VA, USA) was cultured in low glucose DMEM supplemented with 10% FBS and 1% penicillin/streptomycin antibiotic solution. The glutamine concentration of the culture medium was 2 mM. For fluorescence-based assays, cells were seeded in 96-well plates at 2×10^4 cells per well two days prior to experiments to achieve 80-90% confluency at the time of measurement.

Preparation of fatty acid solutions-

FFA stock solutions were prepared by coupling free fatty acids with bovine serum albumin (BSA). First, palmitate or oleate was dissolved in pure ethanol at a concentration of 195 mM so that the final concentration of ethanol in our FFA stock solutions did not exceed 1.5% by volume. This FFA stock solution was then added to a prewarmed 10% w/w BSA solution (37℃) to achieve a final FFA concentration of 3 mM, and this solution was allowed to incubate in a water bath for an additional 10 minutes. The final ratio of FFA to BSA was 2:1. All vehicle treatments were prepared using stocks of 10% w/w BSA with an equivalent volume of ethanol added to match the concentration in FFA stocks. The final concentration of ethanol in all experimental treatments was less than 0.2% by volume.

Detection of ROS-

The radical-sensitive H_2DCFDA dye was used to monitor intracellular ROS production. Cells were seeded on 96-well plates at 2×10^4 cells per well. After treatment with fatty acids and/or inhibitors, cells were washed twice with Hank's Balanced Saline Solution (HBSS) and then incubated with 10 μM H_2DCFDA for one hour at 37ºC in the dark. Oxidation of the dye by

intracellular ROS generates a fluorescent 2,7-dicholorofluorescein (DCF) signal. Fluorescence was measured using the excitation/emission wavelengths 485/530 nm with a Biotek FL600 microplate reader.

Viability/Toxicity assays-

Cell viability was measured using the Promega Cell Titer Blue kit at 24 hours (Fitchburg, WI, USA). Cells were washed twice with HBSS and incubated with dye for 4 hours at 37ºC. The kit measures viability by quantifying resazurin reduction, which indicates metabolic production of reducing equivalents. Fluorescence was measured using the excitation/emission wavelengths 530/590 nm with a Biotek FL600 microplate reader. Additionally, we assessed cell toxicity using the dead-cell stain propidium iodide (PI). PI is an intercalating dye that becomes highly fluorescent with excitation wavelength of 530 nm and emission wavelength of 645 nm when embedded in the exposed double-stranded DNA of dead cells.

Caspase activity-

The Apo-ONE Homogenous Caspase 3/7 Assay kit was used to measure the activities of caspases 3 and 7 as markers of apoptosis. H4IIEC3 hepatoma cells were cultured in 96-well plates as described previously. Cells were then incubated with designated treatments for at least 6 hours. The Apo-ONE kit uses a lysis buffer combined with a caspase 3/7 specific substrate. This substrate, Z-DEVD-R110, becomes fluorescent once its DEVD peptide is removed by the caspases. Fluorescence is then measured at an excitation wavelength of 485 nm and emission wavelength at 530 nm. Caspase 3/7 activation is known to be a reliable indicator of apoptosis initiation in palmitate-treated H4IIEC3 cells, as shown in several previous reports using the Apo-

ONE assay in combination with additional apoptosis markers such as DNA laddering or cytochrome C release .

Metabolite extraction and GC-MS analysis of ^{13}C labeling-

The extraction of intracellular metabolites from H4IIEC3 rat hepatomas and GC-MS analysis of ^{13}C labeling from [U-^{13}C$_5$]glutamine or [U-^{13}C$_{16}$]palmitate was performed as described previously (10). Briefly, cell metabolism was quenched by adding 1 mL of pre-cooled methanol (-80°C) to cultured cells in 10-cm dishes. A biphasic extraction was used to separate polar metabolites into a methanol/water phase and non-polar metabolites into a chloroform phase. Note that this extraction results in mixing of free metabolites from separate subcellular compartments. Polar metabolites were converted to their tert-butylsilyl derivatives using MBTSTFA + 1% TBDMCS (Pierce). Then, 1 μL of each derivatized sample was injected into an Agilent 6890N/5975B GC-MS equipped with a 30m DB-35ms capillary column for analysis of isotopic enrichment.

Oxygen consumption-

Oxygen uptake flux was used as a direct measurement of mitochondrial metabolism. These experiments were performed using the Oroboros Oxygraph-2K, which contains two chambers with separate oxygen probes to monitor on-line changes in oxygen concentration. The instrument was set to a temperature of 32ºC, and the stirring speed for each chamber was 750 rpm. To perform these experiments, H4IIEC3 cells were cultured on 10-cm dishes until 80-90% confluent and subsequently incubated with selected combinations of fatty acids and treatments for 3 hours. Cells were then trypsinized, counted, and resuspended in the same culture medium

at a concentration of 2 million cells per mL. Following resuspension, 2 million cells were injected into the Oxygraph instrument.

Beta-oxidation measurements-

Cell cultures fed tritiated fatty acid produce ^3H_2O at a rate proportional to that of mitochondrial beta-oxidation. Albumin-bound [9,10-^{3}H(N)] palmitic acid (4 µCi ^{3}H/µmol palmitate) was added to cells grown to confluency in 6-well dishes at a final concentration of 400 µM. The final volume of the media solution, including culture medium with glucose and glutamine, inhibitors/activators, and palmitate, was calculated to be exactly 2 mL per well. After 6 hours of incubation, 1.5 mL of media was removed directly from each well and collected in individual round-bottom snap-top tubes. Then 75 µL of 60% perchloric acid was added to each sample for deproteinization and to remove albumin-bound unoxidized palmitate from the sample media. The deproteinization reaction was allowed to continue overnight at 4°C.

Following deproteinization, samples were centrifuged for 30 min. Then, 1.2 mL of sample was collected into a new centrifuge tube and 5 µL of pH indicator dye and 36 µL of 5M K_2CO_3 were added for neutralization. This reaction was allowed to continue overnight at 4°C. After neutralization, samples were centrifuged for 30 min. To remove any remaining palmitate, 0.8 mL of neutralized sample was applied to an individual AG 1-X8 Resin (BioRad, Hercules, CA) column, and the column was allowed to empty under gravity flow. Each column was flushed twice with 0.6 mL of distilled water. The initial charge (0.8 mL) and all subsequent washes (1.2 mL) were collected in a scintillation vial (PerkinElmer, Waltham, MA). 10 mL of EcoLite scintillation cocktail fluid (MP Biomedical, Santa Ana, CA) was added to each sample vial, shaken vigorously, and read in a scintillation counter.

Metabolic flux analysis-

Feeding cells [U-^{13}C$_5$]glutamine isotope tracer results in unique isotopic enrichment patterns in downstream metabolites dependent on the intracellular metabolism (23). It is therefore possible to evaluate the intracellular fluxes that give rise to the measured enrichment patterns by minimizing the lack of fit between measured and simulated mass isotopomer distributions derived from a mathematical model of the metabolic reaction network. We performed ^{13}C MFA on H4IIEC3 rat hepatomas under several treatment conditions in the presence of glucose using custom Matlab-based software that relies on an elementary metabolite unit (EMU) decomposition to efficiently simulate mass isotopomer distributions of intracellular metabolites (24,25). We constructed an isotopomer model to simulate labeling from [U-^{13}C$_5$]glutamine into glutamate, pyruvate, lactate, and several CAC intermediates, which was qualitatively similar to a previous model developed by Noguchi et al. (10). The flux parameters of the model were iteratively adjusted using a Levenberg-Marquardt algorithm until optimal agreement with experimental data was obtained. Flux estimation was repeated a minimum of 50 times from random initial values to ensure a global minimum was achieved. All results were subjected to a chi-square statistical test to assess goodness-of-fit ($\chi = 0.01$), and accurate 95% confidence intervals were computed for all estimated parameters by evaluating the sensitivity of the sum-of-squared residuals to parameter variations (26). A detailed description of the reaction network and modeling assumptions can be found in the Appendix.

Statistical Analysis-

Tests for statistical significance were performed using analysis of variance (Model I ANOVA) and Tukey-Kramer methods for multiple comparisons, or Student's t-test for pair-wise comparisons. Plots indicate +/- one standard error of the mean unless otherwise indicated.

Results

Palmitate overload promotes ROS accumulation and apoptosis

In this study, H4IIEC3 cells were incubated with 400 μM palmitate (PA) as a model of SFA-induced lipotoxicity, consistent with previous studies (10). We have chosen to use the H4IIEC3 rat hepatoma cell line because it has been used in several hallmark papers on the subject of hepatic lipotoxicity and has been shown to accurately recapitulate the response of primary hepatocytes to an elevated PA load (9,10,12). A dose of 400 μM PA was selected to maintain consistency with these prior studies. We confirmed this dose by subjecting H4IIEC3 cells to increasing concentrations of PA and found that 400 μM palmitate provided the maximum lipotoxic effect while remaining in a physiologically relevant range (Figure 3A.1). After 6 hours of treatment, PA-treated cells exhibited a significant increase in ROS accumulation as measured by DCF fluorescence (Figure 3.1A). Additionally, PA-treated cells were marked by elevated caspase 3/7 activity at 12 hours (Figure 3.1B). After 24 hours of PA treatment, cell viability was reduced by approximately two-thirds in comparison to the vehicle-treated (BSA) control group (Figure 3.1C). In contrast, cells treated with the same concentration of oleate (OA) did not exhibit markers of oxidative stress or apoptosis (Figure 3.1 A, B, C).
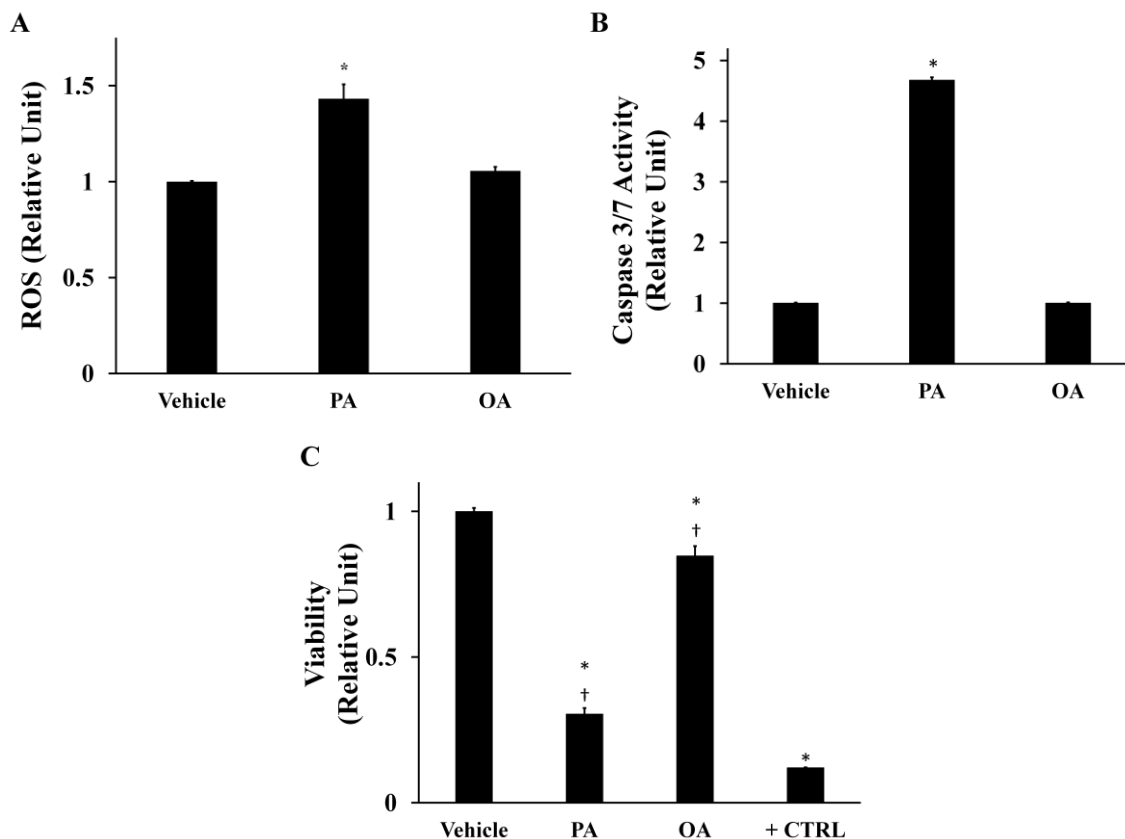
Figure 3.1: Palmitate–induced lipotoxicity is characterized by time-dependent increases in ROS accumulation, caspase activation, and losses in cell viability. H4IIEC3 rat hepatoma cells were incubated with 400 μM palmitate (PA), 400 μM oleate (OA), or 800 μM BSA (vehicle) for the indicated time periods. (A) Normalized ROS accumulation at 6-hour time point measured by DCF fluorescence. (B) Caspase 3/7 activity at 12-hour time point. (C) 24-hour cell viability (resazurin reduction) after incubation with indicated treatments. Positive control cells (+CTRL) were treated with 70% ethanol for 30 minutes. Data represent mean +/- S.E., n=4 for fluorescence assays; *, different from vehicle, $p <.05$; †, different from each other, $p < .05$.

Palmitate stimulates mitochondrial oxidative metabolism

ROS can be produced due to accelerated flux of electrons through the ETC as a result of increased mitochondrial activity. We measured the oxygen consumption of H4IIEC3 cells treated with 400 μM PA to determine if ROS accumulation was associated with elevated mitochondrial metabolism. PA-treated cells were characterized by increased oxygen

consumption (Figure 3.2). Cells treated with 400 μM OA had similar oxygen consumption rates

as vehicle-treated cells. This result confirms that the elevated oxidative phenotype is unique to

cells treated with SFA and that an equal load of MUFA is not sufficient to alter mitochondrial

function.
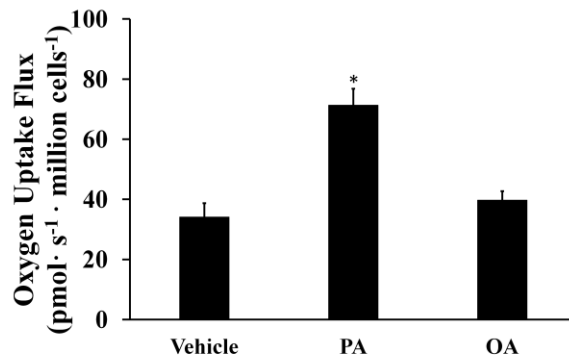
Figure 3.2:   Palmitate stimulates oxidative metabolism while oleate does not.   Oxygen
consumption measurements were performed on cells treated with vehicle, 400 μM palmitate (PA),
and 400 μM oleate (OA) for three hours. Data represent mean +/- S.E., n=3; *different from vehicle,
$p < .05$.

*Antioxidants restore viability by reducing palmitate-induced ROS accumulation without altering
mitochondrial metabolism*

Enhanced ROS accumulation has been proposed as playing a causative role in a variety

of lipotoxic disorders. To determine if increased ROS levels were directly responsible for

reducing cell viability in our system, H4IIEC3 cells were co-incubated with 400 μM PA and 5

mM of the antioxidant N-acetyl cysteine (NAC). NAC co-treatment reduced ROS at 6 hours

(Figure 3.3A), prevented markers of apoptosis at 12 hours (Figure 3.3B), and resulted in a

proportional rescue in cell viability at 24 hours (Figure 3.3C). The antioxidant vitamin E

produced similar reductions in lipotoxicity (Figure 3A.2). The similar effects of both NAC and

vitamin E, despite different mechanisms of ROS scavenging, suggest that NAC acts primarily through its antioxidant function to reduce lipotoxicity. Interestingly, NAC and PA co-treated H4IIEC3 cells had a similar oxygen uptake rate as cells treated with PA alone (Figure 3.3D). This result indicates that palmitate-induced activation of mitochondrial metabolism is independent of ROS accumulation and apoptosis initiation.
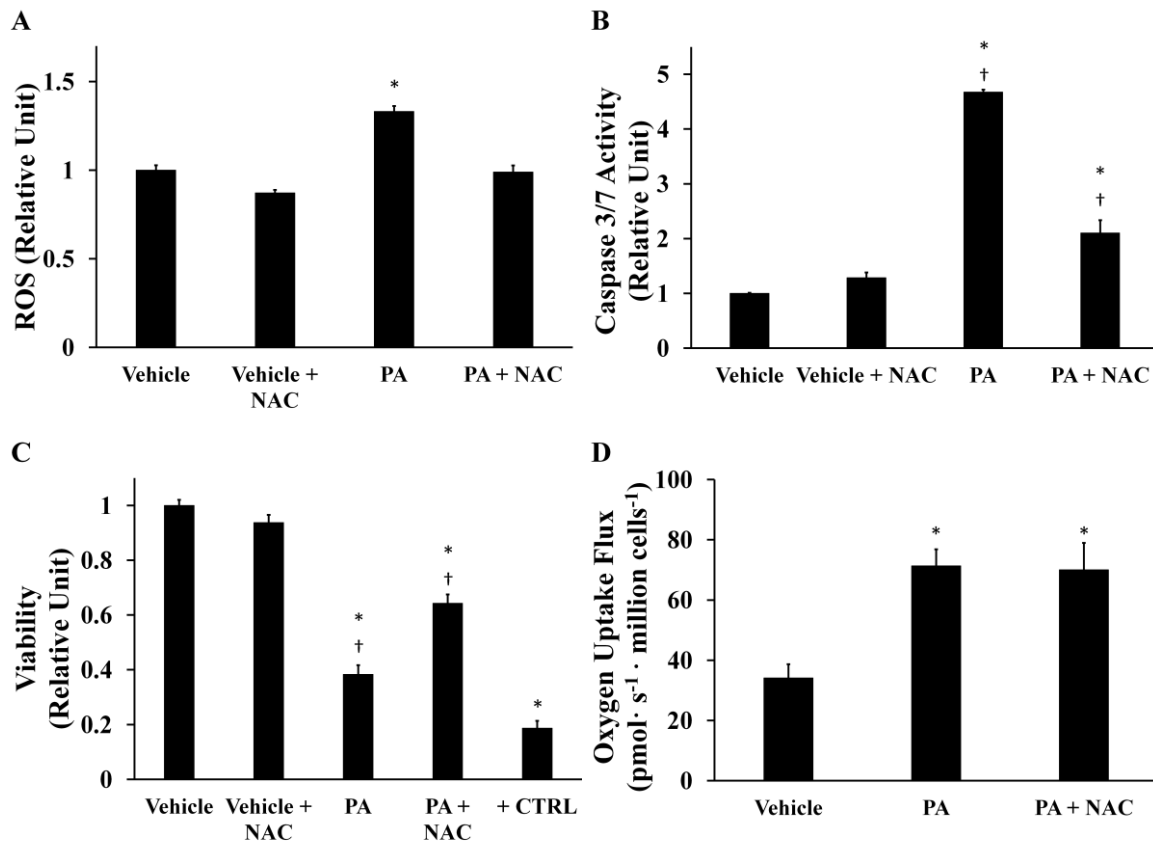
Figure 3.3: Antioxidant treatment reduces intracellular ROS and partially rescues lipotoxic cell death without reversing palmitate-induced activation of oxidative metabolism. The antioxidant N-acetyl cysteine (NAC) was added at a concentration of 5 mM to palmitate-treated (PA, 400 μM) or BSA-treated (vehicle, 800 μM) H4IIEC3 cells. (A) 6-hour ROS accumulation measured by DCF fluorescence. (B) Caspase 3/7 activity at 12-hour time point. (C) 24-hour cell viability assessed by resazurin reduction. Positive control cells (+CTRL) were treated with 70% ethanol for 30 minutes. (D) Oxygen uptake measurements of NAC- and/or PA-treated cells. Data represent mean +/- S.E., n=4 for all fluorescent assays, n=3 for oxygen uptake measurements; * different from vehicle, $p < .05$; † different from each other, $p < .05$.

Direct inhibition of mitochondrial oxidative metabolism suppresses palmitate-induced ROS generation and apoptosis

In a converse experiment, we sought to test whether a direct inhibitor of mitochondrial metabolism could effectively prevent the ability of palmitate to promote ROS accumulation and induce apoptosis. We applied 100 μM phenformin, a mitochondrial complex I antagonist, to H4IIEC3 cells both in the presence and absence of PA. Phenformin reduced PA-induced ROS generation at 6 hours (Figure 3.4A), caspase activation at 12 hours (Figure 3.4B), and long-term cell toxicity at 24 hours (Figure 3.4C) compared to cells treated with PA alone. (In these experiments, we measured PI fluorescence as an indicator of cell toxicity since mitochondrial inhibitors such as phenformin could interfere with accurate assessment of cell viability using resazurin-based dyes.) Experiments using the classical complex I inhibitor rotenone produced similar reductions in ROS accumulation and apoptosis in the presence of 400 μM PA, thus confirming our ability to rescue palmitate-induced apoptosis by inhibiting mitochondrial electron transport (Figure 3A.3). To confirm that phenformin suppressed mitochondrial metabolism at the administered dose, we measured oxygen uptake by cells co-treated with PA and phenformin (Figure 3.4D). The measurements confirmed that phenformin fully normalized oxygen uptake in the presence of palmitate, recapitulating the metabolic phenotype observed in vehicle-treated control cells.
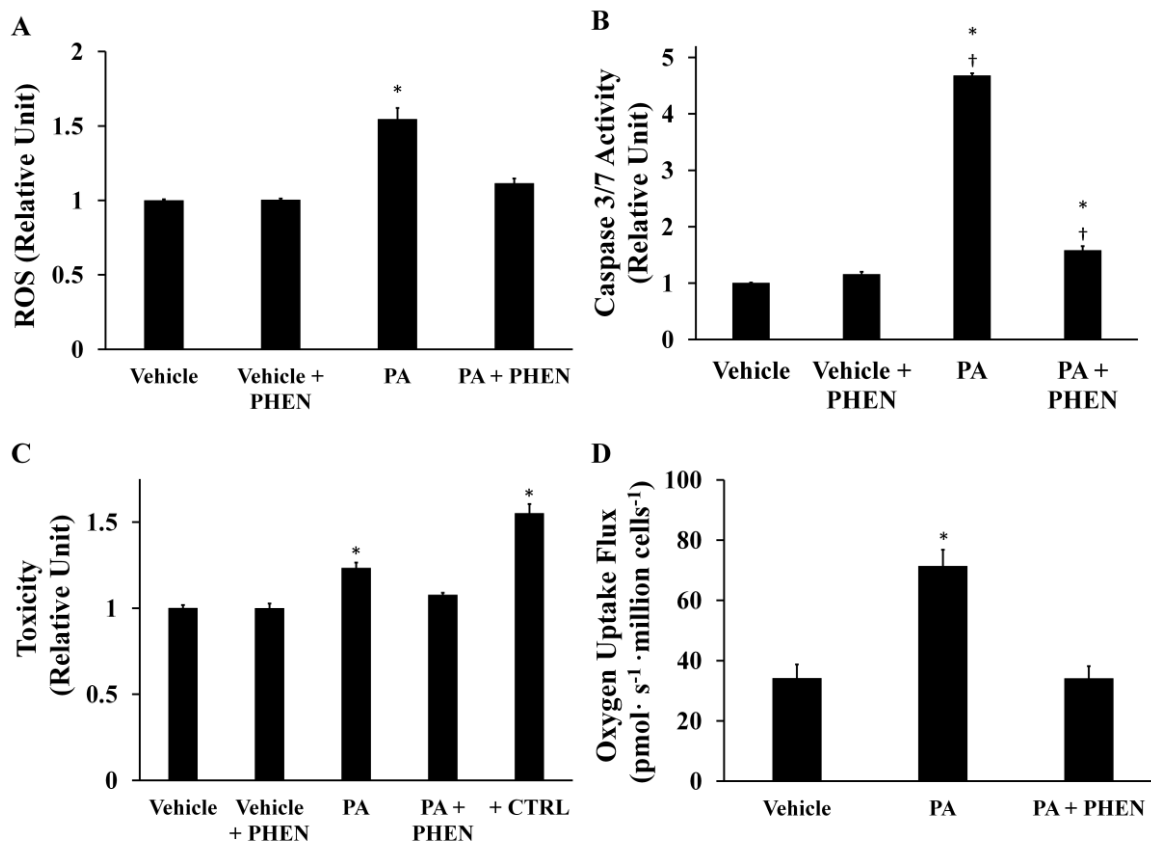
Figure 3.4: Phenformin abolishes palmitate-induced ROS generation, mitochondrial activation, and apoptosis. H4IIEC3 cells were co-treated with 100 μM phenformin (PHEN) and either 400 μM palmitate (PA) or 800 μM BSA (Vehicle) to examine the role of mitochondrial metabolism in ROS accumulation and apoptosis. (A) ROS levels at 6 hours as measured by DCF fluorescence. (B) Caspase 3/7 activity at 12 hours. (C) Cell toxicity at 24 hours assessed by PI fluorescence. Positive control cells (+CTRL) were treated with 70% ethanol for 30 minutes. (D) Oxygen uptake measurements of PHEN- and/or PA-treated cells. Data represent mean +/- S.E., n=4 for all fluorescent assays, n=3 for oxygen uptake measurements; * different from vehicle, $p < .05$; † different from each other, $p < .05$.

Palmitate-induced ROS accumulation is independent of beta-oxidation

There are differing reports on the role of beta-oxidation in promoting *in vitro* lipotoxicity of hepatic cells (9,27). To determine whether the observed ROS accumulation was due to a direct enhancement of beta-oxidation by palmitate addition, H4IIEC3 cells were treated with 400 μM PA and 250 μM etomoxir. Etomoxir is a specific inhibitor of the rate-limiting carnitine

palmitoyltransferase 1 (CPT-1) enzyme that is required to transport long-chain fatty acids across the mitochondrial membrane (28). First, we confirmed that adding etomoxir to [9,10-^{3}H(N)]palmitate-treated cells significantly attenuated beta-oxidation by measuring a decrease in ^{3}H$_2$O production (Figure 3.5A). To further confirm that etomoxir was effective at the selected concentration, we used AICAR to induce beta-oxidation in the presence of exogenous palmitate (29).The effects of AICAR on beta-oxidation were completely reversed by addition of 250 μM etomoxir, confirming that this dose was effective at blocking CPT-1 in H4IIEC3 cells. Next, we observed that co-treatment with PA and etomoxir resulted in no significant change in ROS production in comparison to treatment with PA alone despite the observed reduction in beta-oxidation (Figure 3.5B). Blocking beta-oxidation with etomoxir also did not prevent the appearance of markers of apoptosis (Figure 3.5C, D).
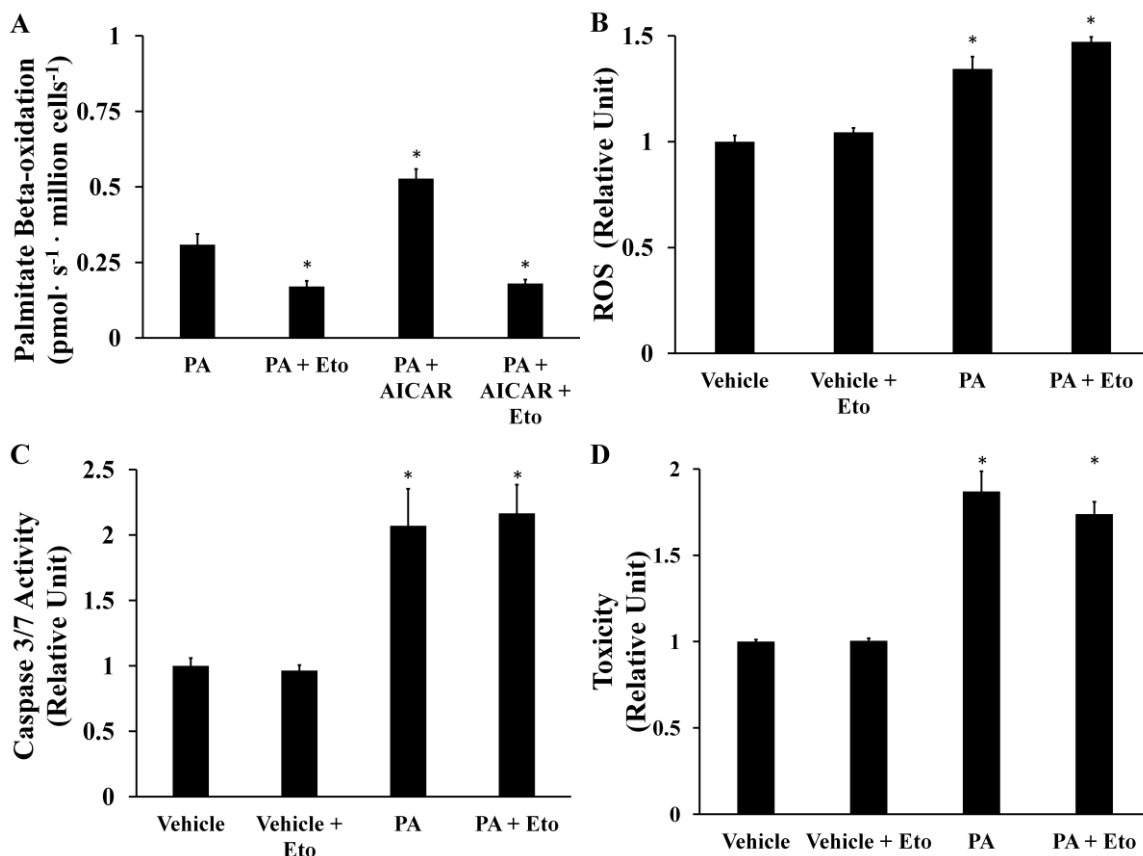
Figure 3.5: Beta-oxidation does not fuel palmitate-induced ROS accumulation. The CPT-1 inhibitor etomoxir (Eto) was added at a concentration of 250 μM to palmitate-treated (PA, 400 μM) or BSA-treated (vehicle, 800 μM) H4IIEC3 cells. (A) Beta-oxidation of [9,10-^{3}H(N)] palmitate assessed by ^{3}H$_2$O production. 500 μM AICAR was used as a positive control. (B) ROS levels at 6 hours measured by DCF fluorescence. (C) Caspase activity of cells treated with palmitate and etomoxir at 12 hours. (D) Cell toxicity at 24 hours assessed by PI fluorescence. Data represent mean +/- S.E., n=4 for fluorescence assays,* different from palmitate in (A), vehicle in (B, C, D), p <.05.

To directly assess the contribution of palmitate toward supplying carbon for CAC intermediates, we treated H4IIEC3 rat hepatomas with [U-^{13}C$_{16}$]palmitate. Intracellular, non-protein-bound metabolites were extracted, derivatized, and analyzed by GC-MS to quantify ^{13}C-enrichment. If carbon from ^{13}C-labeled PA was fully oxidized in the CAC, it would enter the cycle initially as a fully labeled (M+2) acetyl-CoA. This acetyl-CoA would then give rise to M+2 labeled CAC intermediates such as citrate and malate. Therefore, we analyzed ion

fragments of citrate and malate for enrichment of M+2 mass isotopomers (Figure 3.6A). However, we found little to no incorporation of ^{13}C, suggesting that a negligible flux of palmitate carbon was directed into the CAC for complete oxidation.
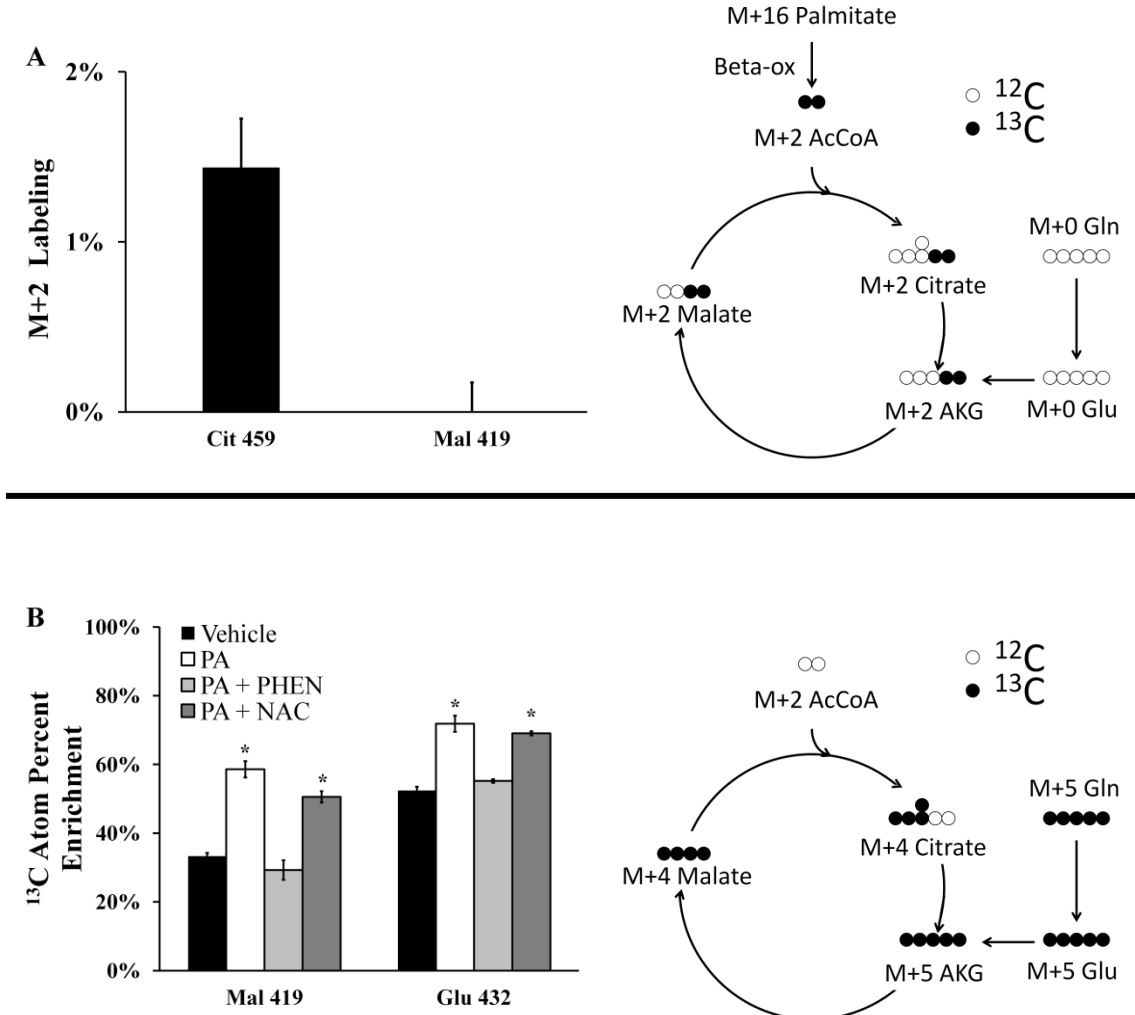
Figure 3.6: Isotopic enrichment of mitochondrial metabolites. Mass isotopomer distributions were corrected for natural isotope abundance using the method of Fernandez et al. (1). (A) M+2 mass isotopomer abundance resulting from incorporation of ^{13}C into malate and citrate following 6 hours of incubation with 400 μM [U-^{13}C$_{16}$]palmitate. Fully oxidized palmitate gives rise to M+2 mass isotopomers as illustrated in the accompanying diagram. (B) Atom percent enrichment (APE) of cells incubated with [U-^{13}C$_5$]glutamine in combination with palmitate and phenformin or NAC co-treatments. APE was calculated using the formula

$$APE = 100\% \times \sum_{i=0}^{N} \frac{Mi \times i}{N}$$, where N is the number of carbon atoms in the metabolite and Mi is

the fractional abundance of the ith mass isotopomer. The diagram illustrates the patterns of isotope incorporation derived from labeled glutamine after one turn of the CAC. Data represent mean +/- S.E., n=3; * different from vehicle, p <.05.

56

Metabolic flux analysis identifies glutamine as a major fuel substrate for palmitate-induced mitochondrial activation

To identify sources of carbon flux into the CAC, we performed further isotope labeling studies by total replacement of medium glutamine with [U-^{13}C$_5$]glutamine. The average ^{13}C-enrichment of a given metabolite therefore reflects the overall contribution of glutamine carbon to the metabolite pool relative to other unlabeled carbon sources (e.g., glucose or FFA). GC-MS analysis of ^{13}C incorporation revealed that malate extracted from PA-treated cells approached 60% enrichment compared to approximately 30% enrichment in vehicle-treated cells (Figure 3.6B). The addition of phenformin to PA-treated cells normalized the isotopic enrichment of malate to the level of control cells. On the other hand, NAC co-supplementation had only a minor effect on malate enrichment. Analysis of isotopic enrichment of glutamate revealed similar enrichment trends. Taken together, these data demonstrate that palmitate treatment is characterized by elevated glutamine consumption and increased entry of glutamine carbon into the CAC relative to other carbon sources. Similar to the oxygen uptake measurements reported in Figure 3.3D and Figure 3.4D, phenformin co-treatment was able to reverse PA-induced alterations to glutamine metabolism while NAC co-treatment was not.

Next, we applied ^{13}C MFA to simultaneously calculate 12 mitochondrial fluxes and their associated 95% confidence intervals by combining mass spectrometric measurements of ^{13}C labeling with the previously measured oxygen consumption rates (Figure 3.7A). H4IIEC3 cells treated with PA alone exhibited higher glutamine consumption, higher malic enzyme flux, and higher citrate synthase flux relative to vehicle-treated cells. Phenformin co-treatment effectively reduced most mitochondrial fluxes, including glutamine uptake and ETC activity. Cells co-treated with NAC and PA exhibited no reduction in mitochondrial metabolic fluxes, suggesting that the palmitate-induced metabolic alterations were not a consequence of elevated ROS and

apoptosis initiation but instead were the result of upstream events in the lipotoxicity cascade that

enhanced mitochondrial metabolic pathways.
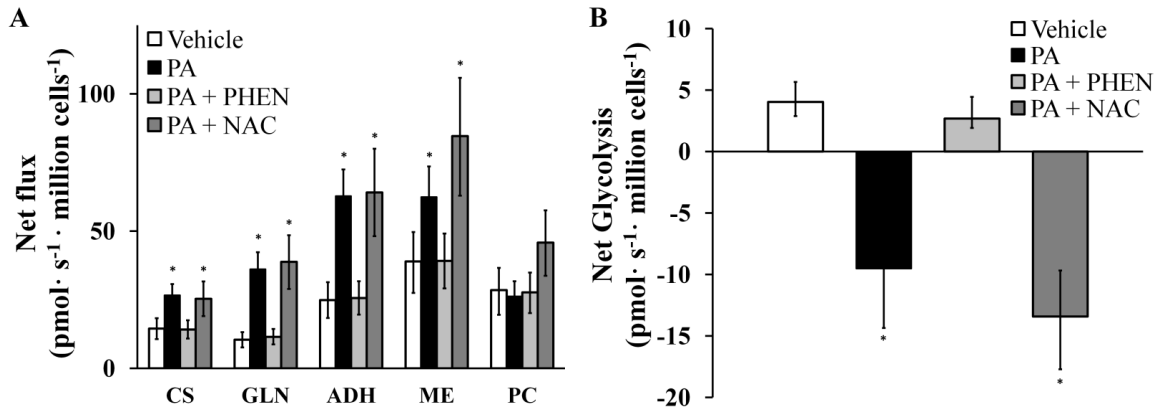
Figure 3.7: ^{13}C flux analysis of mitochondrial metabolism. Fluxes were calculated as described in the Methods section and further detailed in the Supplementary Materials. (A) Major CAC and anaplerotic fluxes of cells treated with BSA (Vehicle) or palmitate (PA) with and without NAC or phenformin (PHEN) co-treatments. Abbreviations: ADH, alpha-ketoglutarate dehydrogenase; CS, citrate synthase; GLN, glutamine uptake; ME, malic enzyme; PC, pyruvate carboxylase. (B) 'Net glycolysis' rate defined as the difference between glycolytic pyruvate production and lactate excretion. Error bars indicate 95% confidence intervals; * different from vehicle, p <.05.

Based on our ^{13}C MFA calculations, we determined the difference between glycolytic

pyruvate production and lactate excretion (Figure 3.7B). We designate this difference as 'net

glycolysis', since it represents the net amount of glycolytic carbon that enters the CAC for

oxidation. If this value is positive, there is net contribution of glucose carbon to the

mitochondrial metabolic pool. If negative, non-glucose carbon derived from the CAC is

contributing to lactate production. For vehicle-treated cells, the net glycolytic rate was positive

since more glucose carbon entered the pyruvate node than was excreted as lactate. Cells treated

with PA, however, were characterized by a negative net glycolytic rate since glutamine entry to

the CAC was elevated relative to glucose. Supplementing PA-treated cells with phenformin, but

not NAC, effectively reversed this phenotype. Complete flux maps of all four treatments are

shown in Figure 3.8.
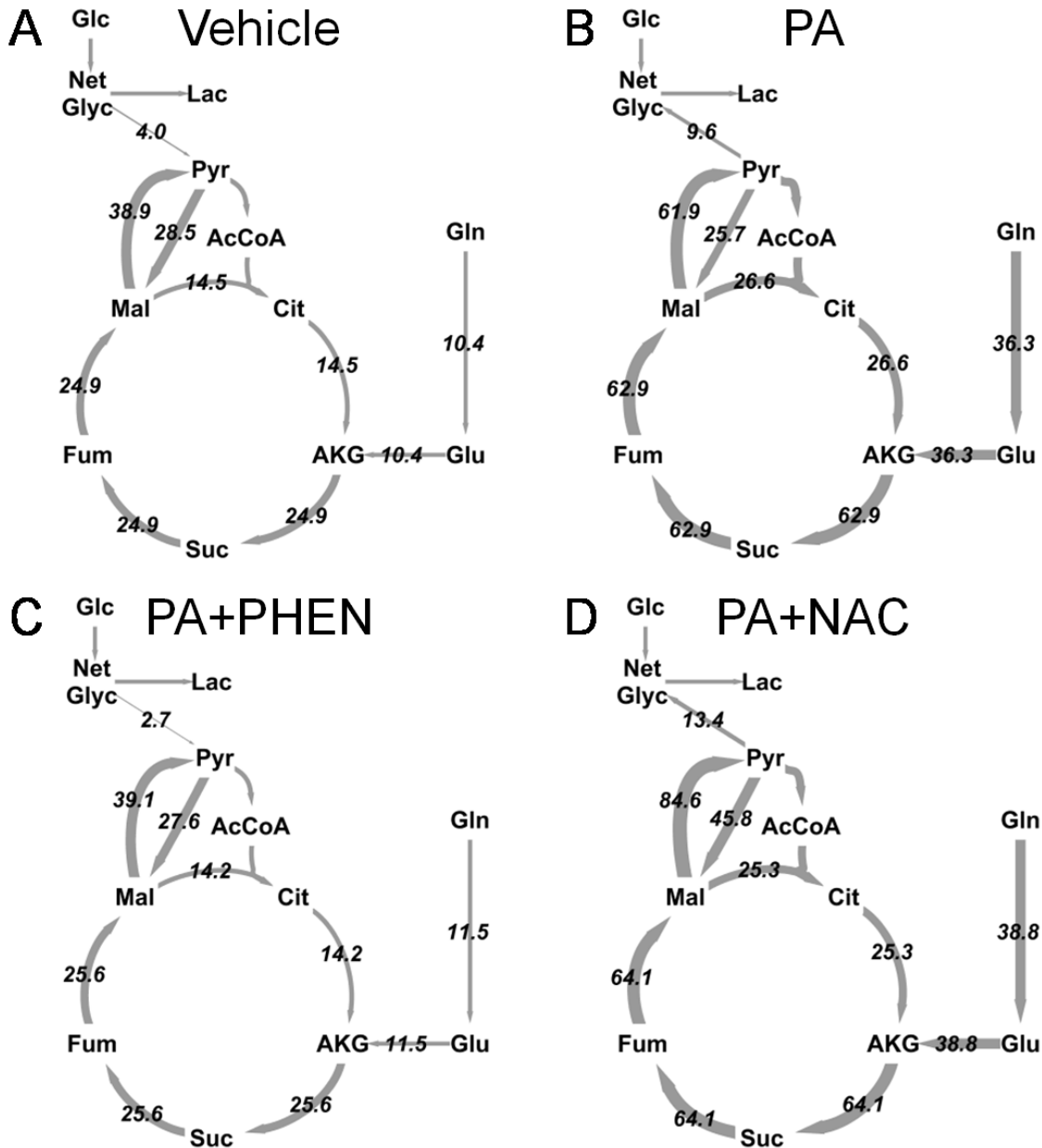
Figure 3.8: Comparison of H4IIEC3 flux maps under various treatments examined in this study. Arrows are weighted according to flux values shown (pmol/million cells/s). (A) Vehicle-treated cells, (B) palmitate (PA) treated cells, (C) palmitate and phenformin (PA + PHEN) co-treated cells, (D) palmitate and NAC (PA + NAC) co-treated cells. Abbreviations: AcCoA, acetyl-CoA; AKG, alpha-ketoglutarate; Cit, citrate; Fum, fumarate; Glc, glucose; Glu, glutamate; Gln, glutamine; Lac, lactate; Mal, malate; Net Glyc, net glycolysis; Pyr, pyruvate; Suc, succinate.

Discussion

Understanding the molecular factors that control hepatic lipotoxicity is a critical step toward developing improved strategies to prevent and treat NAFLD and NASH. A reported feature of palmitate-induced lipotoxicity is increased oxidative stress due to intracellular ROS accumulation, which precedes the onset of apoptosis as indicated by DNA laddering, induction of caspases 3 and 7, and cytochrome C release (10,12,15,22,30). However, the role of ROS in stimulating lipoapoptosis appears to be cell-type dependent. For example, ROS accumulation is a critical event leading to apoptosis of palmitate-treated CHO cells (31), while palmitate-treated neonatal cardiomyocytes undergo apoptosis independently of oxidative stress (32). In our experiments, we measured a burst of ROS at approximately 6 hours following palmitate administration, which was 25-50% higher than cells treated with vehicle (BSA) alone. It has been shown previously in the H4IIEC3 cell line that similar increases in ROS can activate JNK stress pathways, which was sufficient to negatively affect insulin signaling (9). We found that NAC co-treatment effectively normalized PA-induced ROS accumulation, significantly reduced caspase activation, and improved long-term cell viability, indicating that apoptosis initiation is dependent on ROS accumulation in H4IIEC3 cells.

Healthy cells continually produce ROS during mitochondrial oxidative phosphorylation and rely on their enzymatic machinery to manage ROS levels, thereby preventing toxic side effects. Elevated ROS can therefore occur due to either increased oxidative metabolism or deficient antioxidant defenses. To quantify rates of mitochondrial metabolism in palmitate-treated H4IIEC3 cells, we applied ^{13}C MFA based on [U-$^{13}C_5$]glutamine tracing combined with measurements of oxygen consumption flux. Since mitochondria require oxygen to carry out

60

oxidative phosphorylation, increased oxygen consumption is a direct measure of increased mitochondrial metabolism. Palmitate-treated cells exhibited a 2-fold increase in oxygen consumption rate and in most mitochondrial fluxes prior to ROS accumulation. However, NAC co-treatment did not affect palmitate-induced metabolic alterations, indicating that neither elevated ROS nor downstream apoptotic events contributed to mitochondrial activation. Instead, elevated mitochondrial metabolism appears to be an inherent consequence of palmitate overload that is independent of subsequent ROS accumulation and apoptosis initiation.

Next, we sought to determine whether accelerated mitochondrial metabolism is required for palmitate-induced ROS accumulation and apoptosis, or whether these events are primarily attributable to other causes such as failure of antioxidant defenses or activation of NADPH oxidases. To address this question, we employed the complex I antagonist phenformin to directly inhibit mitochondrial metabolism. Phenformin is a lipophilic derivative of the type-2 diabetes drug metformin, which shares the same mechanism of action (33,34). Phenformin co-treatment reduced both ROS accumulation and oxygen uptake in PA-treated H4IIEC3 cells and normalized mitochondrial metabolic fluxes to levels characteristic of vehicle-treated cells. Similar to NAC treatment, this reduction in mitochondria-derived ROS coincided with increased cell viability and decreased caspase activation. Therefore, elevated mitochondrial metabolism is required for ROS accumulation and caspase activation in our model of palmitate lipotoxicity.

Increased fatty acid beta-oxidation has been proposed as the primary fuel source responsible for lipotoxic ROS generation both *in vivo* (2,3) and in the H4IIEC3 cell line (9). In our experiments with the same cell line, however, adding the CPT-1 inhibitor etomoxir to palmitate-treated H4IIEC3 cells had no effect on ROS accumulation or cell viability. These results reveal a novel facet of lipotoxicity in our system: mitochondria-derived ROS

accumulation is independent of fatty acid beta-oxidation. We found little isotopic enrichment of CAC intermediates when H4IIEC3 cells were fed [U-^{13}C$_{16}$]palmitate, indicating that exogenous fatty acid was not being fully oxidized to CO_2. To further investigate the fuel source driving palmitate-induced mitochondrial activation, we relied on ^{13}C MFA to map the flow of carbon entering the CAC from the major non-lipid substrates glucose and glutamine. We found that glutamine provided the primary fuel for elevated mitochondrial metabolism in the presence of palmitate, rather than fatty acid beta-oxidation, and that glutamine consumption could be reduced through co-treatment with phenformin but not NAC. These results demonstrate that ROS accumulation is a direct consequence of mitochondrial activation and can be reversed by inhibiting oxidative phosphorylation, which concomitantly suppresses entry of glutamine carbon into the CAC.

Our ^{13}C MFA results match well with previous *in vivo* ^{2}H/^{13}C NMR studies of NAFLD patients (3) and HFD fed mice (2), both of which reported an approximate 2-fold increase in CAC flux. This was associated with increased oxidative damage in livers of HFD fed mice (2). The authors hypothesized that increased beta-oxidation was fueling the observed enhancement in CAC flux. However, our *in vitro* observations supply an alternative hypothesis, which is that oxidation of non-lipid substrates can also contribute substantially to elevated CAC flux in hepatic lipotoxicity. It should be noted, however, that the *in vivo* flux studies were performed under fasting (i.e., gluconeogenic) conditions, whereas the conditions of our study were representative of a fed (i.e., glycolytic) state. Therefore, it is difficult to make direct quantitative comparisons between our data and those obtained from the prior *in vivo* studies.

Our findings suggest several intriguing questions for further study into the causes and consequences of mitochondrial dysregulation under conditions of FFA lipotoxicity. First, if the

exogenous palmitate load does not directly fuel elevated CAC flux, what other effects of palmitate overexposure might lead to activation of mitochondrial oxidative metabolism? One possible hypothesis is that disruption of normal lipid metabolic pathways may lead to (i) production of lipid-derived signaling molecules or (ii) alteration of intracellular membrane homeostasis that subsequently activates mitochondrial metabolism. This may also involve activation of signaling proteins such as peroxisome proliferator-activated receptors (PPARs) that respond directly to lipid intermediates and can regulate expression of mitochondrial proteins. Although our study provides a detailed picture of metabolic flux rewiring in response to FFA treatments, it does not address the upstream cell signaling and transcriptional regulatory mechanisms that may play a role in mediating the observed metabolic alterations. Second, can direct inhibition of glutamine anaplerosis reverse the lipotoxic metabolic phenotype or will hepatic cells shift to other available carbon sources to maintain elevated CAC flux? Further investigation of both the upstream and downstream molecular events that control palmitate-induced mitochondrial activation in hepatic cells is clearly an important next step.

In summary, we have applied oxygen uptake measurements and ^{13}C MFA to elucidate a critical role for mitochondrial dysregulation in mediating palmitate lipotoxicity of H4IIEC3 cells. We report that a) palmitate-induced metabolic dysregulation is independent of oxidative damage and apoptosis initiation, b) apoptosis is dependent on palmitate-induced metabolic alterations leading to elevated ROS accumulation, and c) glutamine, not fatty acid beta-oxidation, provides the carbon fuel for enhanced CAC flux in response to a palmitate load. Our model also highlights important differences between the protective effects of phenformin and NAC, both of which have direct *in vivo* relevance. Studies using non-diabetic methionine- and choline-deficient mouse models of NASH demonstrate that metformin has the potential to reduce

inflammation after induction of liver injury (35). Additionally, NAC supplementation of HFD

fed Sprague-Dawley rats successfully prevented the appearance of many markers of elevated

oxidative stress such as peroxidized lipid species (36). However, this study reported that NAC

did not reverse potential upstream activators of liver dysfunction such as steatosis and only

partially restored glutathione levels. Clinically, the use of antioxidants as a treatment for NASH

has met with varying degrees of success. For example, the antioxidant vitamin E has been

explored as a potential therapy for persons with NASH. Treatment with vitamin E resulted in

reduced liver injury in adults assessed by a reduction in serum alanine and aspartate

aminotransferase levels but did not improve fibrosis (37). Interestingly, vitamin E trials in

children with NASH report no improvements in alanine aminotransferase levels as a primary

marker of disease but had improved NASH scores (38). These prior *in vivo* studies highlight

how antioxidants can treat some but not all symptoms of NASH, suggesting they do not fully

restore normal redox homeostasis or block other upstream or parallel disease pathways.

Improved understanding of the molecular determinants of lipotoxicity is therefore likely to

suggest novel nutritional and/or pharmacologic interventions to combat the effects of NAFLD

and to prevent its progression toward NASH.

Appendix
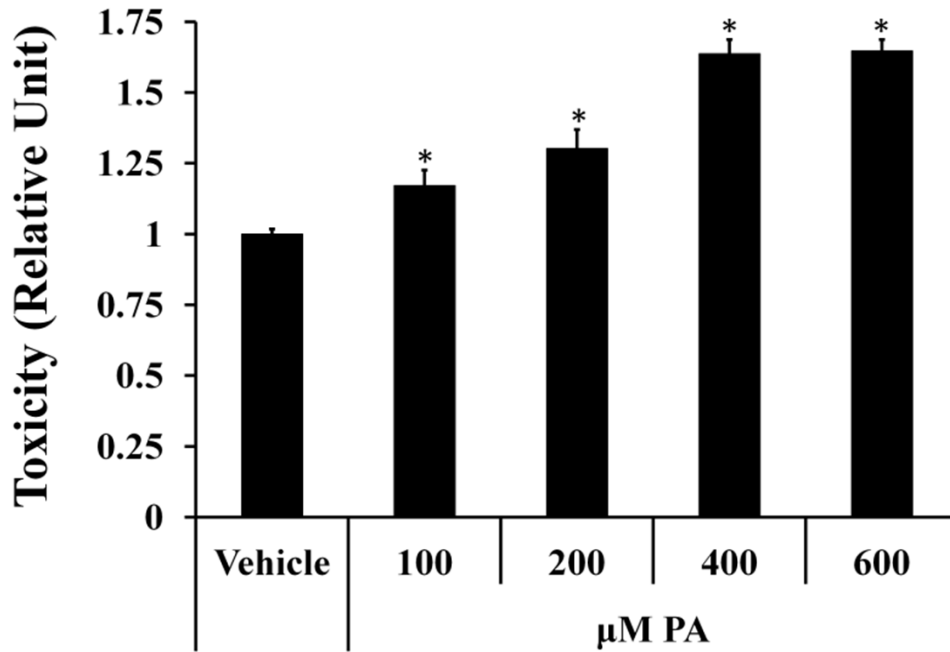
Figure 3A.1: Increasing concentrations of palmitate increases cell death in H4IIEC3 hepatic cells. H4IIEC3 rat hepatic cells were treated with the indicated concentrations of palmitate for 24 hours and cell toxicity was measured by PI fluorescence. 400 µM palmitate doubled PI fluorescence after 24 hours. Data represent mean +/- S.E., n=8 for fluorescence assays; *, different from vehicle, p <.05.
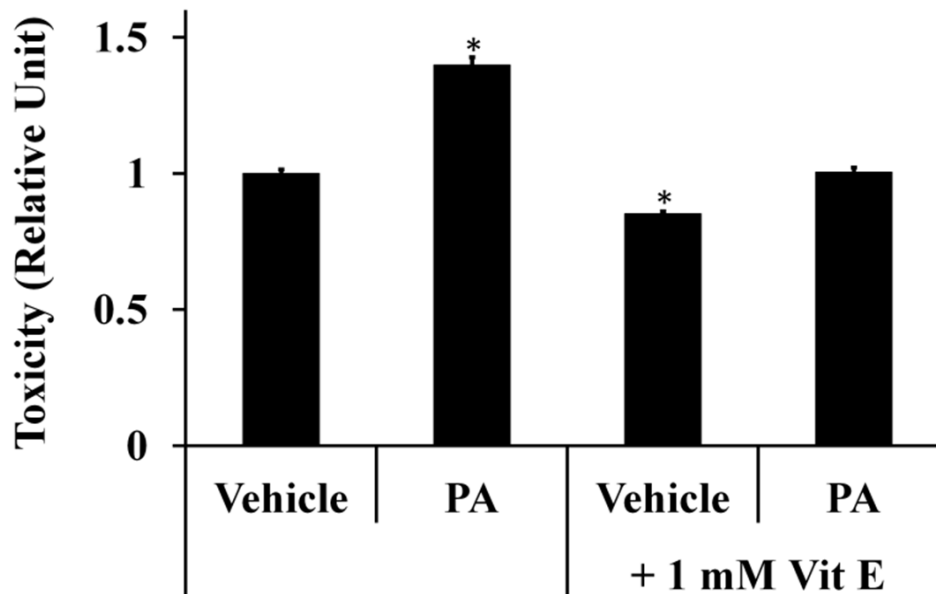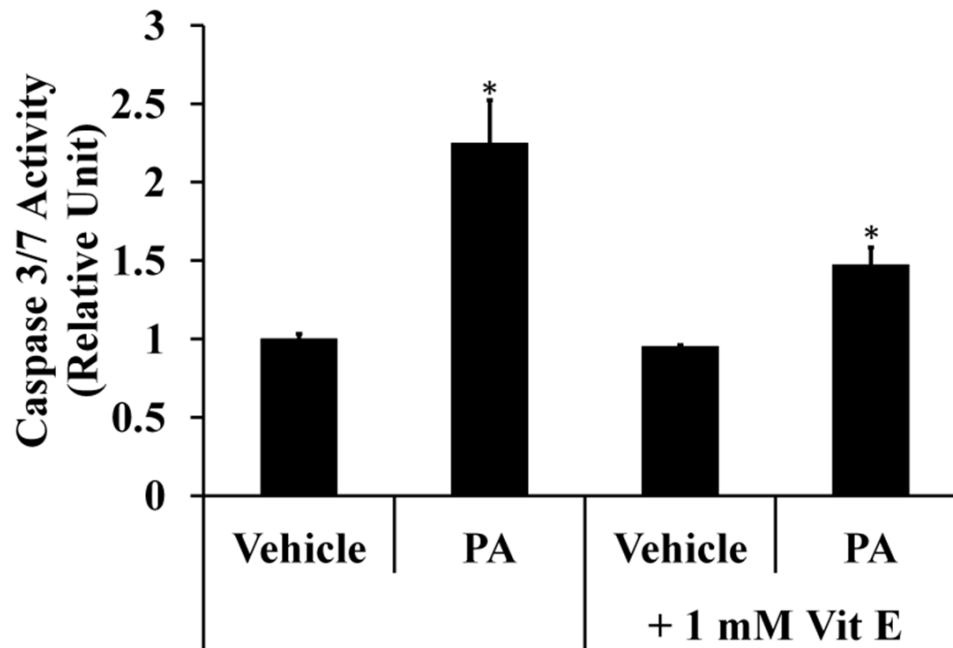
Figure 3A.2: Vitamin E antioxidant supplement prevents lipotoxic cell death. (A) The antioxidant Vitamin E (Vit E, 1 mM) to palmitate-treated (PA, 400 µM) or BSA-treated (vehicle, 800 µM) H4IIEC3 cells and (A) Caspase 3/7 activity was measured after 12 hours. (B) 24-hour cell toxicity was measured by propidium iodide. Vitamin E co-treatment significantly blunts these markers of lipotoxicity. Data represent mean +/- S.E., n=8 for the toxicity assay; * different from vehicle, p <.05.
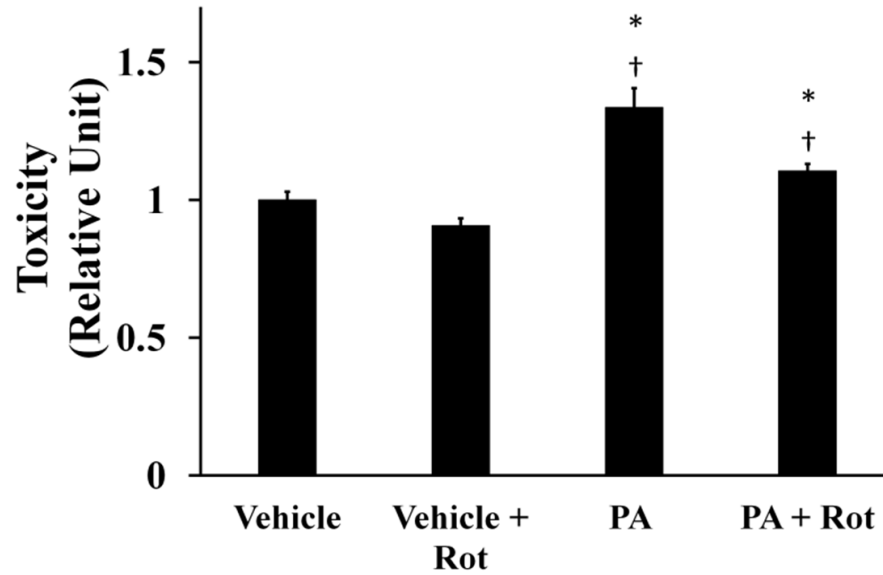
Figure 3A.3: Rotenone addition to palmitate-treated cells reduces cell death. H4IIEC3 cells were co-treated with 100 nM rotenone (ROT) and either 400 µM palmitate (PA) or 800 µM BSA (vehicle) to examine the role of mitochondrial metabolism in ROS accumulation and apoptosis. Toxicity 24-hours post-treatment was assessed using propidium iodide. Data represent mean +/- S.E., n=4 for the toxicity assay; * different from vehicle, p <.05.

Metabolic Flux Analysis (MFA) reaction network and modeling assumptions

In order to calculate intracellular fluxes we used the reaction network listed in Table A1. Our assumptions were as follows:

1) Removal of metabolites for biomass synthesis was negligible due to slow growth of cells.

2) The measured labeling was at isotopic steady state.

3) Labeled CO_2 produced by CAC cycle fluxes was not reincorporated.

4) To constrain the model using oxygen consumption flux, only NADH-producing reactions associated with the CAC cycle were considered. This approach constrains mitochondrial ETC activity to CAC cycle fluxes.

5) ATP citrate lyase activity was assumed to be negligible since the cells were in the presence of excess lipid and cell growth was assumed to be negligible.

6) Major routes of carbon entry were glucose and glutamine. Major routes of carbon exit were complete oxidation to CO_2 and lactate excretion.

7) Lastly, we have included a G dilution parameter to account for lack of isotopic steady state in the aspartate pool. The G parameter represents the fraction of the aspartate pool that had been synthesized in the presence of the tracer (39).

Our model uses oxygen uptake measurements in combination with $[U-^{13}C_5]$glutamine isotope labeling measurements to estimate CAC cycle fluxes. Using oxygen consumption to constrain CAC cycle flux is advantageous because it provides a direct measure of oxidative metabolism. MFA methods that rely solely on carbon balancing to estimate CAC cycle flux are susceptible to errors if reactions are left out of the model (40,41). Detailed MFA results can be found in Figures A3-6 and Tables A3-6 along with the best-fit sum-of-squared residuals (SSR) and the

degrees of freedom (DOF), which characterize the goodness-of-fit for each experiment.

Exchange fluxes are defined as $v_{exch}^{[0,100]} = 100 \times \frac{v_{exch}}{v_{exch}+v_{ref}}$, where v_{ref} is a reference (citrate synthase) flux value (42).

Table 3A.1: Reactions and atom transitions for metabolic flux analysis of H4IIEC3 rat hepatomas. List of metabolite abbreviations can be found below. Dot suffixes denote specific sub-pools of metabolite: .x, extracellular; .t, tracer; .d, dilution.

Pyruvate Metabolism			Reaction Name
Glucose (abcdef)	→	Pyr (abc) + Pyr (fed)	PK
Pyr (abc)	→	Lac (abc)	LDH
Pyr (abc) + CO_2 (d)	→	Mal (abcd)	PC
Mal (abcd)	→	Pyr (abc) + CO_2 (d)	ME
Pyr (abc)	→	AcCoA (bc) + CO_2 (a) + NADH	PDH

CAC Cycle Metabolism			
AcCoA (ab) + Mal (cdef)	→	Cit (fedbac) + NADH	CS
Cit (abcdef)	←→	Akg (abcde) + CO_2 (f) + NADH	IDH
Akg (abcde)	→	Suc (½ abcd + ½ dcba) + CO_2 (a) + NADH	ADH
Suc (½ abcd + ½ dcba)	←→	Fum (½ abcd + ½ dcba)	SDH
Fum (½ abcd + ½ dcba)	←→	Mal (abcd)	FDH

Glutamine anaplerosis			
Gln.x (abcde)	→	Gln (abcde)	Gln uptake
Gln (abcde)	→	Glu (abcde)	GLN
Glu (abcde)	←→	Akg (abcde)	GDH

Net Glycolysis			
Difference between PK and LDH			

Oxygen Consumption			
2·NADH + O_2	→	Sink	

Dilution			
Asp.d (abcd)	→	Asp (abcd)	Asp G parameter

List of abbreviations
AcCoA, acetyl-CoA; **Akg**, alpha-ketoglutarate; **Ala**, alanine; **Asp**, aspartate; **Cit**, citrate; **Fum**, fumarate; **Gln**, glutamine; **Glu**, glutamate; **Lac**, lactate; **Mal**, malate; **Pyr**, pyruvate; **Suc**, succinate; *ADH*, alpha-ketoglutarate dehydrogenase; *CS,* citrate synthase, *FDH*, fumarate dehydrogenase; *GDH,* glutamate dehydrogenase; *GLN,* glutaminase; *IDH,* isocitrate dehydrogenase; *LDH,* lactate dehydrogenase; *ME*, malic enzyme; *PC,* pyruvate carboxylase; *PDH,* pyruvate dehydrogenase; *PK,* pyruvate kinase; *SDH,* succinate dehydrogenase.

Table 3A.2: Measured GC-MS ions used for flux analysis. Standard error (SEM) is representative of the error between biological replicates (n=3).

Metabolite	Mass	Composition	Carbons					SEM %			
								Vehicle	PA	PA + PHEN	PA + NAC
Lac	233	$C_{10}H_{25}O_2Si_2$		2	3			0.65	0.54	0.50	0.65
Lac	261	$C_{11}H_{25}O_3Si_2$	1	2	3			0.80	0.74	0.50	0.50
Mal	419	$C_{18}H_{39}O_5Si_3$	1	2	3	4		1.7	0.88	0.80	0.59
Asp	390	$C_{17}H_{40}O_3NSi_3$		2	3	4		1.1	1.6	1.0	0.75
Asp	418	$C_{18}H_{40}O_4NSi_3$		2	3	4	5	0.86	1.5	1.2	0.73
Glu	330	$C_{16}H_{36}O_2NSi_2$		2	3	4	5	0.75	1.1	0.63	0.87
Glu	432	$C_{19}H_{42}O_4NSi_3$	1	2	3	4	5	0.56	1.0	0.50	0.60
Gln	431	$C_{19}H_{43}N_2O_3Si_3$	1	2	3	4	5	0.70	0.50	0.50	0.50

Table 3A.3 Calculated absolute flux parameters and 95% confidence intervals for untreated cells. Net flux units are pmol/million cells/s. Exchange fluxes and dilution parameters are scaled from 0 to 100%. SSR = 62.0 (32 DOF).

Parameter	Value	95% Confidence Interval
Net Flux		
PK	32.2	[23.4, 41.7]
PDH	14.5	[10.6, 18.2]
CS	14.5	[10.6, 18.2]
IDH	14.5	[10.6, 18.2]
GLN	10.4	[7.6, 13.2]
GDH	10.4	[7.6, 13.2]
ADH	24.9	[18.3, 31.4]
SDH	24.9	[18.3, 31.4]
FDH	24.9	[18.3, 31.4]
ME	38.9	[28.1, 50.3]
PC	28.5	[20.4, 37.5]
LDH	60.3	[43.6, 78.5]
O_2 Consumption	34.1	[25.1, 43.0]
Net Glycolysis		
PK – LDH	4.0	[2.9, 5.7]
Exchange Flux		
IDH	0	[0, 100]
SDH	20	[0, 100]
FDH	100	[60.1, 100]
GDH	100	[92.5, 100]
Dilution		
Asp G Parameter	85.5	[84.4, 86.6]
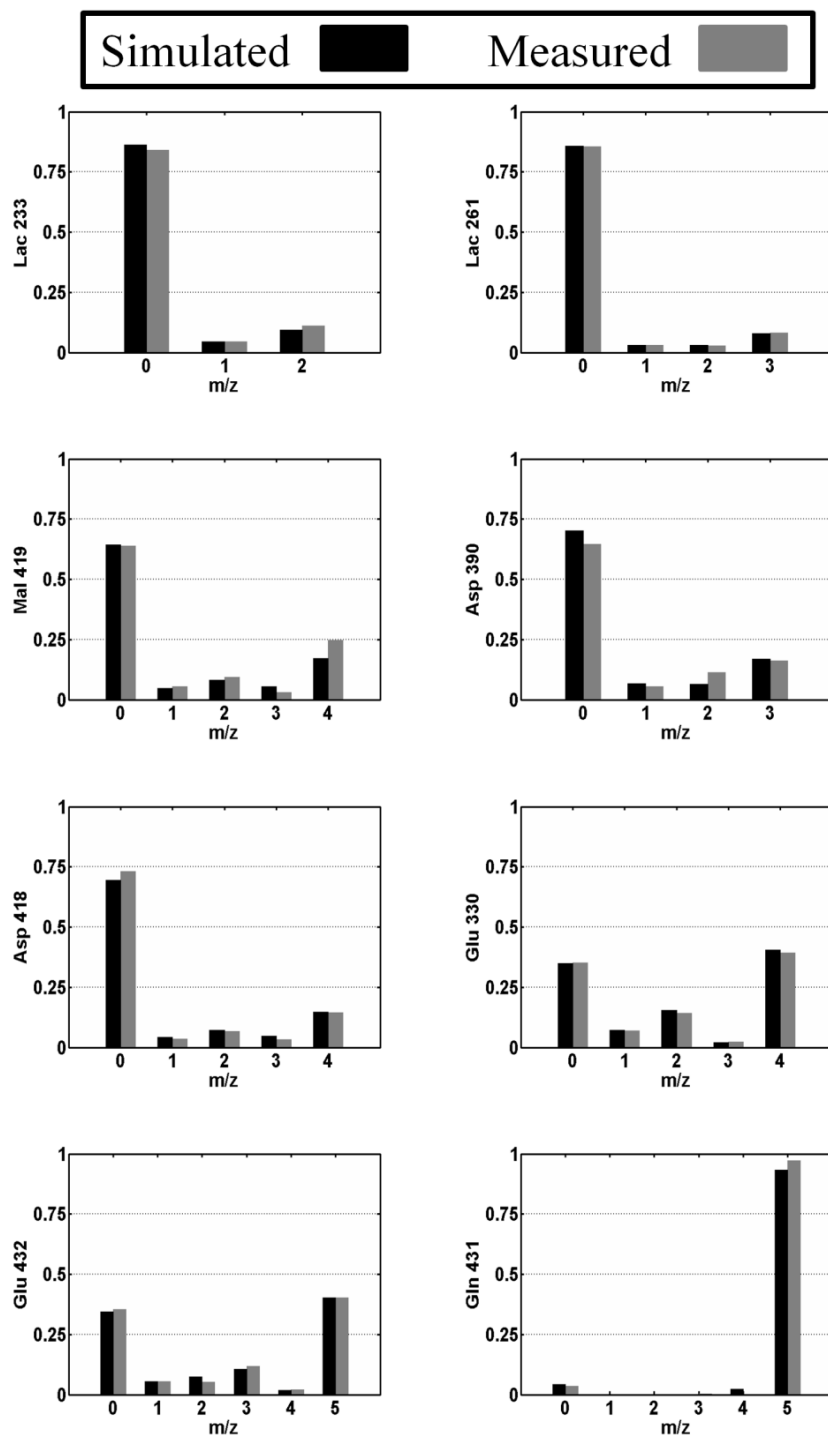
Figure 3A.4: Simulated and measured mass isotopomer distributions for vehicle-treated cells. Simulated distributions are shown for the best-fit flux estimates. Data are corrected for natural isotope abundance.

Table 3A.4: Calculated absolute flux parameters and 95% confidence intervals for palmitate treated cells. Net flux units are pmol/million cells/s. Exchange fluxes and dilution parameters are scaled from 0 to 100%. SSR = 40 (35 DOF).

Parameter	Value	95% Confidence Interval
Net Flux		
PK	64.5	[52.9, 78.8]
PDH	26.6	[22.5, 30.7]
CS	26.6	[22.5, 30.7]
IDH	26.6	[22.5, 30.7]
GLN	36.3	[30.1, 43]
GDH	36.3	[30.1, 43]
ADH	62.9	[53.2, 72.8]
SDH	62.9	[53.2, 72.8]
FDH	62.9	[53.2, 72.8]
ME	61.9	[50.9, 74.5]
PC	25.7	[20.3, 32.1]
LDH	139.6	[112.4, 171.4]
O_2 Consumption	71.3	[60.6, 82.1]
Net Glycolysis		
PK – LDH	-9.6	[-14.6, -5.6]
Exchange Flux		
IDH	8.9	[0, 100]
SDH	70.3	[0, 100]
FDH	100	[0, 100]
GDH	94.7	[87.2, 100]
Dilution		
Asp G Parameter	78.5	[77.7, 79.0]
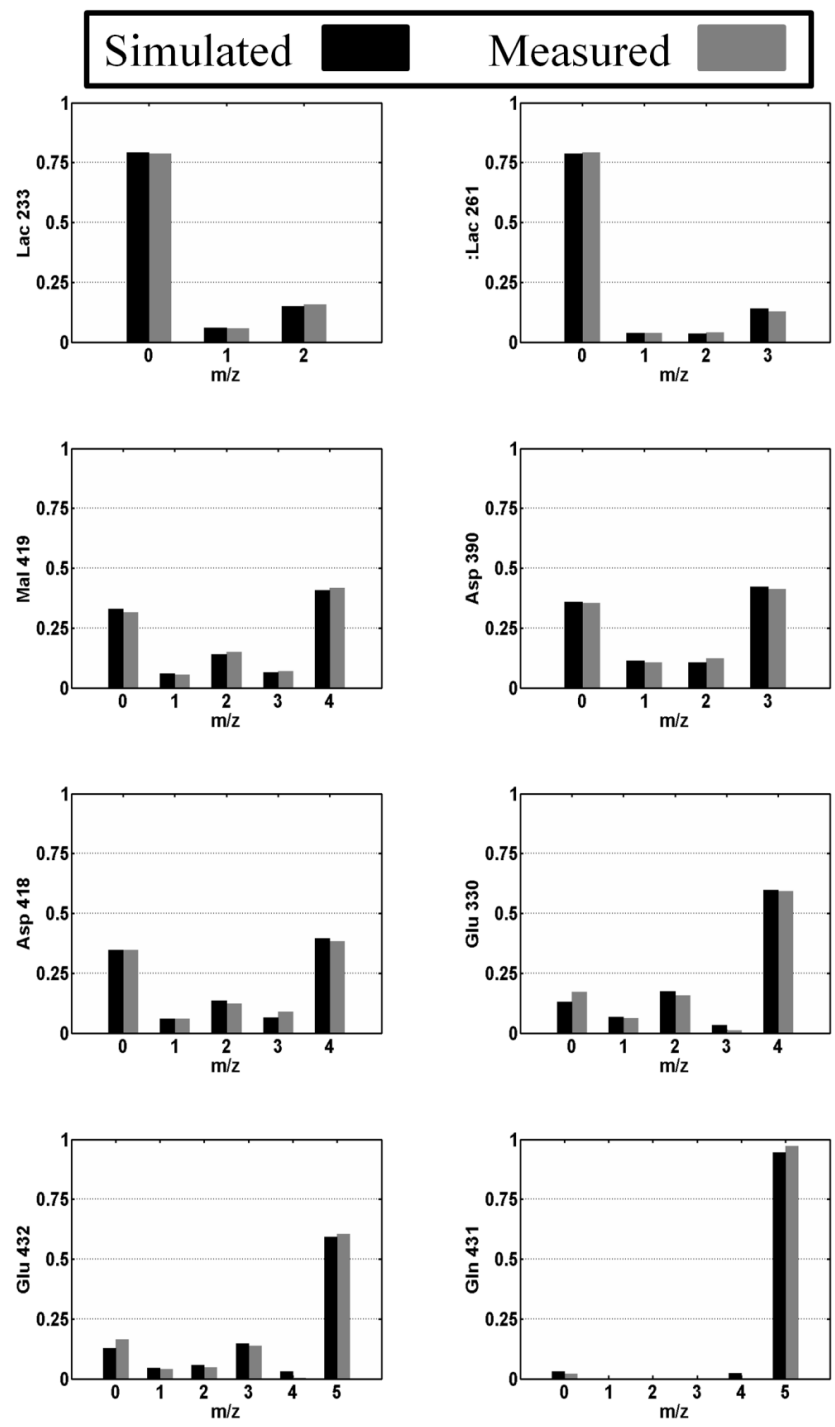
Figure 3A.5: Simulated and measured mass isotopomer distributions for palmitate-treated cells. Simulated distributions are shown for the best-fit flux estimates. Data are corrected for natural isotope abundance.

Table 3A.5: Calculated absolute flux parameters and 95% confidence intervals for palmitate and phenformin co-treated cells. Net flux units are pmol/million cells/s. Exchange fluxes and dilution parameters are scaled from 0 to 100%. SSR = 68.4 (35 DOF).

Parameter	Value	95% Confidence Interval	
Net Flux			
PK	40.8	[30.3,	51.6]
PDH	14.2	[10.8,	17.5]
CS	14.2	[10.8,	17.5]
IDH	14.2	[10.8,	17.5]
GLN	11.5	[8.6,	14.2]
GDH	11.5	[8.6,	14.2]
ADH	25.6	[19.5,	31.6]
SDH	25.6	[19.5,	31.6]
FDH	25.6	[19.5,	31.6]
ME	39.1	[29.1,	49.1]
PC	27.6	[20.3,	35.1]
LDH	79.0	[58.2,	100.1]
O_2 Consumption	34.0	[26.0,	42.0]
Net Glycolysis			
PK – LDH	2.7	[1.9,	4.5]
Exchange Flux			
IDH	31.1	[0,	100]
SDH	1.8	[0,	100]
FDH	100	[66.3,	100]
GDH	100	[92.1,	100]
Dilution			
Asp G Parameter	86.4	[85.4,	87.3]
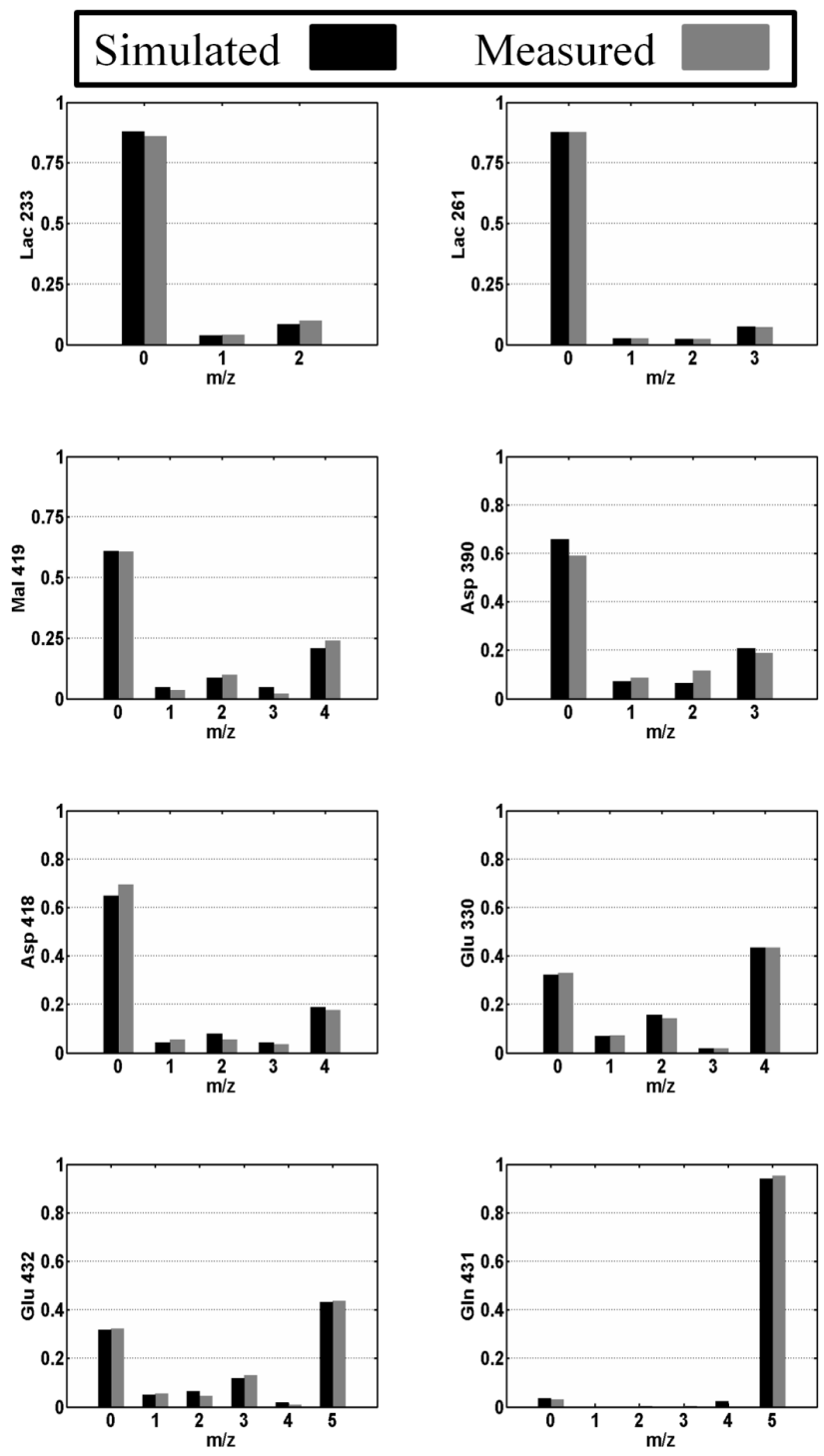
Figure 3.A6: Simulated and measured mass isotopomer distributions for palmitate and phenformin co-treated cells. Simulated distributions are shown for the best-fit flux estimates. Data are corrected for natural isotope abundance.

Table 3A.6: Calculated absolute flux parameters and 95% confidence intervals for palmitate and N-acetyl cysteine co-treated cells. Net flux units are pmol/million cells/s. Exchange fluxes and dilution parameters are scaled from 0 to 100%. SSR = 63.5 (34 DOF).

Parameter	Value	95% Confidence Interval	
Net Flux			
PK	99.4	[73.9,	126.5]
PDH	25.3	[19.0,	31.6]
CS	25.3	[19.0,	31.6]
IDH	25.3	[19.0,	31.6]
GLN	38.8	[29.0,	48.6]
GDH	38.8	[29.0,	48.6]
ADH	64.1	[48.2,	80.0]
SDH	64.1	[48.2,	80.0]
FDH	64.1	[48.2,	80.0]
ME	84.6	[63.3,	106.3]
PC	45.8	[34.1,	57.9]
LDH	212.3	[157.8,	270.2]
O_2 Consumption	70.0	[52.7,	87.4]
Net Glycolysis			
PK − LDH	-13.4	[-17.7	-9.7]
Exchange Flux			
IDH	4.6	[0,	100]
SDH	18.3	[0,	100]
FDH	91.1	[0,	100]
GDH	100	[96.5,	100]
Dilution			
Asp G Parameter	79.8	[78.3,	79.9]
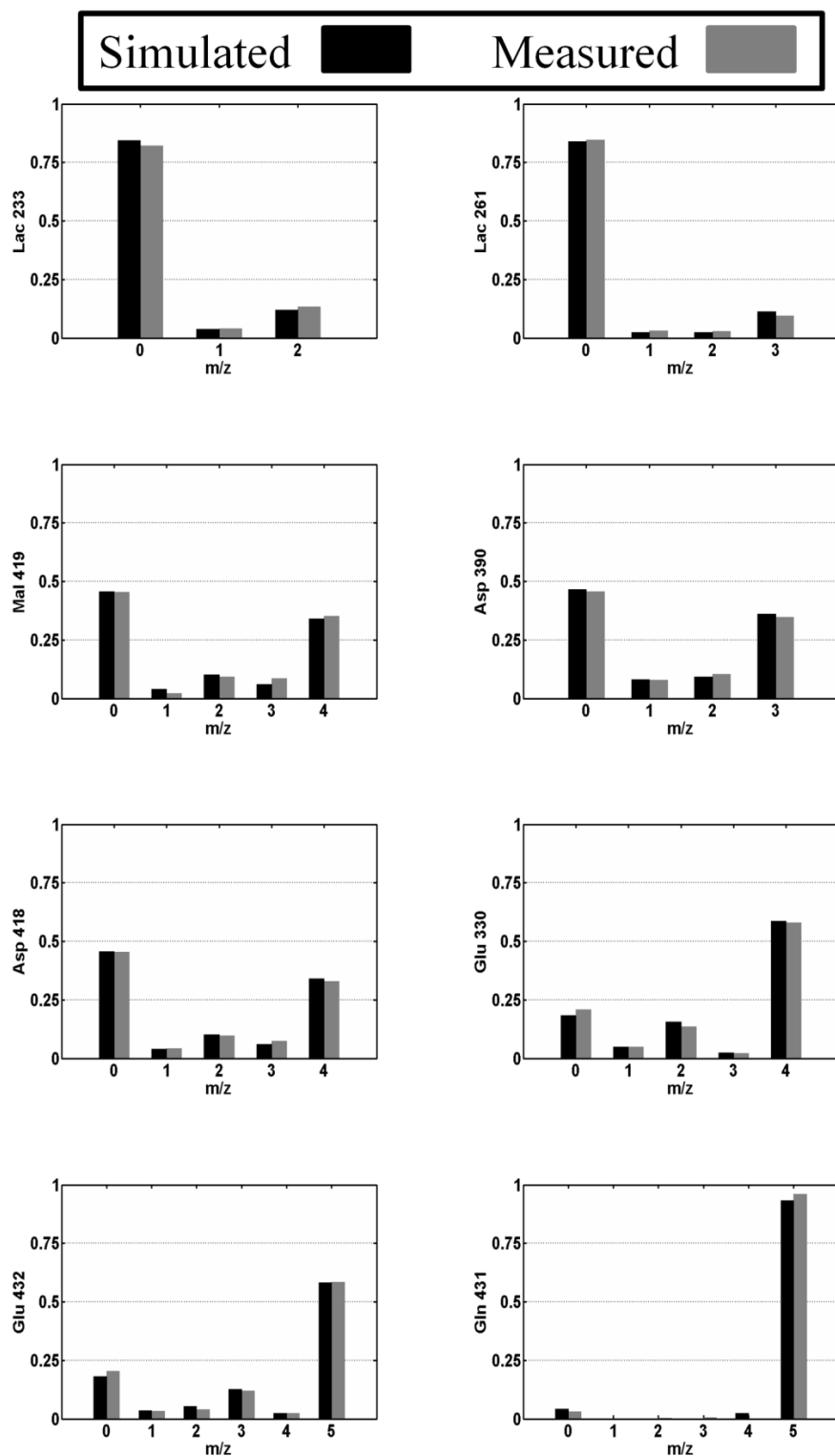
Figure 3A.7: Simulated and measured mass isotopomer distributions for palmitate and N-acetyl cysteine co-treated cells. Simulated distributions are shown for the best-fit flux estimates. Data are corrected for natural isotope abundance.

Acknowledgements

References

1. Fernandez, C. A., Des Rosiers, C., Previs, S. F., David, F., and Brunengraber, H. (1996) Correction of 13C mass isotopomer distributions for natural stable isotope abundance. *J Mass Spectrom* **31**, 255-262

2. Satapati, S., Sunny, N. E., Kucejova, B., Fu, X., He, T. T., Mendez-Lucas, A., Shelton, J. M., Perales, J. C., Browning, J. D., and Burgess, S. C. (2012) Elevated TCA cycle function in the pathology of diet-induced hepatic insulin resistance and fatty liver. *Journal of lipid research* **53**, 1080-1092

3. Sunny, N. E., Parks, E. J., Browning, J. D., and Burgess, S. C. (2011) Excessive hepatic mitochondrial TCA cycle and gluconeogenesis in humans with nonalcoholic fatty liver disease. *Cell metabolism* **14**, 804-810

4. Samuel, V. T., Liu, Z. X., Qu, X., Elder, B. D., Bilz, S., Befroy, D., Romanelli, A. J., and Shulman, G. I. (2004) Mechanism of hepatic insulin resistance in non-alcoholic fatty liver disease. *The Journal of biological chemistry* **279**, 32345-32353

5. Savage, D. B., Petersen, K. F., and Shulman, G. I. (2007) Disordered lipid metabolism and the pathogenesis of insulin resistance. *Physiological reviews* **87**, 507-520

6. Sanyal, A. J., Campbell-Sargent, C., Mirshahi, F., Rizzo, W. B., Contos, M. J., Sterling, R. K., Luketic, V. A., Shiffman, M. L., and Clore, J. N. (2001) Nonalcoholic steatohepatitis: association of insulin resistance and mitochondrial abnormalities. *Gastroenterology* **120**, 1183-1192

7. Serviddio, G., Bellanti, F., Tamborra, R., Rollo, T., Capitanio, N., Romano, A. D., Sastre, J., Vendemiale, G., and Altomare, E. (2008) Uncoupling protein-2 (UCP2) induces mitochondrial proton leak and increases susceptibility of non-alcoholic steatohepatitis (NASH) liver to ischaemia-reperfusion injury. *Gut* **57**, 957-965

8. Pessayre, D., and Fromenty, B. (2005) NASH: a mitochondrial disease. *Journal of hepatology* **42**, 928-940

9. Nakamura, S., Takamura, T., Matsuzawa-Nagata, N., Takayama, H., Misu, H., Noda, H., Nabemoto, S., Kurita, S., Ota, T., Ando, H., Miyamoto, K., and Kaneko, S. (2009) Palmitate Induces Insulin Resistance in H4IIEC3 Hepatocytes through Reactive Oxygen Species Produced by Mitochondria. *Journal of Biological Chemistry* **284**, 14809-14818

10. Noguchi, Y., Young, J., Aleman, J., Hansen, M., Kelleher, J., and Stephanopoulos, G. (2009) Effect of Anaplerotic Fluxes and Amino Acid Availability on Hepatic Lipoapoptosis. *Journal of Biological Chemistry* **284**, 33425-33436

11.   Malhi, H., Bronk, S. F., Werneburg, N. W., and Gores, G. J. (2006) Free fatty acids induce JNK-dependent hepatocyte lipoapoptosis. *Journal of Biological Chemistry* **281**, 12093-12101

12.   Pfaffenbach, K., Gentile, C., Nivala, A., Wang, D., Wei, Y., and Pagliassotti, M. (2010) Linking endoplasmic reticulum stress to cell death in hepatocytes: roles of C/EBP homologous protein and chemical chaperones in palmitate-mediated cell death. *American Journal of Physiology-Endocrinology and Metabolism* **298**, E1027-E1035

13.   Leamy, A. K., Egnatchik, R. A., and Young, J. D. (2013) Molecular mechanisms and the role of saturated fatty acids in the progression of non-alcoholic fatty liver disease. *Progress in lipid research* **52**, 165-174

14.   Listenberger, L., Ory, D., and Schaffer, J. (2001) Palmitate-induced apoptosis can occur through a ceramide-independent pathway. *Journal of Biological Chemistry* **276**, 14890-14895

15.   Wei, Y., Wang, D., Topczewski, F., and Pagliassotti, M. (2006) Saturated fatty acids induce endoplasmic reticulum stress and apoptosis independently of ceramide in liver cells. *American Journal of Physiology-Endocrinology and Metabolism* **291**, E275-E281

16.   Listenberger, L., Han, X., Lewis, S., Cases, S., Farese, R., Ory, D., and Schaffer, J. (2003) Triglyceride accumulation protects against fatty acid-induced lipotoxicity. *Proceedings of the National Academy of Sciences of the United States of America* **100**, 3077-3082

17.   Gao, D., Nong, S., Huang, X., Lu, Y., Zhao, H., Lin, Y., Man, Y., Wang, S., Yang, J., and Li, J. (2010) The effects of palmitate on hepatic insulin resistance are mediated by

NADPH Oxidase 3-derived reactive oxygen species through JNK and p38MAPK pathways. *The Journal of biological chemistry* **285**, 29965-29973

18. Adam-Vizi, V., and Chinopoulos, C. (2006) Bioenergetics and the formation of mitochondrial reactive oxygen species. *Trends in Pharmacological Sciences* **27**, 639-645

19. Brookes, P. S., Yoon, Y. S., Robotham, J. L., Anders, M. W., and Sheu, S. S. (2004) Calcium, ATP, and ROS: a mitochondrial love-hate triangle. *American Journal of Physiology-Cell Physiology* **287**, C817-C833

20. Kamata, H., Honda, S., Maeda, S., Chang, L., Hirata, H., and Karin, M. (2005) Reactive oxygen species promote TNF alpha-induced death and sustained JNK activation by inhibiting MAP kinase phosphatases. *Cell* **120**, 649-661

21. Srivastava, S., and Chan, C. (2007) Hydrogen peroxide and hydroxyl radicals mediate palmitate-induced cytotoxicity to hepatoma cells: Relation to mitochondrial permeability transition. *Free Radical Research* **41**, 38-49

22. Wei, Y., Wang, D., Gentile, C., and Pagliassotti, M. (2009) Reduced endoplasmic reticulum luminal calcium links saturated fatty acid-mediated endoplasmic reticulum stress and cell death in liver cells. *Molecular and Cellular Biochemistry* **331**, 31-40

23. Wiechert, W., Mollney, M., Isermann, N., Wurzel, W., and de Graaf, A. (1999) Bidirectional reaction steps in metabolic networks: III. Explicit solution and analysis of isotopomer labeling systems. *Biotechnology and Bioengineering* **66**, 69-85

24. Antoniewicz, M. R., Kelleher, J. K., and Stephanopoulos, G. (2007) Elementary metabolite units (EMU): A novel framework for modeling isotopic distributions. *Metabolic Engineering* **9**, 68-86

25.   Young, J., Walther, J., Antoniewicz, M., Yon, H., and Stephanopoulos, G. (2008) An Elementary Metabolite Unit (EMU) based method of isotopically nonstationary flux analysis. *Biotechnology and Bioengineering* **99**, 686-699

26.   Antoniewicz, M. R., Kelleher, J. K., and Stephanopoulos, G. (2006) Determination of confidence intervals of metabolic fluxes estimated from stable isotope measurements. *Metab Eng* **8**, 324-337

27.   Srivastava, S., and Chan, C. (2008) Application of metabolic flux analysis to identify the mechanisms of free fatty acid toxicity to human hepatoma cell line. *Biotechnology and Bioengineering* **99**, 399-410

28.   Cook, G. A., and Gamble, M. S. (1987) REGULATION OF CARNITINE PALMITOYLTRANSFERASE BY INSULIN RESULTS IN DECREASED ACTIVITY AND DECREASED APPARENT KI VALUES FOR MALONYL-COA. *Journal of Biological Chemistry* **262**, 2050-2055

29.   Kaushik, V. K., Young, M. E., Dean, D. J., Kurowski, T. G., Saha, A. K., and Ruderman, N. B. (2001) Regulation of fatty acid oxidation and glucose metabolism in rat soleus muscle: effects of AICAR. *American Journal of Physiology-Endocrinology and Metabolism* **281**, E335-E340

30.   Pagliassotti, M., Wei, Y., and Wang, D. (2005) Saturated fatty acids induce cytotoxicity in hepatocytes via effects on the endoplasmic reticulum. *Obesity Research* **13**, A31-A31

31.   Borradaile, N. M., Han, X., Harp, J. D., Gale, S. E., Ory, D. S., and Schaffer, J. E. (2006) Disruption of endoplasmic reticulum structure and integrity in lipotoxic cell death. *Journal of Lipid Research* **47**, 2726-2737

32. Hickson-Bick, D. L. M., Sparagna, G. C., Buja, L. M., and McMillin, J. B. (2002) Palmitate-induced apoptosis in neonatal cardiomyocytes is not dependent on the generation of ROS. *American Journal of Physiology-Heart and Circulatory Physiology* **282**, H656-H664

33. Hawley, S. A., Ross, F. A., Chevtzoff, C., Green, K. A., Evans, A., Fogarty, S., Towler, M. C., Brown, L. J., Ogunbayo, O. A., Evans, A. M., and Hardie, D. G. (2010) Use of Cells Expressing gamma Subunit Variants to Identify Diverse Mechanisms of AMPK Activation. *Cell Metabolism* **11**, 554-565

34. Owen, M. R., Doran, E., and Halestrap, A. P. (2000) Evidence that metformin exerts its anti-diabetic effects through inhibition of complex 1 of the mitochondrial respiratory chain. *Biochemical Journal* **348**, 607-614

35. Kita, Y., Takamura, T., Misu, H., Ota, T., Kurita, S., Takeshita, Y., Uno, M., Matsuzawa-Nagata, N., Kato, K.-i., Ando, H., Fujimura, A., Hayashi, K., Kimura, T., Ni, Y., Otoda, T., Miyamoto, K.-i., Zen, Y., Nakanuma, Y., and Kaneko, S. (2012) Metformin Prevents and Reverses Inflammation in a Non-Diabetic Mouse Model of Nonalcoholic Steatohepatitis. *Plos One* **7**

36. Baumgardner, J. N., Shankar, K., Hennings, L., Albano, E., Badger, T. M., and Ronis, M. J. J. (2008) N-acetylcysteine attenuates progression of liver pathology in a rat model of nonalcoholic steatohepatitis. *Journal of Nutrition* **138**, 1872-1879

37. Sanyal, A. J., Chalasani, N., Kowdley, K. V., McCullough, A., Diehl, A. M., Bass, N. M., Neuschwander-Tetri, B. A., Lavine, J. E., Tonascia, J., Unalp, A., Van Natta, M., Clark, J., Brunt, E. M., Kleiner, D. E., Hoofnagle, J. H., Robuck, P. R., and Nash, C. R. N.

(2010) Pioglitazone, Vitamin E, or Placebo for Nonalcoholic Steatohepatitis. *New England Journal of Medicine* **362**, 1675-1685

38.   Lavine, J. E., Schwimmer, J. B., Van Natta, M. L., Molleston, J. P., Murray, K. F., Rosenthal, P., Abrams, S. H., Scheimann, A. O., Sanyal, A. J., Chalasani, N., Tonascia, J., Uenalp, A., Clark, J. M., Brunt, E. M., Kleiner, D. E., Hoofnagle, J. H., Robuck, P. R., and Nonalcoholic Steatohepatitis, C. (2011) Effect of Vitamin E or Metformin for Treatment of Nonalcoholic Fatty Liver Disease in Children and Adolescents The TONIC Randomized Controlled Trial. *Jama-Journal of the American Medical Association* **305**, 1659-1668

39.   Antoniewicz, M. R., Kraynie, D. F., Laffend, L. A., González-Lergier, J., Kelleher, J. K., and Stephanopoulos, G. (2007) Metabolic flux analysis in a nonstationary system: Fed-batch fermentation of a high yielding strain of E. coli producing 1,3-propanediol. *Metabolic Engineering* **9**, 277-292

40.   Altamirano, C., Illanes, A., Becerra, S., Cairo, J. J., and Godia, F. (2006) Considerations on the lactate consumption by CHO cells in the presence of galactose. *Journal of Biotechnology* **125**, 547-556

41.   Ahn, W. S., and Antoniewicz, M. R. (2013) Parallel labeling experiments with [1,2-13C]glucose and [U-13C]glutamine provide new insights into CHO cell metabolism. *Metabolic Engineering* **15**, 34-47

42.   Wiechert, W., Siefke, C., deGraaf, A. A., and Marx, A. (1997) Bidirectional reaction steps in metabolic networks .2. Flux estimation and statistical analysis. *Biotechnology and Bioengineering* **55**, 118-135

CHAPTER 4

ER CALCIUM RELEASE PROMOTES MITOCHONDRIAL DYSFUNCTION AND
HEPATIC CELL LIPOTOXICITY IN RESPONSE TO PALMITATE OVERLOAD

Abstract

Elevations in palmitate induce hepatic cell dysfunction characterized by enhanced apoptosis, depleted ER calcium stores, oxidative stress, and altered citric acid cycle (CAC) metabolism; however, the mechanism of how this occurs is not well understood. We hypothesize that elevated saturated fatty acids such as palmitate disrupt intracellular calcium homeostasis resulting in a net flux of calcium from the ER to mitochondria, which activates aberrant oxidative metabolism and oxidative stress. We treated primary hepatocytes and H4IIEC3 cells with fatty acids and calcium chelators to identify the roles of intracellular calcium flux in lipotoxicity. We then applied ^{13}C metabolic flux analysis (MFA) to determine the impact of calcium in promoting palmitate-stimulated mitochondrial alterations. We found that elevated palmitate enhanced oxygen consumption and glutamate anaplerosis in hepatic cells. Co-treatment with the calcium-specific chelator BAPTA resulted in a suppression of ROS accumulation, apoptosis markers, and oxygen consumption. Additionally, ^{13}C MFA revealed that BAPTA co-treated cells had reduced CAC fluxes compared to cells treated with palmitate alone. Our results suggest that SFA-induced lipoapoptosis in hepatic cells is dependent on calcium-stimulated mitochondrial activation and ROS accumulation.

Introduction

The obese and steatotic liver is marked by elevated fatty acids, ER stress, and metabolic alterations that give rise to hepatocyte dysfunction (1-5). Non-alcoholic fatty liver disease (NAFLD) is a chronic condition resulting from excess lipid accumulation, which affects up to 30% of the U.S. population and is the leading cause of referrals to hepatology clinics (1,6). Although simple steatosis does not always lead to complications, around 10% of NAFLD patients are at increased risk of developing more serious liver injuries such as nonalcoholic steatohepatitis (NASH) and hepatocellular carcinoma (8). Free fatty acid (FFA) levels are present in higher concentrations in the plasma of these individuals, suggesting that *in vivo* alterations in FFA metabolism are linked to corresponding changes in disease severity (9,10).

Systematic hepatic dysfunction induced by obesity ranges from oxidative stress, dysresgulated metabolism, ER stress, and abnormally elevated apoptosis (11). *In vitro* experiments have demonstrated that saturated fatty acids (SFAs), but not monounsaturated fatty acids (MUFAs), are potent inducers of ER stress, reactive oxygen species (ROS) accumulation, and apoptosis in hepatic cells (5,12-17). However, a mechanistic explanation for the differing lipotoxic effects of SFAs and MUFAs is currently lacking. It has been shown that markers of ER stress such as CHOP/GADD135 formation and depletion of ER calcium stores appear soon after cells are treated with long-chain SFAs, but not MUFAs (18). ER calcium is depleted shortly after SFA exposure, suggesting a mechanism of SFA toxicity that involves rapid disruption of ER homeostasis (19-21). The exact role of this calcium efflux in mediating lipotoxicity is unknown, although intracellular calcium levels impact many critical aspects of cell function. Calcium is integral in two important aspects of cell biology: oxidative metabolism and apoptosis. Calcium ions act as essential cofactors by activating enzymes involved in the citric acid cycle

(CAC), particularly dehydrogenases and transporters involved in the malate-aspartate redox shuttle (22-25). Calcium fluxes also initiate mitochondrial apoptotic pathways. Pro- and anti-apoptotic proteins of the Bax, Bcl, and Bim families have been shown to regulate the net movement of calcium into and out of the mitochondria (26-28).

Altered energy metabolism is an additional characteristic of both human and mouse fatty livers that has been observed in both *in vitro* and *in vivo* studies of lipotoxicity. *In vivo* flux analysis using ^{2}H/^{13}C NMR reported a ~2-fold increase in CAC flux in NAFLD patients compared to patients with normal intrahepatic triglyceride content (29). Complementary studies performed in high-fat diet (HFD) fed mice revealed similar increases in CAC activity that were associated with elevated markers of oxidative stress (30). The authors hypothesized that CAC activation was required to meet energetic demands in the face of reduced respiratory efficiency resulting from mitochondrial oxidative damage. However, prior *in vitro* studies of hepatic cells using ^{13}C metabolic flux analysis (MFA) have shown that FFAs can enhance mitochondrial metabolism independently of beta-oxidation through a mechanism that precedes the onset of oxidative damage (12,31). These studies revealed that palmitate drastically enhanced CAC fluxes relative to glycolytic fluxes in H4IIEC3 cells within 6h of treatment, but this increase in mitochondrial metabolism was largely fueled by increased glutamine oxidation by palmitate-treated cells. Consistent with the *in vivo* mouse studies, these changes in CAC fluxes coincided with enhanced ROS accumulation, suggesting that altered mitochondrial metabolism may be the cause, rather than a consequence, of enhanced oxidative stress observed in obesity and NAFLD. To confirm this, we performed experiments using antioxidants and mitochondrial inhibitors to demonstrate that these mitochondrial alterations were both critical for cellular dysfunction and did not require prior ROS accumulation (31). Although these *in vivo* and *in vitro* studies present

a consistent picture of the metabolic response to hepatic FFA overload, they do not explain the mechanism by which mitochondrial metabolism is activated by palmitate treatment.

Because of the rapid appearance of ER stress markers in response to palmitate treatment, we hypothesized that disruption of ER homeostasis may be the initial insult that is responsible for subsequent changes in mitochondrial function. We hypothesized that elevated levels of the SFA palmitate would compromise the ability of the ER to maintain calcium stores, resulting in net efflux of ER calcium that would enhance CAC flux, stimulate oxidative metabolism and ROS production, and ultimately lead to cellular dysfunction and apoptosis. To test this, we treated primary rat hepatocytes and immortalized H4IIEC3 hepatic cells with lipotoxic doses of palmitate, either with or without the intracellular calcium chelator BAPTA-AM. Palmitate-treated cells exhibited decreased ER calcium, elevated mitochondrial calcium, reduced mitochondrial potential, and enhanced oxygen consumption, all of which preceded the onset of apoptotic cell death. BAPTA co-treatment abrogated these lipotoxic phenotypes. Further ^{13}C MFA experiments revealed that palmitate-treated cells exhibited enhanced CAC flux and increased mitochondrial glutamine metabolism that were associated with ROS accumulation. BAPTA co-treatment also suppressed glutamine-dependent CAC activation and reduced oxidative stress. These results offer a mechanistic explanation for the close association between ER stress and ROS accumulation reported in prior lipotoxicity studies, in which calcium serves as a major linchpin connecting changes in ER homeostasis to the onset of mitochondrial dysfunction.

Materials and Methods

Materials-

The fluorescent dyes 2', 7'-dichlorodihydrofluorescein diacetate (H_2DCFDA), propidium iodide (PI), Fura-2 AM, and JC-1 were purchased from Invitrogen (Carlsbad, CA, USA). The calcium-specific chelator BAPTA-AM was also obtained from Invitrogen. The fatty acids palmitate and oleate, bovine serum albumin (BSA), and low glucose Dulbecco's modified Eagle's medium (DMEM) were purchased from Sigma Aldrich (St. Louis, MO, USA). Primary hepatocytes were cultured on plates coated with Collagen I (Rat Tail) from BD Biosciences (San Jose, CA).

Primary rat hepatocyte isolation-

Primary hepatocytes were isolated from male Sprague-Dawley rats as described previously (32). The portal vein and inferior vena cava of anesthetized animals were cannulated and perfused with 37°C oxygenated perfusion media, pH 7.4, containing 118 mM NaCl, 5.9 mM KCl, 1.2 mM $MgSO_4$, 1.2 mM NaH_2PO_4, 25 mM $NaHCO_3$, 0.2 mM EGTA and 5 mM glucose. After 15 minutes, the liver was excised from the animal and perfused with liver digest medium (Invitrogen, Grand Island NY). Then the cells were dispersed, washed four times, and suspended in attachment media, which consisted of 20 mM glucose DMEM supplemented with 30 mg/L proline, 100 mg/L ornithine, 0.544 mg/L $ZnCl_2$, 0.75 mg/L $ZnSO_4$ $7H_2O$, 0.2 mg/L $CuSO_4$ $5H_2O$, 0.25 mg/L $MnSO_4$, 2 g/L bovine serum albumin (Sigma), 5 nM insulin, 100 nM dexamethasone, 100,000 U penicillin, 100,000 U streptomycin, and 2 mM glutamine. After four hours of incubation in the attachment media, the primary hepatocytes were switched to a

maintenance media identical to the attachment media except it had a concentration of 1 nM (instead of 5 nM) insulin.

H4IIEC3 cell culture-

The H4IIEC3 rat hepatoma cell line was purchased from ATCC (American Type Culture Collection, Manassas, VA, USA). The cells were cultured in 5 mM glucose DMEM supplemented with 2 mM glutamine, 10% FBS, and 1% penicillin/streptomycin antibiotic solution.

Fatty acid preparation-

FFA stock solutions were prepared by coupling free fatty acids with BSA. First, palmitate or oleate was dissolved in pure ethanol at a concentration of 195 mM so that the final concentration of ethanol in our FFA stock solutions did not exceed 1.5% by volume. This solution was then added to a prewarmed 10% w/w BSA solution (37℃) to achieve a final FFA concentration of 3 mM, and this solution was allowed to incubate in a water bath for an additional 10 minutes. The final ratio of FFA to BSA was 2:1. All vehicle treatments were prepared using stocks of 10% w/w BSA with an equivalent volume of ethanol added to match the concentration in FFA stocks. The final concentration of ethanol in all experimental treatments was less than 0.2% by volume.

ROS accumulation-

Levels of intracellular ROS were assessed using the radical-sensitive dye H_2DCFDA, which is oxidized to the fluorescent 2, 7-dicholorofluorescein (DCF) upon exposure to ROS.

Following treatment with indicated reagents, the cells were washed with Hank's Balanced Saline Solution (HBSS) twice. Dye was added at a concentration of 10 μM H₂DCFDA and incubated for one hour at 37ºC in darkness. Fluorescence was measured using the excitation/emission wavelengths 485/530 nm with a Biotek FL600 microplate reader.

Toxicity assays-

Propidium iodide (PI), an intercalating dye, was used to measure cell death induced by elevated fatty acids using excitation and emission wavelengths of 530 nm and 645 nm. Fluorescence was measured using the Biotek FL600 microplate reader.

Apoptosis measurements-

To monitor cellular apoptosis as a function of caspase 3 and 7 activities, we utilized the commercial Apo-ONE Homogenous Caspase 3/7 Assay kit that combines a lysis buffer with Z-DEVD-R110, a caspase-3/7 specific substrate. Upon exposure to active caspases, the DEVD peptide is cleaved and the molecule becomes fluorescent (ex/em, 485/530 nm).

Oxygen consumption flux-

To determine overall mitochondrial activity, we measured the direct oxygen uptake flux of cells treated with fatty acids, vehicle, or inhibitors using the Oroboros Oxygraph-2K. This instrument uses two separate chambers with individual oxygen probes to detect real-time changes in media oxygen concentration at a constant temperature of 32ºC and stirring speed of 750 rpm. Briefly, H4IIEC3 hepatic cells were cultured on 10-cm dishes until 90% confluent. Cells were then treated with designated fatty acids or inhibitors for 3 hours, trypsinized, counted,

and then re-suspended in the same media for uptake measurements. Two million cells were placed in the Oroboros chamber to measure oxygen consumption.

Mitochondrial potential-

JC-1 is a dye which exists in a monomeric form in non-polarized mitochondria and fluoresces in the green (em: 530) spectrum when excited at 485 nm. The dye accumulates in the mitochondria based upon the potential. This accumulation is accompanied by formation of dye aggregates shifting the fluorescence to the red (em: 590 nm) spectrum when excited at 485 nm. Therefore red/green ratio indicates alterations in the mitochondrial potential between different cells and treatments.

ER calcium release assays-

To measure ER calcium levels, H4IIEC3 cells were loaded with the ratiometric, cytosolic calcium dye Fura-2 AM following a method developed for pancreatic islets (33). Cells were cultured at 500,000 cells per dish on Mattek imaging dishes, loaded with 3 μM Fura-2 for 30 minutes, washed three times, and then perfused with imaging buffer containing 119 mM NaCl, 25 mM HEPES, 4.7 mM KCl, 2.5 mM CaCl2.[(H2O)6], 1.2 mM $MgSO_4$, 1.2 mM KH_2PO_4. Fura-2 fluorescence imaging was performed using a Nikon TE2000-U microscope at excitations of 340 and 380 nm every 5 seconds. Once a baseline was established, 1 μM thapsigargin was perfused across the dish to prevent ER calcium reuptake, and fluorescence was measured every 5 seconds. The data shown are expressed in normalized fluorescence units with excitation at 340/380 nm for 5 individual plates with 30-50 cells analyzed per plate.

Mitochondrial calcium-

The mitochondrial calcium indicator Rhod-2, AM (Invitrogen) was used to assess mitochondrial calcium in H4IIEC3 cells. Cells were pre-treated with indicated treatments and then loaded with 10 μM Rhod-2. Cells were loaded with the dye for one hour, washed three times, and given fresh DMEM. Fluorescence was measured at ex/em of 552/581 using a Biotek Synergy plate reader.

Polar metabolite extraction and GC-MS analysis of ^{13}C enrichment-

Intracellular metabolites from H4IIEC3 rat hepatomas were extracted as previously described (12). To quench cell metabolism, 1 mL of -80°C methanol was added to cells cultured on 10-cm dishes. Cells were scraped and placed into a separate tube containing water and chloroform, centrifuged, and the polar phase was collected and dried for GC-MS analysis. The *tert*-butylsilyl derivatives of the polar metabolites were generated by incubating with MBTSTFA + 1% TBDMCS (Pierce). ^{13}C isotopic enrichment of the derivatized sample was analyzed using an Agilent 6890N/5975B GC-MS equipped with a 30m DB-35ms capillary column.

Metabolic flux analysis-

^{13}C MFA was performed using the INCA software package (34) and a previously developed model of hepatic metabolism comprising glycolysis, CAC, and anaplerotic pathways (31). Our experiments involved replacing the unlabeled glutamine in normal DMEM with a [U-$^{13}C_5$]glutamine isotope tracer. When consumed by cells in culture, this tracer gives rise to unique ^{13}C enrichment patterns in downstream metabolites that depend on the atom rearrangements that occur within intervening metabolic pathways. These enrichment patterns

95

provide quantitative information on the relative fluxes through intracellular metabolic pathways. By minimizing the lack-of-fit between experimentally measured mass isotopomer abundances and computationally simulated mass isotopomer distributions, the INCA program can be used to calculate metabolic flux maps associated with each of our chosen treatments (35,36). Fluxes were estimated a minimum of 50 times starting from random initial values to identify a global best-fit solution. Once this solution was achieved, a chi-square test was used to assess the goodness-of-fit. Additionally, 95% confidence intervals were calculated for all estimated parameters by assessing the sensitivity of the sum-of-squared residuals to parameter variations (37). Comprehensive ^{13}C MFA results and a detailed description of our network model are available in the Appendix.

Statistical Analysis-

Analysis of variance (Model I ANOVA) and Tukey-Kramer methods for multiple comparisons, along with Student's t-test for pair-wise comparisons, were utilized to determine statistical significance amongst the experimental data. Results are presented as +/- one standard error of the mean (SEM) unless otherwise indicated.

Results

Elevated concentrations of palmitate, but not oleate, induce cell death marked by loss of mitochondrial potential and apoptosis in hepatic cells

Primary rat hepatocytes treated with elevated concentrations of the SFA palmitate exhibit cell death in a dose-dependent manner as indicated by increasing PI fluorescence (Figures 1A). Elevated doses of the MUFA oleate had no effect on cell viability in primary hepatocytes. Based

on these results and previously published studies, we chose 400 μM palmitate as the lipotoxic concentration used in all further experiments (12). Similar to primary rat hepatocytes, H4IIEC3 rat hepatoma cells also exhibited increased cell death after 24 hours of palmitate treatment (Figure 4.1A). Additionally, primary hepatocyte and H4IIEC3 cells exhibited elevated caspase activity following 12 hours of palmitate treatment, while oleate did not induce markers of apoptosis (Figure 4.1B). While both primary hepatocytes and H4IIEC3 cells exhibited significantly increased apoptosis in response to elevated palmitate, the effects were both more rapid and more pronounced in H4IIEC3 cells.

To determine if palmitate lipotoxicity was associated with loss of mitochondrial potential, primary rat hepatocytes and H4IIEC3 cells were incubated with FFA treatments for 6 hours followed by staining with the mitochondrial potential dye JC-1. Both primary hepatocytes and H4IIEC3 cells exhibited decreased mitochondrial potential after 6 hours of palmitate treatment (Figure 4.1C). While elevated palmitate decreased the mitochondrial potential of both cell types, the effect was more significant in hepatoma cells. Taken together, we posit that H4IIEC3 cells provide a representative model of hepatocyte response to FFA overload in the context of NAFLD and NASH, because they recapitulate all of the qualitative features of lipotoxicity observed in primary rat hepatoctyes while exhibiting enhanced sensitivity to acute palmitate treatments.

97
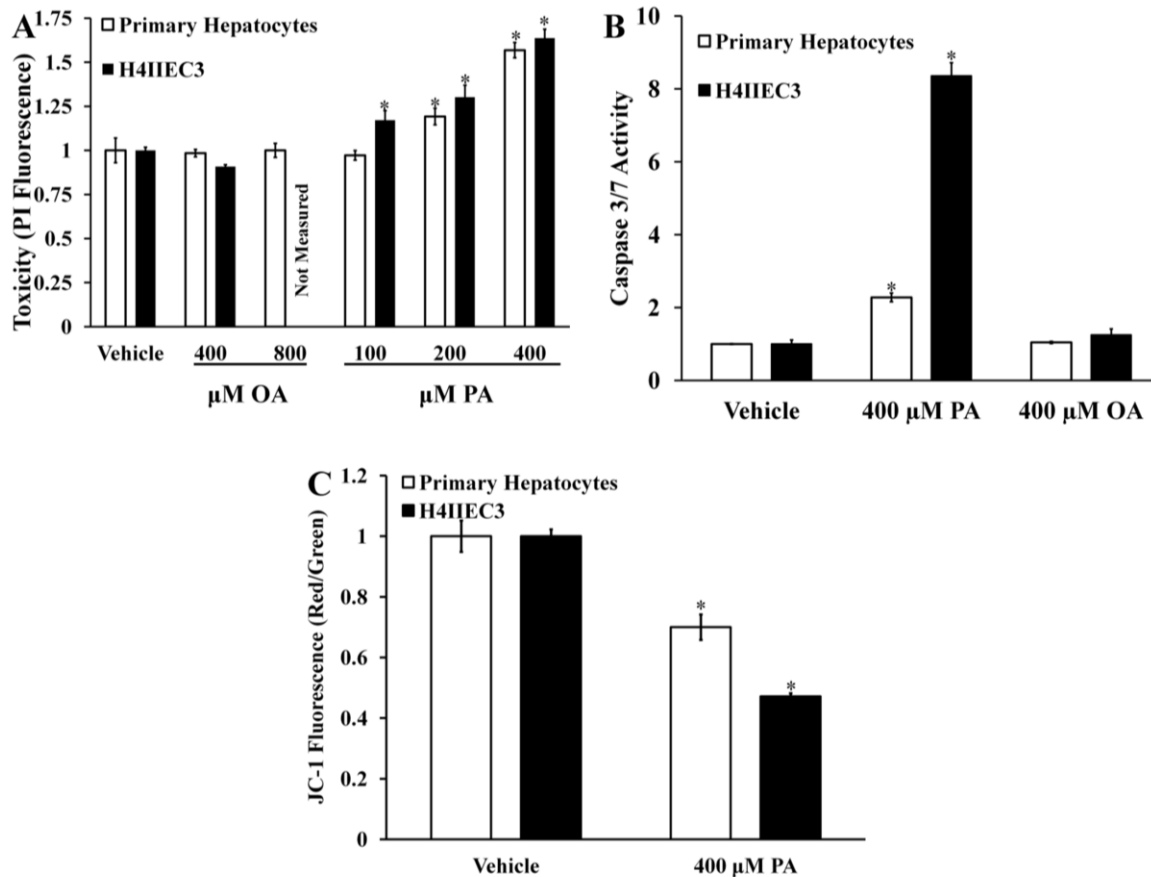
Figure 4.1: Elevated doses of palmitate, but not oleate, induce lipotoxicity in primary rat hepatocytes and H4IIEC3 hepatic cells. Cells were incubated with increasing doses of palmitate (PA) or oleate (OA), followed by measurements of cell death and mitochondrial potential. (A) Cell death measured by PI fluorescence for primary hepatocytes and H4IIEC3 cells treated with increasing doses of palmitate or oleate for 24 hours. (B) 12-hour caspase activity measured for primary hepatocytes and H4IIEC3 hepatic cells treated with 400 μM palmitate. (C) JC-1 fluorescence for primary hepatocytes and H4IIEC3 hepatic cells treated with vehicle (BSA) or 400 μM palmitate (PA) for 6 hours. JC-1 fluorescence is depicted as the ratio between red and green fluorescent signals. Data represent mean +/- S.E., n=8; *, different from vehicle, $p < .05$. All fatty acid treatments are normalized to equal volume vehicle (BSA) controls.

Palmitate lipotoxicity is marked by a redistribution of intracellular calcium

Previous studies have observed reduced ER calcium stores and increased markers of ER stress following palmitate treatment in primary rat hepatocytes and CHO cells (38,39). To test if our lipotoxicity model exhibits the same decrease in ER luminal calcium, we assessed the

relative levels of ER calcium in H4IIEC3 cells treated with 400 μM palmitate for 6 hours. Compared to vehicle treatment, cells treated with palmitate exhibited a smaller fold change in Fura-2 fluorescence following thapsigargin treatment, indicating depleted ER calcium stores (Figure 4.2A). Additionally, we calculated the area under the curve (AUC) from the point of initial thapsigargin treatment to the peak of Fura-2 fluorescence to estimate the relative difference in total ER calcium release between vehicle- and palmitate-treated H4IIEC3 cells (Figure 4.2B). H4IIEC3 cells treated with 400 μM palmitate had a decreased AUC, confirming that total luminal calcium was diminished by palmitate treatment. Next, we sought to determine if decreased ER calcium was associated with increased mitochondrial calcium. After 6 hours of treatment with 400 μM palmitate, H4IIEC3 cells were incubated with the mitochondrial calcium indicator Rhod-2 AM. Palmitate-treated cells exhibited an approximate 50% increase in Rhod-2 fluorescence, indicating elevated mitochondrial calcium levels (Figure 4.2C).
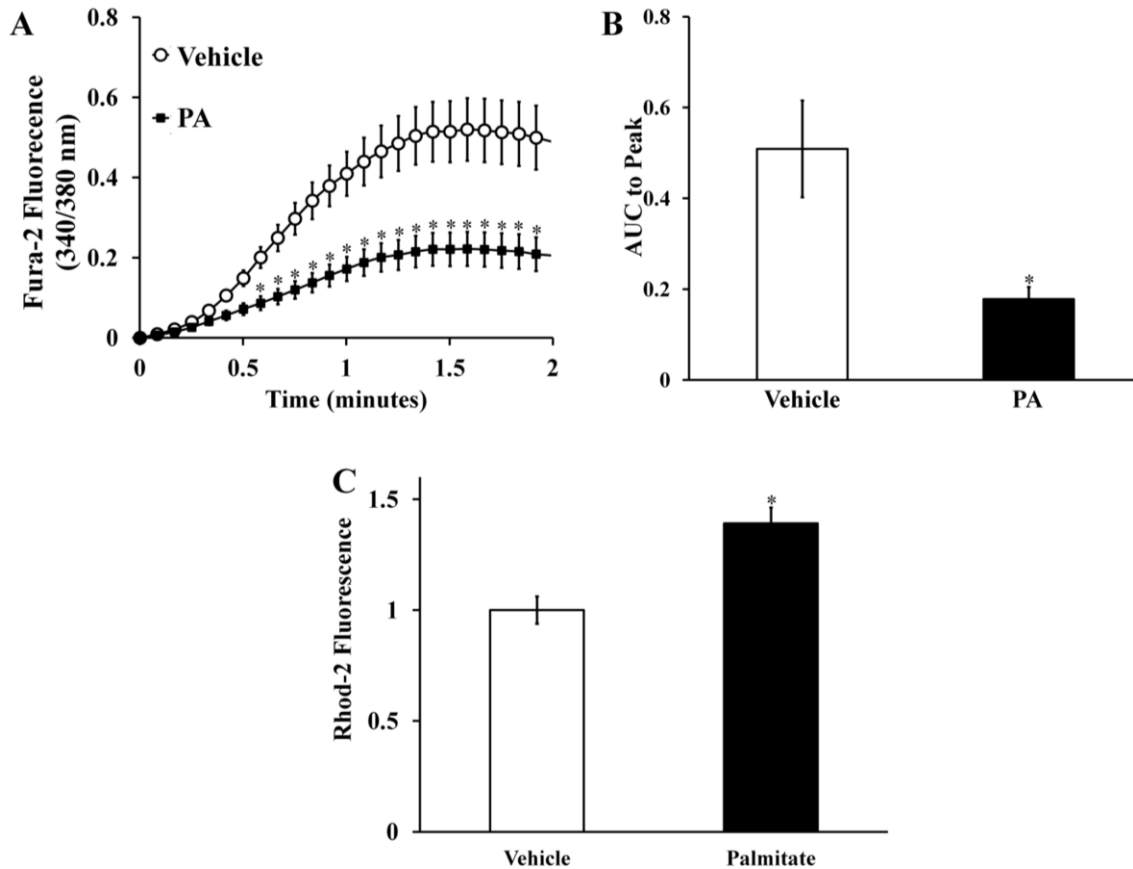
Figure 4.2: Lipotoxic palmitate redistributes intracellular calcium. (A) To assess ER calcium, H4IIEC3 hepatic cells pre-treated with vehicle (BSA) or 400 µM palmitate (PA) for 6 hours were then perfused with thapsigargin (1 µM) while changes in cystolic Fura-2 fluorescence were recorded. (B) Calculated area under curve (AUC) to peak fluorescence was used to quantify relative calcium load released by ER. (C) Relative mitochondrial calcium levels assessed by Rhod-2 fluorescence for H4IIEC3 hepatic cells treated with vehicle (BSA) or 400 µM palmitate (PA) for 6 hours. Data represent mean +/- S.E., n=5 plates with 25-30 cells per plate for thapsigargin assays, n=6 for Rhod-2 measurements; * different from vehicle, p <.05.

ER calcium release promotes ROS overproduction, enhanced oxygen consumption, and apoptosis in response to a palmitate load

To test whether these other lipotoxic phenotypes were dependent on the observed ER-to-mitochondrial calcium translocation, the cell-permeable calcium chelator BAPTA-AM was administered to H4IIEC3 cells in both the presence and absence of palmitate treatments. Primary hepatocytes and H4IIEC3 hepatic cells co-treated with 40 µM BAPTA and 400 µM

palmitate exhibited decreased apoptotic markers relative to cells treated with palmitate alone (Figure 4.3A). The ability of BAPTA to reduce lipotoxic cell death was in agreement with previous reports (38).While palmitate treatment was characterized by ROS accumulation, reduction in mitochondrial potential, and enhanced oxygen uptake by H4IIEC3 cells, BAPTA co-treatment suppressed all of these palmitate-induced metabolic phenotypes (Figure 4.3B, C, D). To confirm that BAPTA was rescuing cells by chelating intracellular calcium, cells were also treated with the calcium chelator EGTA. Similar reductions in lipotoxicity as assessed by PI fluorescence were observed in cells co-treated with palmitate and EGTA (data not shown).
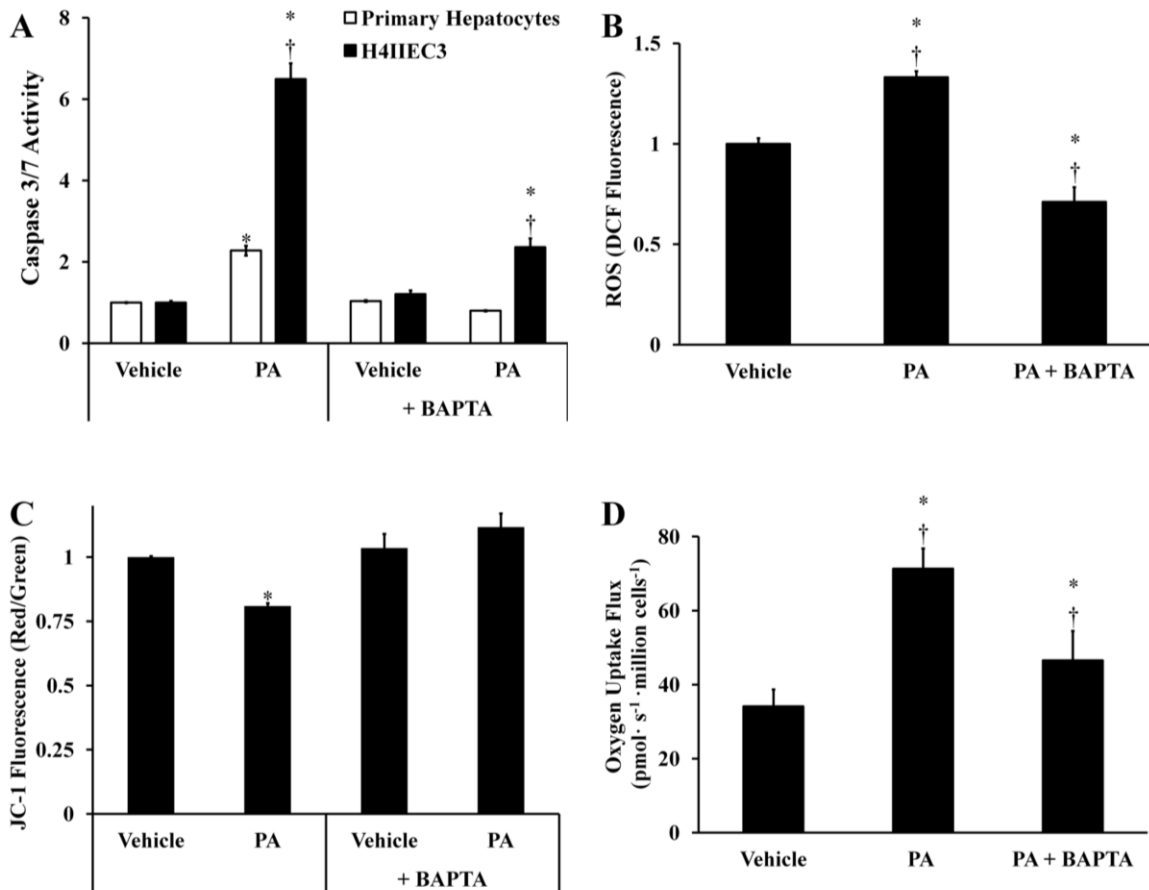
Figure 4.3: Co-treatment with the intracellular calcium chelator BAPTA-AM reduces the lipotoxic effects of palmitate. Hepatic cells were treated with either vehicle (BSA) or 400 μM palmitate (PA) in the presence or absence of 40 μM BAPTA to examine the role of redistributed calcium stores on apoptosis, ROS accumulation, and mitochondrial metabolism. (A) Caspase 3/7 activity was measured at 12 hours to assess the effect of BAPTA treatment on apoptosis in both primary hepatocytes and H4IIEC3 cells. (B) ROS levels at 6 hours were measured by DCF fluorescence in H4IIEC3 cells. (C) Mitochondrial membrane potential at 6 hours was assessed by JC-1 fluorescence in H4IIEC3 cells. (D) Oxygen uptake measurements of BAPTA- and/or PA-treated H4IIEC3 cells. Data represent mean +/- S.E., n=4 for DCF, n=3 for oxygen uptake measurements, n=8 for JC-1, caspase activity, and toxicity assays; * different from vehicle, $p < .05$; † different from each other, $p < .05$.

^{13}C flux analysis demonstrates that chelation of intracellular calcium reverses metabolic alterations associated with lipotoxicity

Hepatic cells treated with palmitate exhibit an altered metabolic phenotype marked by

elevated CAC flux, enhanced glutamine metabolism, and increased oxygen consumption (31).

Prior work in our lab has shown that these changes are the primary cause of subsequent ROS accumulation and apoptosis in H4IIEC3 cells, and are not simply byproducts of the apoptosis cascade (31). To examine how BAPTA affects intracellular metabolism, we performed experiments by replacing unlabeled glutamine in DMEM with the stable isotope tracer [U-$^{13}C_5$]glutamine. First, we examined the ^{13}C atom percent enrichment (APE) of several intermediate metabolites. The APE values indicate the fractional contribution of exogenous glutamine to the biosynthesis of these intermediates, relative to other unlabeled sources of carbon (e.g., glucose). GC-MS analysis of intracellular malate and glutamate extracted from palmitate-treated H4IIEC3 cells revealed that their APEs approached 60% and 75%, respectively, compared to 30% and 55% for vehicle-treated cells (Figure 4.4). BAPTA co-treatment reduced the isotopic enrichment of these metabolites back to vehicle-treated levels. These results demonstrate that (a) palmitate lipotoxicity is characterized by increased glutamine conversion to glutamate and subsequent entry of glutamate carbon to the CAC, relative to unlabeled carbon sources and (b) stimulation of this anaplerotic pathway is calcium-dependent.
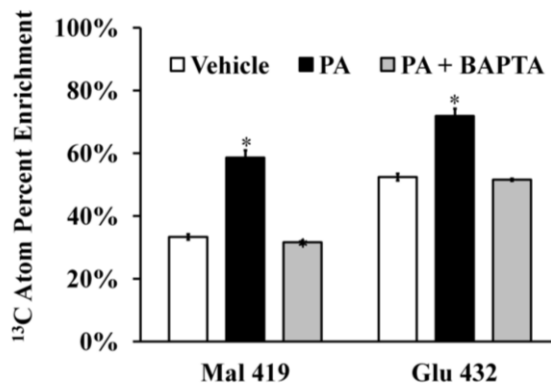
Figure 4.4: Isotopic enrichment of mitochondrial metabolites. H4IICE3 hepatic cells were incubated with [U-^{13}C$_5$]glutamine and treated with vehicle (BSA), palmitate (PA), or PA + BAPTA for 6 hours. Intracellular metabolism was then quenched and metabolites were analyzed using GC-MS. The resulting mass isotopomer distributions were corrected for natural isotope abundance using the method of Fernandez et al. (7). The atom percent enrichment (APE) of cells was calculated using the formula $APE = 100\% \times \sum\limits_{i=0}^{N} \frac{Mi \times i}{N}$, where N is the number of carbon atoms in the metabolite and Mi is the fractional abundance of the ith mass isotopomer. APE represents the fractional incorporation of ^{13}C from the labeled isotope tracer (i.e., glutamine) to the measured metabolite fragment ion. The fragment ion Mal 419 contains all four malate carbons. The fragment ion Glu 432 contains all five glutamate carbons. Data represent mean +/- S.E., n=3; * different from vehicle, p <.05.

By combining ^{13}C mass isotopomer measurements of malate, lactate, glutamate, and aspartate fragment ions derived from GC-MS with measured rates of oxygen consumption, we applied ^{13}C MFA to calculate 12 metabolic fluxes (Figure 4.5) and their associated 95% confidence intervals for vehicle-treated, palmitate-treated, and palmitate + BAPTA co-treated H4IIEC3 cells. Hepatic cells fed 400 μM palmitate were characterized by higher rates of glutamine uptake (Figure 4.6A), alpha-ketoglutarate dehydrogenase flux (Figure 4.6C), citrate synthase flux (Figure 4.6D), and malic enzyme flux (Figure 4.6E) in comparison to vehicle-treated control cells. BAPTA co-treatment led to reductions in the estimated alpha-ketoglutarate, malic enzyme, and glutaminase fluxes. On the other hand, similar measurements of pyruvate

carboxylase (Figure 4.6F) flux across all treatments suggest that this mode of anaplerosis was not sensitive to palmitate or BAPTA exposure. Rather, the increases in CAC flux and its suppression by BAPTA appear to be glutamine-dependent.

Our experiments were performed under physiological glucose concentrations and in the absence of glucagon or other hormones that stimulate gluconeogenesis. Therefore, cells exhibited glycolytic metabolism with net conversion of glucose to pyruvate. The ^{13}C MFA calculations allowed us to determine the difference between pyruvate production by glycolysis and its consumption to form lactate, which we denote as 'net glycolysis' (Figure 4.6B). We found that palmitate-treated H4IIEC3 cells were characterized by a negative net glycolytic rate, indicating that excess anaplerotic carbon was exported from the CAC and was excreted as lactate. On the other hand, BAPTA supplementation reverted palmitate-treated cells back to a positive net glycolytic phenotype, similar to that exhibited by vehicle-treated cells, thus demonstrating a suppression of palmitate-induced glutamate anaplerosis by BAPTA.
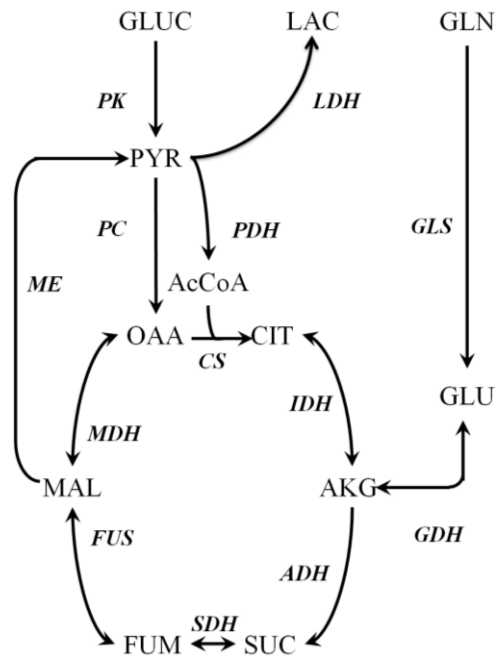
Figure 4.5: Metabolic network used for ^{13}C MFA. Presented is the network model used for MFA. Oxygen consumption was also included in calculations.
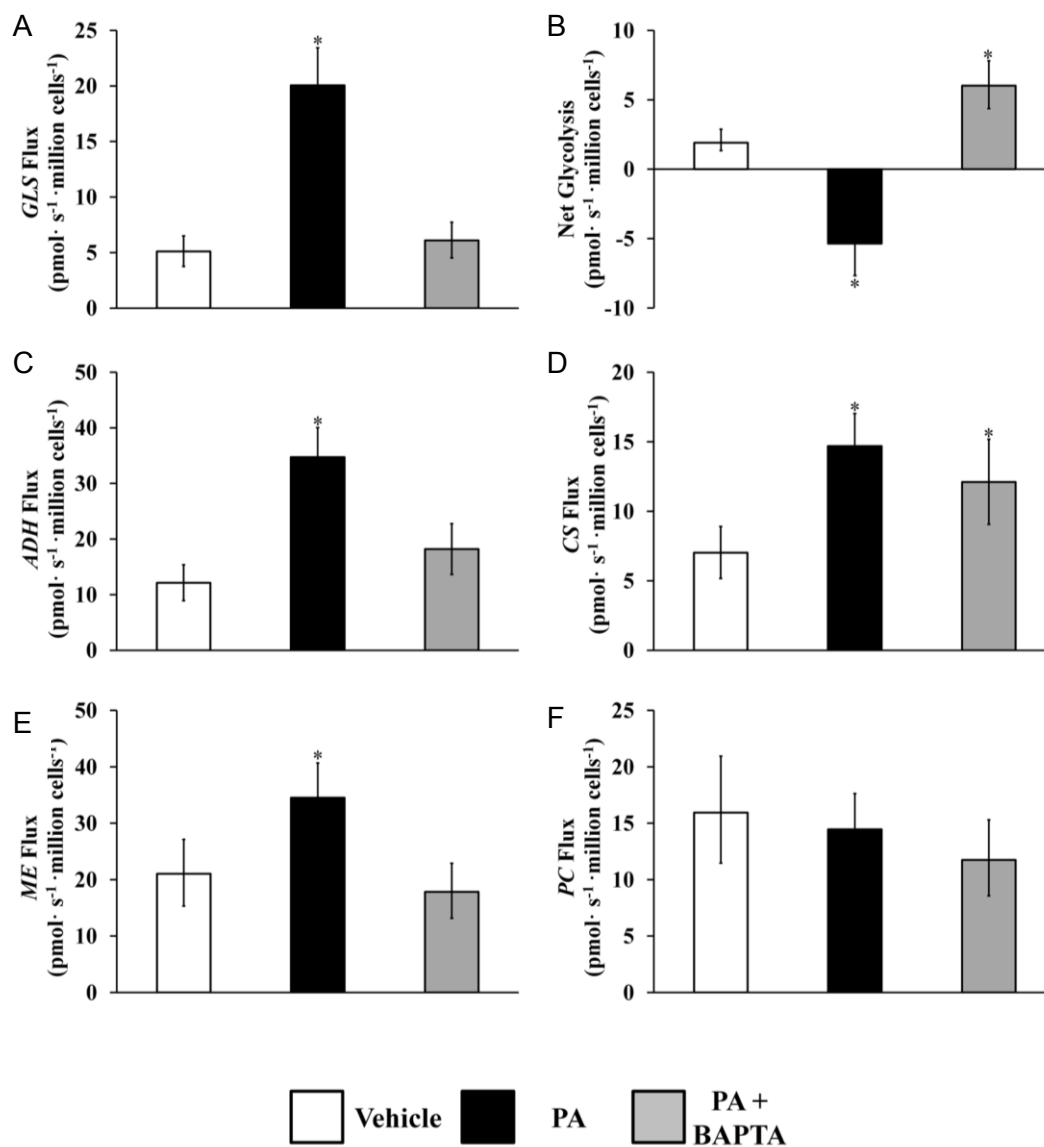
Figure 4.6: ^{13}C flux analysis of mitochondrial metabolism. We performed ^{13}C MFA as detailed in the Methods and the Appendix. Intracellular CAC and anaplerotic fluxes were calculated for H4IIEC3 cells treated with vehicle (BSA), palmitate (PA), or PA + BAPTA. Calculated fluxes for (A) glutamine uptake, (B) 'Net glycolysis' defined as the difference between lactate secretion and glycolytic pyruvate production, (C) alpha-ketoglutarate dehydrogenase, (D) citrate synthase, (E) malic enzyme, and (F) pyruvate carboxylase. Abbreviations: ADH, alpha-ketoglutarate dehydrogenase; CS, citrate synthase; GLN, glutamine uptake; ME, malic enzyme; PC, pyruvate carboxylase. Error bars indicate 95% confidence intervals; * different from vehicle, p <.05.

Discussion

Oxidative stress, ER stress, and elevated CAC flux in the liver are characteristics of obesity, NAFLD/NASH, and hepatic lipotoxicity (3,4,12,18,40). In the current study, we demonstrate that lipotoxic concentrations of the SFA palmitate are associated with the net redistribution of intracellular calcium from the ER to the mitochondria. Our results demonstrate that blocking this calcium translocation can reverse several markers of lipotoxicity in primary rat hepatocytes and H4IIEC3 cells. Experiments co-treating hepatic cells with palmitate plus the calcium chelator BAPTA were able to partially rescue cell death while reducing ROS accumulation and caspase activation. Furthermore, our novel ^{13}C MFA studies revealed that BAPTA prevented the acceleration of CAC metabolism and glutamate anaplerosis associated with palmitate treatment. Our results suggest that altered ER calcium homeostasis provides a critical link between ER stress, ROS accumulation, and altered metabolic phenotypes that contribute to palmitate lipotoxicity.

Perturbed ER homeostasis is one hypothesized initiator of cellular lipotoxicity (1). Features of ER impairment in these models include activation of the unfolded protein response (UPR) and decreased ER calcium stores. However, the role of these ER stress markers in mediating other aspects of lipotoxicity has been unclear. For example, CHOP is a pro-apoptotic protein that is expressed during prolonged periods of UPR. While CHOP is upregulated in response to lipotoxic loads of palmitate, siRNA silencing of CHOP does not prevent apoptosis in H4IIEC3 cells (18). Additionally, primary hepatocytes from *Chop -/-* mice exhibited no resistance to elevated palmitate concentrations *in vitro*. These results confirm that palmitate alters ER function, but do not fully define how ER stress contributes to apoptosis and mitochondrial dysfunction in palmitate-treated hepatic cells. Therefore, CHOP expression is

effectively a marker of lipotoxicity but is not required for apoptosis. Although the literature implies that alternate products of ER stress signaling may mediate lipotoxicity, these intermediates have not been previously identified.

Like CHOP expression, ER calcium homeostasis is perturbed in obesity and lipotoxic conditions in both hepatic and non-hepatic cells (1,20,38). Our use of calcium chelators demonstrates that calcium signaling is critical for palmitate-induced apoptosis, in agreement with previous reports (38). However, these previous studies did not provide a possible mechanism for how ER calcium release can stimulate apoptosis or promote other markers of lipotoxicity such as oxidative stress or mitochondrial dysfunction. While calcium is a known contributor to the intrinsic apoptotic pathway (26), our experiments demonstrate a unique, direct connection between ER stress and metabolic derangements associated with palmitate lipotoxicity. Our prior work has shown that these metabolic alterations persist even when ROS accumulation and apoptosis are inhibited by antioxidant co-treatments (31), thus implying that they are not simply a byproduct of apoptotic signaling but instead function to promote lipotoxicity. In the current study, we were able to prevent palmitate-induced activation of CAC flux by quenching cytosolic calcium levels with BAPTA co-treatment. Consistent with our prior studies, this normalization of mitochondrial fluxes was associated with reductions in ROS accumulation and caspase activity. Our data therefore demonstrates that alterations in ER calcium storage and trafficking may be an initiating event that causally precedes several downstream aspects of hepatocyte lipotoxicity.

Normally, ER calcium is maintained by sarcoendoplasmic reticulum calcium ATPase (SERCA), which functions to pump calcium into the ER lumen from the cytosol. The activity of the SERCA pump is known to be impaired in the obese liver (1) and cholesterol-loaded

macrophages (41). Under normal physiological conditions, the ER membrane is highly fluid due to a low ratio of free cholesterol to phospholipids. Increasing the saturation of ER membranes or perturbing the phosphatidylcholine/phosphatidylethanolamine (PC/PE) ratio has been shown to effectively limit the ability of the SERCA pump to buffer cytosolic calcium. In fact, overexpressing SERCA *in vivo* is enough to reduce liver ER stress in obese mice, demonstrating that SERCA function is critical to the activation of ER stress in obesity (1). We hypothesize that saturated fatty acids may be preferentially incorporated into the ER phospholipid membrane and thereby disrupt SERCA function by increasing the membrane saturation. This may, in turn, lead to a net efflux of ER calcium that subsequently translocates to the mitochondria. As shown by the present study, this ER-to-mitochondrial calcium flux is responsible for promoting several downstream markers of palmitate lipotoxicity, including ROS accumulation, elevated CAC flux, glutamate anaplerosis, and caspase activation (Figure 4.7).
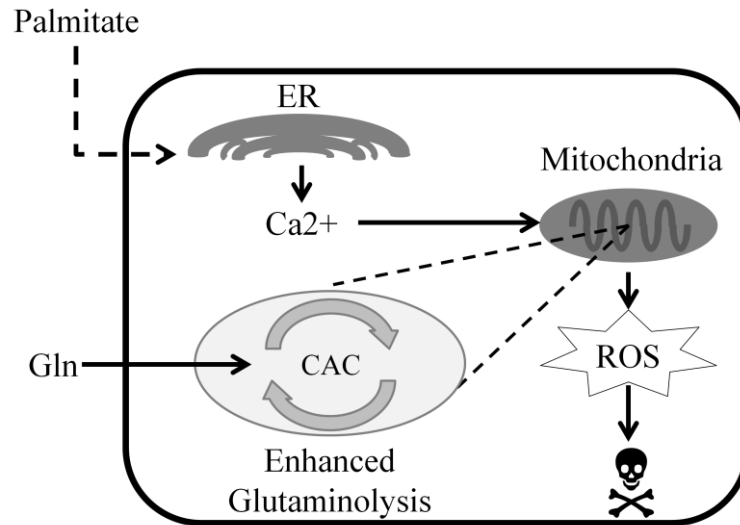
Figure 4.7: Hypothetical mechanism of palmitate lipotoxicity. Our results demonstrate that lipotoxic concentrations of the saturated fatty acid palmitate alter ER calcium stores and induce mitochondrial dysfunction characterized by elevated glutamine consumption, CAC flux, oxygen consumption, and ROS accumulation. We propose that calcium efflux from ER directly stimulates these altered mitochondrial phenotypes leading to apoptosis. Co-treating hepatic cells with the calcium chelator BAPTA both suppresses PA-induced apoptosis and the associated metabolic disorders, supporting our hypothesis.

Although it has been shown that low doses of palmitate (100 μM) impair ER calcium through a possible ROS dependent mechanism (42), our previous studies demonstrated that the addition of antioxidants do not affect palmitate-induced metabolic dysfunction (31). Combined with our current study, our antioxidant experiments indicate that transient increases in cytosolic calcium stimulate mitochondrial ROS accumulation. Transient increases in cytosolic calcium due to ER release can directly impact mitochondrial metabolism through two mechanisms, both of which may explain the observed increases in glutamine and O_2 consumption by palmitate-treated cells. After uptake through the mitochondrial calcium uniporter, calcium can directly affect the enzymatic activities of pyruvate dehydrogenase (PDH), isocitrate dehydrogenase (IDH), and alpha-ketoglutarate dehydrogenase (ADH). In the case of ADH, calcium increases

the enzyme's affinity for its substrate alpha-ketoglutarate (aKG), thus driving the reaction in the forward direction. Activation of ADH may therefore deplete mitochondrial aKG levels and promote increased anaplerosis from glutamate. Our measurement of increased mitochondrial calcium in palmitate-treated H4IIEC3 cells supports this potential mechanism.

Alternatively, calcium can amplify O_2 consumption without being taken up by the uniporter. Gellerich et al. (24) inhibited mitochondrial calcium uptake in isolated mitochondria and still observed changes in mitochondrial oxygen consumption that were sensitive to extramitochondrial calcium levels. Interestingly, this phenotype is also associated with increased glutamate metabolism. Calcium can alter the malate-aspartate shuttle by enhancing the activity of the glutamate/aspartate antiporter encoded by *SLC25A13* and *SLC25A12*. These are given the common names of citrin (for liver) and aralar (for most other cells). The malate-aspartate shuttle functions to transport reducing equivalents (e.g., derived from cytosolic NADH) into the mitochondria. It has been shown that the respiration rate of isolated brain mitochondria can be affected solely by calcium and glutamate levels. Elevated cytosolic levels of calcium could therefore impact mitochondrial metabolic activity by enhancing the capacity of the malate-aspartate shuttle to transport reducing equivalents into the mitochondria, which could result in increased O_2 consumption.

Our ^{13}C MFA studies revealed that calcium directly stimulates metabolic alterations, in particular to CAC and associated anaplerotic pathways, in the context of palmitate lipotoxicity. The results indicate that lipotoxic treatments were marked by enhanced oxidative metabolism, which could be abrogated by BAPTA co-treatment. This reduction in CAC flux was dependent on the potential ability of BAPTA to modify glutamate anaplerosis as revealed by the reduction in the ^{13}C enrichment of intracellular glutamate and malate of cells fed [U-$^{13}C_5$]glutamine.

Similarly, Noguchi et al. (12) found that glutamate supplementation enhanced palmitate-induced ROS accumulation and apoptosis in palmitate-treated H4IIEC3 cells, and that its effect was strongest of all single amino acids tested. Combined with our current observation that BAPTA co-treatment suppresses glutamine conversion to glutamate and the subsequent entry of glutamate carbon into the CAC, this finding suggests that upregulation of calcium-stimulated glutamine metabolism is a critical arm of hepatic lipotoxicity.

Understanding the potential downstream effects of ER stress activation in the context of obesity is important to design potential therapies to prevent the progression of NAFLD toward NASH and other severe liver disorders. Because of the rapid appearance of ER stress markers in response to palmitate treatment, we hypothesized that disruption of ER homeostasis may be the initial insult that is responsible for subsequent changes in mitochondrial function. Our experiments outline a novel role for intracellular calcium transport in mediating hepatocyte lipotoxicity. Our cell imaging and ^{13}C MFA results demonstrate that net efflux of ER calcium activates mitochondrial metabolism, thus complementing the findings of Wei et al. (38) that show ER stress playing a central role in palmitate lipotoxicity. For the first time, we show that BAPTA improves hepatic cell viability and reduces caspase activation through the suppression of mitochondrial metabolism and ROS accumulation in the context of a lipotoxic fatty acid load. Specifically, BAPTA co-treatment blunted both ROS accumulation and caspase activation at 6- and 12-hour time points. Our unique ^{13}C MFA approach demonstrates that BAPTA suppresses these lipotoxic phenotypes by preventing palmitate-stimulated mitochondrial dysfunction involving enhanced glutamine-fueled CAC flux. Clearly, BAPTA co-treatment is capable of significantly changing and delaying the normal sequence of events in the mechanism of palmitate lipotoxicity. Our data provides a novel mechanism connecting elevated palmitate, ER

calcium stores, and dysregulated mitochondrial metabolism implicating a role for impaired SERCA function and calcium signaling in lipotoxic oxidative stress.

Appendix

Metabolic Flux Analysis (MFA) reaction network and modeling assumptions

To calculate the intracellular fluxes in the reaction network listed in Table A1 using the metabolites in Table A2, we made the following assumptions:

1) All measurements were performed at isotopic steady state.

2) Labeled CO_2 produced in the CAC was not reincorporated into central metabolism.

3) Metabolite usage for biomass synthesis was minor due to the short experimental time and slow growth of the cells.

4) Due to excess lipid and minimal cell growth, ATP citrate lyase activity was assumed to be negligible.

5) Beta-oxidation of palmitate was not considered due to our previous finding that beta-oxidation does not supply significant carbon during lipotoxicity (43). Therefore, carbon can enter the system as glucose or glutamine and leave as lactate or CO_2.

6) The oxygen consumption flux was assumed to satisfy the requirements for re-oxidizing NADH produced in both the CAC and glycolysis, in order to maintain redox balance. Our model cannot discriminate between NADH- and NADPH-dependent isoforms of IDH or malic enzyme. Therefore, we have modeled these enzymatic reactions as NADH-dependent due to the presence of mitochondrial transhydrogenase that can interconvert NADPH and NADH. This assumption will produce the most conservative estimates for flux differences between the tested treatments.

114

7) To account for incomplete isotopic steady state in the measured aspartate pool, we have included a *G* parameter. This value represents the fraction of the total aspartate pool that was synthesized in the presence of the isotopic tracer (44).

To estimate CAC flux, our metabolic model combines [U-^{13}C$_5$]glutamine isotope labeling with oxygen consumption. This enables quantification of absolute carbon fluxes in addition to relative flux ratios, and avoids potential errors associated with models that rely solely on carbon balancing to calculate CAC flux (45,46). Detailed flux results are provided in Figures A1-3 along with Tables A3-5. We report both the degrees of freedom (DOF) and the best-fit sum-of-squared residuals (SSR), which together indicate the goodness-of-fit for each experiment. We define exchange fluxes as $v_{exch}^{[0,100]} = 100 \times \frac{v_{exch}}{v_{exch}+v_{ref}}$, where v_{ref} is the citrate synthase flux value (47).

Table 4A.1: Reactions and atom transitions for metabolic flux analysis of H4IIEC3 rat hepatomas. Dot suffixes denote specific sub-pools of metabolite: .x, extracellular; .t, tracer; .d, dilution.

Pyruvate Metabolism			Reaction Name
½ Glucose (abcdef)	→	½ Pyr (cba) + ½ Pyr (def) + NADH	PK
Pyr (abc) + NADH	→	Lac (abc)	LDH
Pyr (abc) + CO_2 (d)	→	Mal (abcd)	PC
Mal (abcd)	→	Pyr (abc) + CO_2 (d) + NADH	ME
Pyr (abc)	→	AcCoA (bc) + CO_2 (a) + NADH	PDH
CAC Metabolism			
AcCoA (ab) + Mal (cdef)	→	Cit (fedbac) + NADH	CS
Cit (abcdef)	←→	Akg (abcde) + CO_2 (f) + NADH	IDH
Akg (abcde)	→	Suc (½ bcde + ½ edcb) + CO_2 (a) + NADH	ADH
Suc (½ abcd + ½ dcba)	←→	Fum (½ abcd + ½ dcba) + $FADH_2$	SDH
Fum (½ abcd + ½ dcba)	←→	Mal (abcd)	FUS
Glutamine anaplerosis			
Gln (abcde)	→	Glu (abcde)	GLS
Glu (abcde)	←→	Akg (abcde)	GDH
Net Glycolysis			
Difference between PK and LDH			
Oxygen Consumption			
2 NADH + O_2	→	2 H_2O	
2 $FADH_2$ + O_2	→	2 H_2O	
Dilution			
Asp.d (abcd)	→	Asp (abcd)	Asp G parameter

Table 4A.2: GC-MS ions used for metabolic flux analysis. The reported standard error (SEM) is representative of the calculated error amongst n=3 biological replicates.

Metabolite	Mass	Composition	Carbons					SEM (mol%)		
								Veh	PA	PA+ BAPTA
Gln	431	$C_{19}H_{43}O_3N_2Si_3$	1	2	3	4	5	0.7	0.5	0.5
Glu	432	$C_{19}H_{42}O_4NSi_3$	1	2	3	4	5	0.57	1.0	0.68
Glu	330	$C_{16}H_{36}O_2NSi_2$		2	3	4	5	0.77	1.0	0.5
Mal	419	$C_{18}H_{39}O_5Si_3$	1	2	3	4		1.67	0.88	0.7
Asp	390	$C_{17}H_{40}O_3NSi_3$		2	3	4		1.5	1.3	0.88
Asp	418	$C_{18}H_{40}O_4NSi_3$	1	2	3	4		0.86	0.9	0.82
Lac	233	$C_{10}H_{25}O_2Si_2$		2	3			0.65	0.5	0.5
Lac	261	$C_{11}H_{25}O_3Si_2$	1	2	3			0.6	0.64	0.5

Table 4A.3: Calculated absolute flux parameters and 95% confidence intervals for vehicle cells. Net flux units are pmol/million cells/s. Exchange fluxes and dilution parameters are scaled from 0 to 100%. SSR = 46.9 (32 DOF).

Parameter	Value	95% Confidence Interval	
Net Flux			
PK	32.3	[23.4,	42.0]
PDH	7.0	[5.2,	8.9]
CS	7.0	[5.2,	8.9]
IDH	7.0	[5.2,	8.9]
GLS	5.1	[3.8,	6.5]
GDH	5.1	[3.8,	6.5]
ADH	12.1	[8.9,	15.4]
SDH	12.1	[8.9,	15.4]
FUS	12.1	[8.9,	15.4]
ME	21.3	[15.3,	28.2]
PC	15.9	[11.5,	21.0]
LDH	30.4	[22.0,	39.7]
O_2 Consumption	34.1	[25.2,	43.0]
Net Glycolysis			
PK – LDH	1.9	[1.3,	2.9]
Exchange Flux			
IDH	0.9	[0,	100]
SDH	0.0	[0,	100]
FUS	100	[4.2,	100]
GDH	100	[11.5,	100]
Dilution			
Asp G Parameter	80.8	[72.8,	89.4]
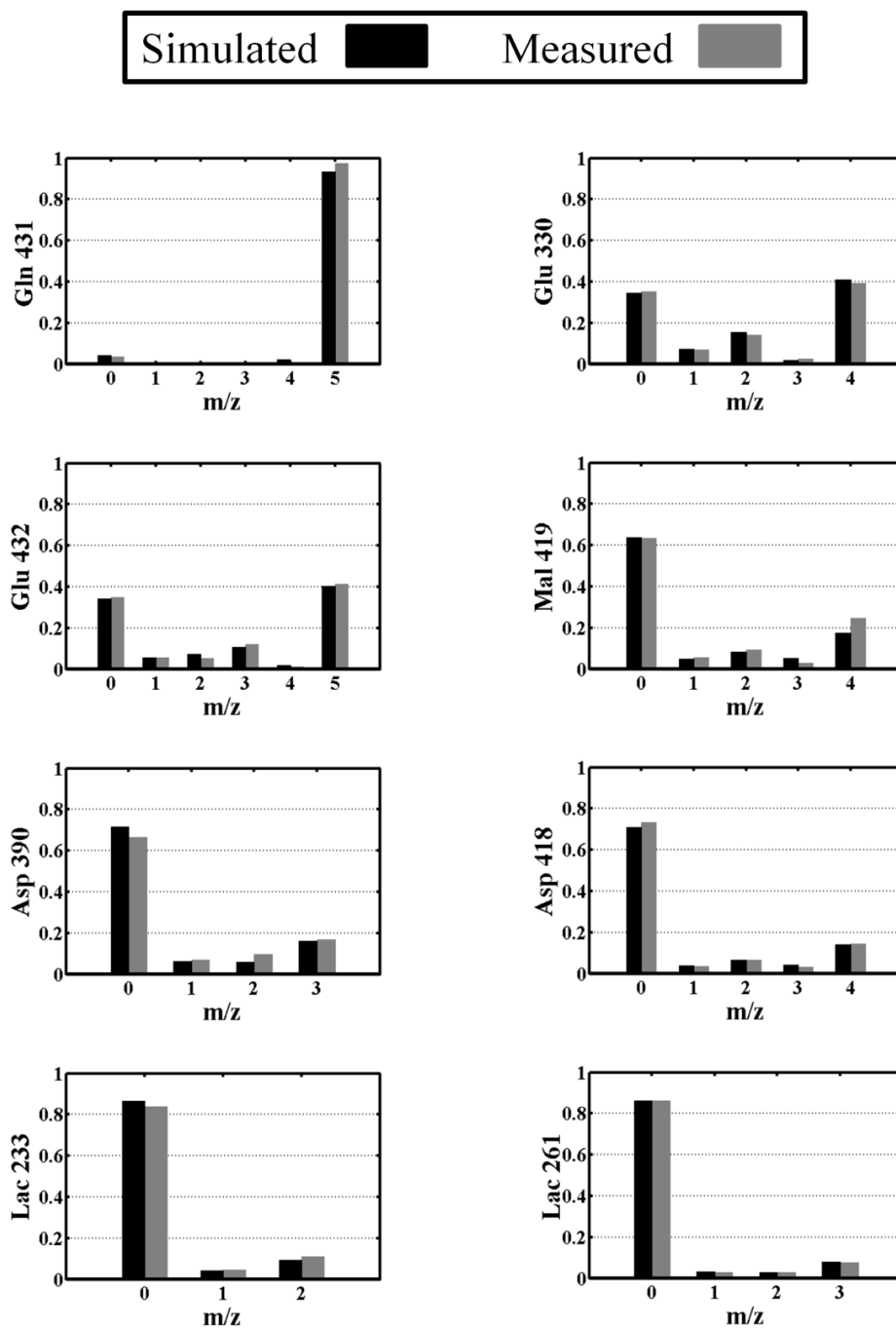
Figure 4A.1: Measured and simulated mass isotopomer distributions for vehicle-treated hepatic cells. Mass isotopomer distributions are corrected for natural isotope abundance. Simulated distributions are the result of best-fit flux estimates.

Table 4A.4: Calculated absolute flux parameters and 95% confidence intervals for palmitate-treated cells. Net flux units are pmol/million cells/s. Exchange fluxes and dilution parameters are scaled from 0 to 100%. SSR = 42.6 (35 DOF).

Parameter	Value	95% Confidence Interval	
Net Flux			
PK	71.7	[59.3.	85.4]
PDH	14.7	[12.4,	17.0]
CS	14.7	[12.4,	17.0]
IDH	14.7	[12.4,	17.0]
GLS	20.0	[16.8,	23.4]
GDH	20.0	[16.8,	23.4]
ADH	34.7	[29.5,	40.0]
SDH	34.7	[29.5,	40.0]
FUS	34.7	[29.5,	40.0]
ME	34.5	[28.8,	40.8]
PC	14.5	[11.7,	17.6]
LDH	77.1	[63.3,	92.6]
O_2 Consumption	71.3	[60.6,	82.1]
Net Glycolysis			
PK – LDH	-5.4	[-7.7,	-3.4]
Exchange Flux			
IDH	0.1	[0,	100]
SDH	0	[0,	100]
FUS	100	[0,	100]
GDH	100	[8.2,	100]
Dilution			
Asp G Parameter	97.7	[93.9,	100]
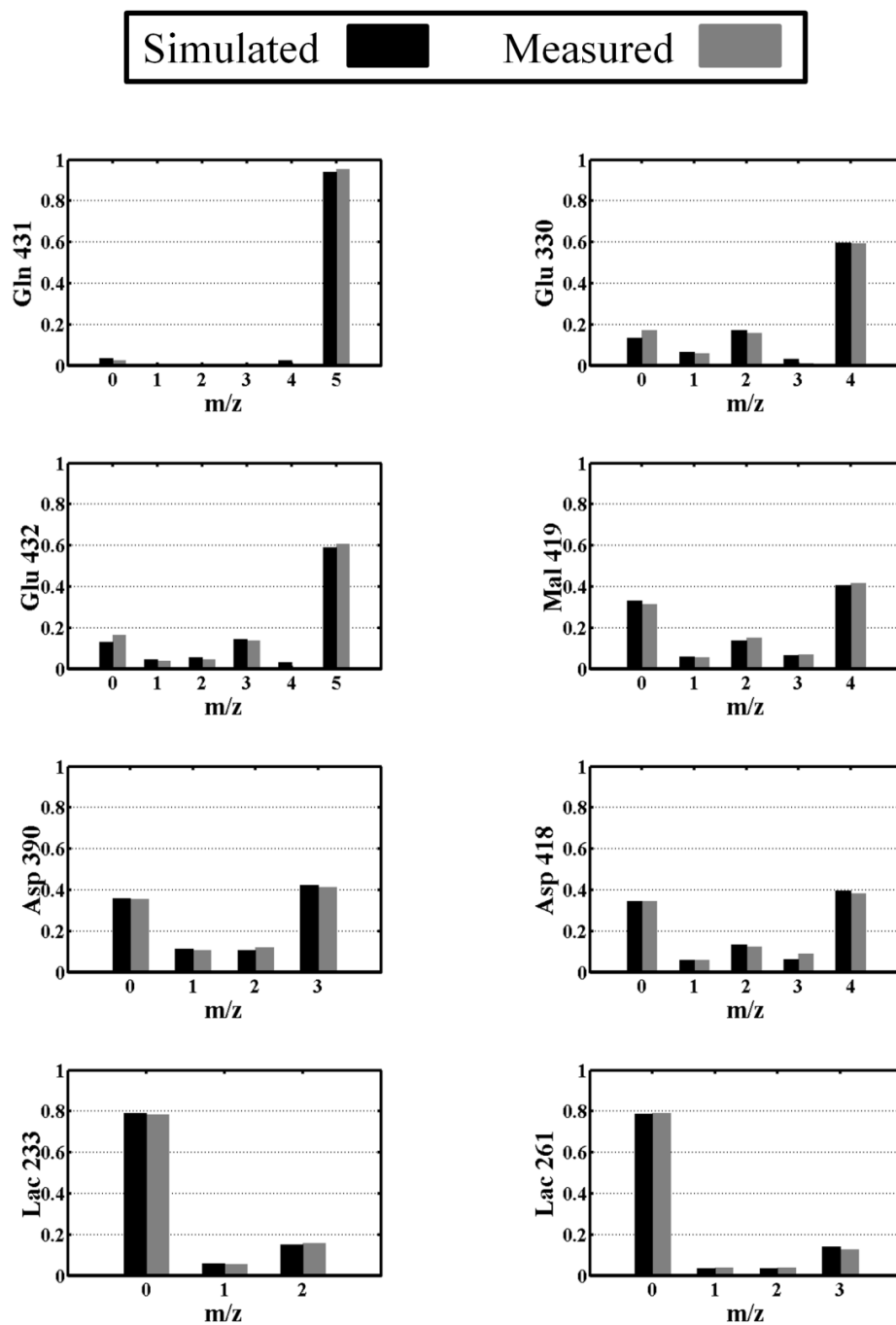
Figure 4A.2: Measured and simulated mass isotopomer distributions for palmitate-treated hepatic cells. Mass isotopomer distributions are corrected for natural isotope abundance. Simulated distributions are the result of best-fit flux estimates.

Table 4A.5: Calculated absolute flux parameters and 95% confidence intervals for cells treated with both palmitate and BAPTA. Net flux units are pmol/million cells/s. Exchange fluxes and dilution parameters are scaled from 0 to 100%. SSR = 62.0 (32 DOF).

Parameter	Value	95% Confidence Interval
Net Flux		
PK	43.6	[31.9, 56.6]
PDH	12.1	[9.1, 15.2]
CS	12.1	[9.1, 15.2]
IDH	12.1	[9.1, 15.2]
GLS	6.1	[4.5, 7.7]
GDH	6.1	[4.5, 7.7]
ADH	18.2	[13.6, 22.8]
SDH	18.2	[13.6, 22.8]
FUS	18.2	[13.6, 22.8]
ME	17.8	[13.1, 22.9]
PC	11.7	[8.6, 15.3]
LDH	37.6	[27.1, 49.8]
O_2 Consumption	48.3	[36.2, 60.4]
Net Glycolysis		
PK – LDH	6.0	[4.4, 7.8]
Exchange Flux		
IDH	0.3	[0, 100]
SDH	20	[0, 100]
FUS	50	[0, 100]
GDH	100	[92.5, 100]
Dilution		
Asp G Parameter	70.6	[65.6, 75.6]
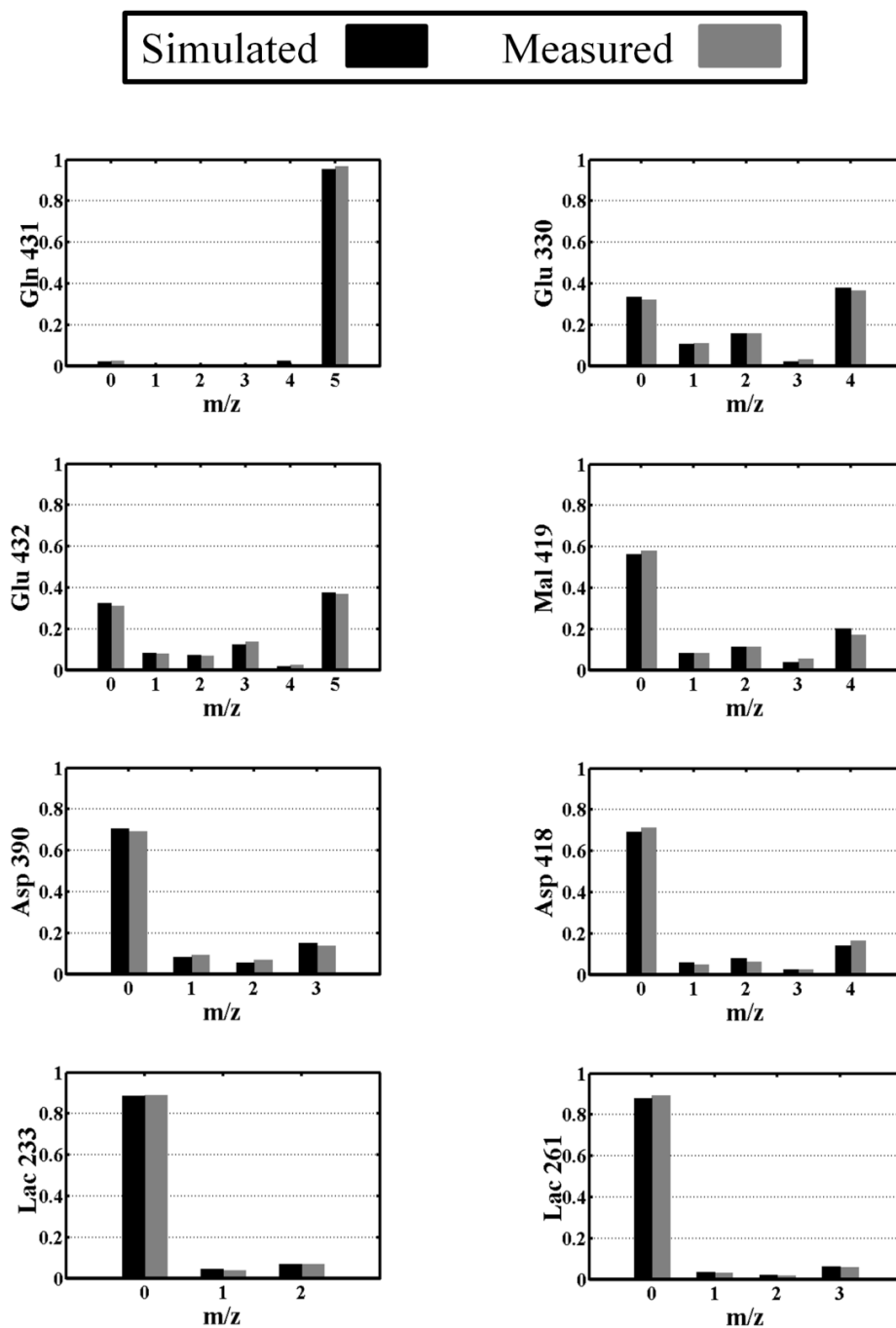
Figure 4A.3: Measured and simulated mass isotopomer distributions for palmitate and BAPTA co-treated hepatic cells. Mass isotopomer distributions are corrected for natural isotope abundance. Simulated distributions are the result of best-fit flux estimates.

References

1. Fu, S., Yang, L., Li, P., Hofmann, O., Dicker, L., Hide, W., Lin, X., Watkins, S. M., Ivanov, A. R., and Hotamisligil, G. S. (2011) Aberrant lipid metabolism disrupts calcium homeostasis causing liver endoplasmic reticulum stress in obesity. *Nature* **473**, 528-531

2. Sunny, N. E., Parks, E. J., Browning, J. D., and Burgess, S. C. (2011) Excessive Hepatic Mitochondrial TCA Cycle and Gluconeogenesis in Humans with Nonalcoholic Fatty Liver Disease. *Cell Metab* **14**, 804-810

3. Ozcan, U., Cao, Q., Yilmaz, E., Lee, A., Iwakoshi, N., Ozdelen, E., Tuncman, G., Gorgun, C., Glimcher, L., and Hotamisligil, G. (2004) Endoplasmic reticulum stress links obesity, insulin action, and type 2 diabetes. *Science* **306**, 457-461

4. Satapati, S., Sunny, N. E., Kucejova, B., Fu, X. R., He, T. T., Mendez-Lucas, A., Shelton, J. M., Perales, J. C., Browning, J. D., and Burgess, S. C. (2012) Elevated TCA cycle function in the pathology of diet-induced hepatic insulin resistance and fatty liver. *Journal of Lipid Research* **53**, 1080-1092

5.   Feldstein, A., Canbay, A., Angulo, P., Taniai, M., Burgart, L., Lindor, K., and Gores, G. (2003) Hepatocyte apoptosis and Fas expression are prominent features of human nonalcoholic steatohepatitis. *Gastroenterology* **125**, 437-443

6.   Angulo, P., and Lindor, K. D. (2002) Non-alcoholic fatty liver disease. *Journal of Gastroenterology and Hepatology* **17**, S186-S190

7.   Fernandez, C. A., Des Rosiers, C., Previs, S. F., David, F., and Brunengraber, H. (1996) Correction of 13C mass isotopomer distributions for natural stable isotope abundance. *J Mass Spectrom* **31**, 255-262

8.   Neuschwander-Tetri, B. A., and Caldwell, S. H. (2003) Nonalcoholic steatohepatitis: summary of an AASLD Single Topic Conference. *Hepatology* **37**, 1202-1219

9.   Li, Z. Z., Berk, M., McIntyre, T. M., and Feldstein, A. E. (2009) Hepatic Lipid Partitioning and Liver Damage in Nonalcoholic Fatty Liver Disease ROLE OF STEAROYL-CoA DESATURASE. *Journal of Biological Chemistry* **284**, 5637-5644

10.   Puri, P., Baillie, R. A., Wiest, M., Mirshahi, F., and Sanyal, A. J. (2006) A lipidomic analysis of non-alcoholic fatty liver disease (NAFLD). *Journal of Hepatology* **44**, S260-S261

11.   Leamy, A. K., Egnatchik, R. A., and Young, J. D. (2013) Molecular mechanisms and the role of saturated fatty acids in the progression of non-alcoholic fatty liver disease. *Progress in Lipid Research* **52**, 165-174

12.   Noguchi, Y., Young, J., Aleman, J., Hansen, M., Kelleher, J., and Stephanopoulos, G. (2009) Effect of Anaplerotic Fluxes and Amino Acid Availability on Hepatic Lipoapoptosis. *Journal of Biological Chemistry* **284**, 33425-33436

13. Gu, X., Li, K., Laybutt, D. R., He, M.-l., Zhao, H.-L., Chan, J. C. N., and Xu, G. (2010) Bip overexpression, but not CHOP inhibition, attenuates fatty-acid-induced endoplasmic reticulum stress and apoptosis in HepG2 liver cells. *Life Sciences* **87**, 724-732

14. Barreyro, F., Kobayashi, S., Bronk, S., Werneburg, N., Malhi, H., and Gores, G. (2007) Transcriptional regulation of Bim by FoxO3A mediates hepatocyte lipoapoptosis. *Journal of Biological Chemistry* **282**, 27141-27154

15. Srivastava, S., and Chan, C. (2007) Hydrogen peroxide and hydroxyl radicals mediate palmitate-induced cytotoxicity to hepatoma cells: Relation to mitochondrial permeability transition. *Free Radical Research* **41**, 38-49

16. Cazanave, S. C., Mott, J. L., Elmi, N. A., Bronk, S. F., Werneburg, N. W., Akazawa, Y., Kahraman, A., Garrison, S. P., Zambetti, G. P., Charlton, M. R., and Gores, G. J. (2009) JNK1-dependent PUMA Expression Contributes to Hepatocyte Lipoapoptosis. *Journal of Biological Chemistry* **284**, 26591-26602

17. Malhi, H., Bronk, S. F., Werneburg, N. W., and Gores, G. J. (2006) Free fatty acids induce JNK-dependent hepatocyte lipoapoptosis. *Journal of Biological Chemistry* **281**, 12093-12101

18. Pfaffenbach, K., Gentile, C., Nivala, A., Wang, D., Wei, Y., and Pagliassotti, M. (2010) Linking endoplasmic reticulum stress to cell death in hepatocytes: roles of C/EBP homologous protein and chemical chaperones in palmitate-mediated cell death. *American Journal of Physiology-Endocrinology and Metabolism* **298**, E1027-E1035

19. Padilla, A., Descorbeth, M., Almeyda, A. L., Payne, K., and De Leon, M. (2011) Hyperglycemia magnifies Schwann cell dysfunction and cell death triggered by PA-induced lipotoxicity. *Brain Research* **1370**, 64-79

20.   Borradaile, N. M., Han, X., Harp, J. D., Gale, S. E., Ory, D. S., and Schaffer, J. E. (2006) Disruption of endoplasmic reticulum structure and integrity in lipotoxic cell death. *Journal of Lipid Research* **47**, 2726-2737

21.   Wei, Y., Wang, D., Topczewski, F., and Pagliassotti, M. (2006) Saturated fatty acids induce endoplasmic reticulum stress and apoptosis independently of ceramide in liver cells. *American Journal of Physiology-Endocrinology and Metabolism* **291**, E275-E281

22.   Brookes, P. S., Yoon, Y. S., Robotham, J. L., Anders, M. W., and Sheu, S. S. (2004) Calcium, ATP, and ROS: a mitochondrial love-hate triangle. *American Journal of Physiology-Cell Physiology* **287**, C817-C833

23.   Barron, J. T., Gu, L. P., and Parrillo, J. E. (1998) Malate-aspartate shuttle, cytoplasmic NADH redox potential, and energetics in vascular smooth muscle. *Journal of Molecular and Cellular Cardiology* **30**, 1571-1579

24.   Gellerich, F. N., Gizatullina, Z., Trumbeckaite, S., Nguyen, H. P., Pallas, T., Arandarcikaite, O., Vielhaber, S., Seppet, E., and Striggow, F. (2010) The regulation of OXPHOS by extramitochondrial calcium. *Biochimica Et Biophysica Acta-Bioenergetics* **1797**, 1018-1027

25.   Contreras, L., and Satrustegui, J. (2009) Calcium Signaling in Brain Mitochondria INTERPLAY OF MALATE ASPARTATE NADH SHUTTLE AND CALCIUM UNIPORTER/MITOCHONDRIAL DEHYDROGENASE PATHWAYS. *Journal of Biological Chemistry* **284**, 7091-7099

26.   Gyorgy, H., Gyrogy, C., Das, S., Garcia-Perez, C., Saotome, M., Roy, S., and Yi, M. (2006) Mitochondrial calcium signalling and cell death: Approaches for assessing the role of mitochondrial Ca2+ uptake in apoptosis. *Cell Calcium* **40**, 553-560

27.   Nutt, L., Chandra, J., Pataer, A., Fang, B., Roth, J., Swisher, S., O'Neil, R., and McConkey, D. (2002) Bax-mediated Ca2+ mobilization promotes cytochrome c release during apoptosis. *Journal of Biological Chemistry* **277**, 20301-20308

28.   White, C., Li, C., Yang, J., Petrenko, N., Madesh, M., Thompson, C., and Foskett, J. (2005) The endoplasmic reticulum gateway to apoptosis by Bcl-X-L modulation of the InsP(3)R. *Nature Cell Biology* **7**, 1021-U1135

29.   Sunny, N. E., Parks, E. J., Browning, J. D., and Burgess, S. C. (2011) Excessive hepatic mitochondrial TCA cycle and gluconeogenesis in humans with nonalcoholic fatty liver disease. *Cell Metab* **14**, 804-810

30.   Satapati, S., Sunny, N. E., Kucejova, B., Fu, X., He, T. T., Mendez-Lucas, A., Shelton, J. M., Perales, J. C., Browning, J. D., and Burgess, S. C. (2012) Elevated TCA cycle function in the pathology of diet-induced hepatic insulin resistance and fatty liver. *Journal of lipid research* **53**, 1080-1092

31.   Egnatchik, R. A., Leamy, A. K., Noguchi, Y., Shiota, M., and Young, J. D. (2013) Palmitate-induced Activation of Mitochondrial Metabolism Promotes Oxidative Stress and Apoptosis in H4IIEC3 Rat Hepatocytes. *Metabolism: clinical and experimental*

32.   Shiota, M., Inagami, M., Fujimoto, Y., Moriyama, M., Kimura, K., and Sugano, T. (1995) Cold acclimation induces zonal heterogeneity in gluconeogenic responses to glucagon in rat liver lobule. *American Journal of Physiology* **268**, E1184-E1191

33.   Jacobson, D. A., Weber, C. R., Bao, S. Z., Turk, J., and Philipson, L. H. (2007) Modulation of the pancreatic islet beta-cell-delayed rectifier potassium channel Kv2.1 by the polyunsaturated fatty acid arachidonate. *Journal of Biological Chemistry* **282**, 7442-7449

34.   Young, J. D. (2014) INCA: A computational platform for isotopically nonstationary metabolic flux analysis. *Bioinformatics*

35.   Antoniewicz, M. R., Kelleher, J. K., and Stephanopoulos, G. (2007) Elementary metabolite units (EMU): A novel framework for modeling isotopic distributions. *Metabolic Engineering* **9**, 68-86

36.   Young, J., Walther, J., Antoniewicz, M., Yon, H., and Stephanopoulos, G. (2008) An Elementary Metabolite Unit (EMU) based method of isotopically nonstationary flux analysis. *Biotechnology and Bioengineering* **99**, 686-699

37.   Antoniewicz, M. R., Kelleher, J. K., and Stephanopoulos, G. (2006) Determination of confidence intervals of metabolic fluxes estimated from stable isotope measurements. *Metab Eng* **8**, 324-337

38.   Wei, Y., Wang, D., Gentile, C., and Pagliassotti, M. (2009) Reduced endoplasmic reticulum luminal calcium links saturated fatty acid-mediated endoplasmic reticulum stress and cell death in liver cells. *Molecular and Cellular Biochemistry* **331**, 31-40

39.   Borradaile, N. M., Harp, J. D., and Schaffer, J. E. (2006) Palmitate-induced changes in endoplasmic reticulum structure and function: A central role for the ER in lipotoxicity. *Arteriosclerosis Thrombosis and Vascular Biology* **26**, E49-E49

40.   Puri, P., Mirshahi, F., Cheung, O., Natarajan, R., Maher, J. W., Kellum, J. M., and Sanyal, A. J. (2008) Activation and Dysregulation of the Unfolded Protein Response in Nonalcoholic Fatty Liver Disease. *Gastroenterology* **134**, 568-576

41.   Li, Y. K., Ge, M. T., Ciani, L., Kuriakose, G., Westover, E. J., Dura, M., Covey, D. F., Freed, J. H., Maxfield, F. R., Lytton, J., and Tabas, I. (2004) Enrichment of endoplasmic reticulum with cholesterol inhibits sarcoplasmic-endoplasmic reticulum calcium ATPase-

2b activity in parallel with increased order of membrane lipids - Implications for depletion of endoplasmic reticulum calcium stores and apoptosis in cholesterol-loaded macrophages. *Journal of Biological Chemistry* **279**, 37030-37039

42.   Zhang, J., Li, Y., Jiang, S., Yu, H., and An, W. (2013) Enhanced endoplasmic reticulum SERCA activity by overexpression of hepatic stimulator substance gene prevents liver cells from ER stress-induced apoptosis. *American Journal of Physiology - Cell Physiology*

43.   Egnatchik, R. A., Leamy, A. K., Noguchi, Y., Shiota, M., and Young, J. D. Palmitate-induced Activation of Mitochondrial Metabolism Promotes Oxidative Stress and Apoptosis in H4IIEC3 Rat Hepatocytes. *Metabolism*

44.   Antoniewicz, M. R., Kraynie, D. F., Laffend, L. A., González-Lergier, J., Kelleher, J. K., and Stephanopoulos, G. (2007) Metabolic flux analysis in a nonstationary system: Fed-batch fermentation of a high yielding strain of E. coli producing 1,3-propanediol. *Metabolic Engineering* **9**, 277-292

45.   Altamirano, C., Illanes, A., Becerra, S., Cairo, J. J., and Godia, F. (2006) Considerations on the lactate consumption by CHO cells in the presence of galactose. *Journal of Biotechnology* **125**, 547-556

46.   Ahn, W. S., and Antoniewicz, M. R. (2013) Parallel labeling experiments with [1,2-13C]glucose and [U-13C]glutamine provide new insights into CHO cell metabolism. *Metabolic Engineering* **15**, 34-47

47.   Wiechert, W., Siefke, C., deGraaf, A. A., and Marx, A. (1997) Bidirectional reaction steps in metabolic networks .2. Flux estimation and statistical analysis. *Biotechnology and Bioengineering* **55**, 118-135

CHAPTER 5

GLUTAMATE OXALOACETATE TRANSAMINASE ACTIVITY PROMOTES HEPATIC
CELL LIPOTOXICITY THROUGH ENHANCED CAC ANAPLEROSIS

Abstract

Hepatic lipotoxicity is characterized by enhanced mitochondrial anaplerosis which
predisposes the cell to oxidative stress and apoptosis. Previously, we have shown that calcium
regulates the anaplerotic state of hepatic mitochondria treated with elevated palmitate. We
hypothesized elevated calcium increased α-ketoglutarate dehydrogenase oxidation of α-
ketoglutarate necessitating increased CAC anaplerosis. To test this hypothesis, hepatic cells
were treated with lipotoxic palmitate in the absence or presence of glutamine, glutamate, and α-
ketoglutarate. It was found that co-incubating primary hepatocytes and α-ketoglutarate resulted
in increased cell death compared to cells treated without α-ketoglutarate. To dissect the
metabolic pathway producing this α-ketoglutarate, we treated H4IIEC3 cells with siRNA for
glutamate dehydrogenase, cytosolic glutamate oxaloacetate transaminase (GOT1), or
mitochondrial glutamate oxaloacetate transaminase (GOT2). Knockdown of GOT2 greatly
reduced the lipotoxic effects of elevated palmitate while knockdown of Glud1 had no effect.
Additionally co-treating H4IIEC3 hepatic cells with palmitate and the pan-transaminase inhibitor
AOA confirmed these results by reducing lipotoxicity and lipotoxic mitochondrial alterations
characterized by increased oxygen consumption and anaplerosis. Taken together, these results
demonstrate that lipotoxicity disrupts the anaplerotic state of mitochondria, causing a shift to
aberrant transaminase metabolism which fuels CAC dysregulation.

Introduction

The liver is a central metabolic hub of the body, regulating glucose, lipid, and amino acid metabolism. As such, many hepatic pathologies are associated with altered metabolic capacity. In particular, NAFLD and NASH, as the hepatic manifestations of the metabolic syndrome, are associated with insulin resistance and altered mitochondrial capacity including impaired fatty acid oxidation and increased anaplerosis (1-5). While plasma free fatty acid concentrations are often elevated in these pathologies (6,7), the biochemical mediators and metabolic pathways linking elevated plasma fatty acid concentrations to mitochondrial metabolic dysfunction are currently unclear. In addition to alterations of plasma free fatty acid profiles, clinical and animal models of NASH and fatty liver have demonstrated significant alterations in plasma amino acid levels suggesting systemic dysregulation of amino acid metabolism (8-10).

Altered plasma glutamine and glutamate levels have recently been identified as markers in patients with the metabolic syndrome and NASH (8,11). In particular, decreases in the ratio between glutamine and glutamate are associated with enhanced systemic glucose intolerance as glutamate can potentiate the formation of alanine, and therefore gluconeogenesis. Additionally, abnormal glutamatyl-dipeptide synthesis has been associated with many liver diseases including NASH and hepatocellular carcinoma (12). This was attributed to inefficient synthesis of glutathione to combat oxidative stress associated with liver disease. Conversely, it has been recently hypothesized that the NAFLD biomarkers glutamate pyruvate transaminase (GPT, or alanine aminotransferase) and glutamate oxaloacetate transaminase (GOT, or aspartate aminotransferase) may participate in a more causative mechanism of disease progression (13).

Consistent with the hypothesis that alterations in glutamate metabolism could potentiate disease, *in vitro* models of lipotoxicity have shown that hepatic cells treated with an overload of

the saturated fatty acid palmitate are characterized by altered mitochondrial metabolism which favors glutamate anaplerosis and enhanced oxidative flux (14). Additionally, replacing extracellular glutamine with alternative amino acids revealed that glutamate had the greatest effect in promoting oxidative stress and losses in cell viability characteristic of palmitate lipotoxicity (14). This finding agrees with several *in vivo* studies which show that elevations in intrahepatic lipids are associated with elevations in mitochondrial anaplerosis and CAC oxidation (15). The addition of exogenous antioxidants to *in vitro* hepatic cells did not reverse these metabolic abnormalities, indicating that anaplerotic flux of glutamine/glutamate carbon entering the CAC was not simply a response to combat lipotoxic ROS accumulation (16).

We have previously demonstrated that addition of the calcium chelator BAPTA to hepatic cells treated with elevated levels of palmitate are characterized by attenuations in CAC anaplerosis and oxidative stress (Chapter 4). This indicated that alterations in intracellular calcium predispose the mitochondria to an enhanced anaplerotic phenotype that contributes to lipotoxicity. Calcium is a known regulator of α-ketoglutarate dehydrogenase (ADH) as well as the glutamate aspartate uniporter citrin, the action of which can lead to increased oxidation of α-ketoglutarate (22, 23). Therefore, we hypothesized that glutamine and glutamate anaplerosis is upregulated in response to palmitate treatment in order to maintain CAC α-ketoglutarate levels. As such, the deregulation of carbon entry to the CAC at the α-ketoglutarate node represents one potential mechanism by which intracellular calcium can impact the rate of lipotoxicity.

To test the hypothesis that CAC anaplerosis controls the rate of palmitate lipotoxicity in hepatic cells, we altered extracellular media concentrations of glutamine, glutamate, and α-ketoglutarate to determine if the presence of these anaplerotic substrates predisposed hepatic cells to enhanced apoptosis in the presence of lipotoxic concentrations of palmitate. Additionally,

we employed pharmacologic and siRNA-mediated knockdown of glutamate dehydrogenase (Glud1) and the glutamate oxaloacetate (GOT) pathways of CAC anaplerosis (Figure 5.1). We found that attenuation of GOT activity, but not Glud1, significantly decreased hepatic lipoapoptosis in H4IIEC3 cells. Pharmacologic inhibition of transaminase metabolism using the pan transaminase inhibitor amino oxyacetic acid (AOA) reduced the enhanced oxygen consumption flux we had previously observed as a characteristic of palmitate lipotoxicity. Similarly, ^{13}C MFA revealed that AOA reduced absolute glutamine anaplerosis and CAC flux compared to hepatic cells treated with palmitate alone. Taken together, these results indicate that upstream events in hepatic lipotoxicity (i.e., abnormal ER calcium release) predispose the mitochondria to utilize extracellular glutamate carbon to replenish CAC intermediates. Uninhibited, this mechanism leads to the characteristic metabolic dysfunction and oxidative stress associated with hepatic lipotoxicity (16).
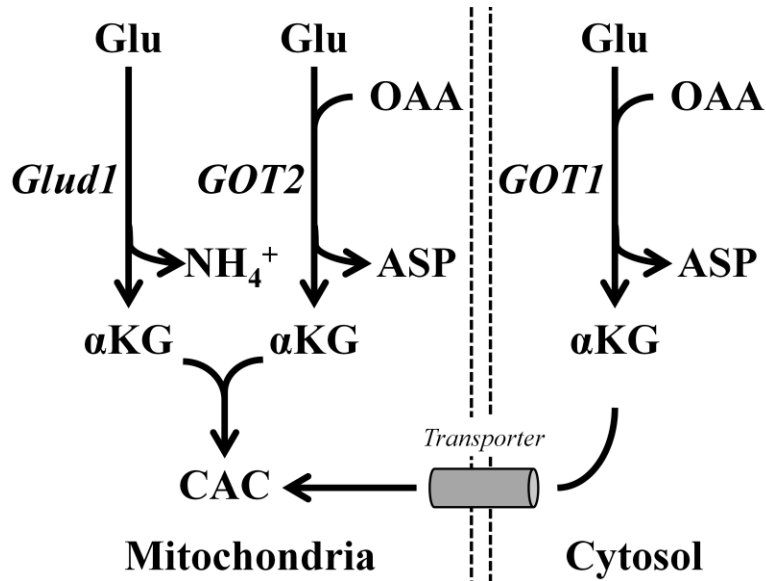
Figure 5.1: Enzymatic pathways by which glutamate can provide α-ketoglutarate for CAC anaplerosis. Extracellular glutamine is metabolized in the mitochondria to glutamate (Glu) by glutaminase. Glutamate can be metabolized through glutamate dehydrogenase (*Glud1*) or glutamate oxaloacetate transaminase 2 (*GOT2*) to α-ketoglutarate (αKG). Similarly cytosolic, glutamate oxaloacetate transaminase 1 (*GOT1*) produces αKG from Glu which must then be transported (through a malate/ αKG antiporter) across the mitochondrial membrane to enter CAC metabolism. The GOT pathways additionally consume oxaloacetate (OAA) and produce aspartate (ASP).

Methods

Materials-

Dulbecco's modified Eagle's medium (DMEM), amino oxyacetic acid (AOA), dimethyl alpha-ketoglutarate, aspartic acid, glutamic acid, bovine serum albumin (BSA), palmitate, and oleate were purchased from Sigma (St. Louis, MO, USA). The dead-cell stain propidium iodide (PI) was obtained from Invitrogen (Carlsbad, CA, USA).

H4IIEC3 hepatic cell culture-

The H4IIEC3 rat hepatoma cell line was used as a model of *in vitro* hepatic lipotoxicity (American Type Culture Collection, Manassas, VA, USA). Cells were cultured in low glucose DMEM (1g/L) with 10% FBS and 1% penicillin/streptomycin antibiotic solution with a basal 2 mM glutamine concentration. For measurements of toxicity and apoptosis, cells were plated at a density of 2×10^4 cells per well in a 96-well plate and allowed to grow for two days (until confluent) prior to the experiment.

Primary rat hepatocyte isolation and culture-

Primary hepatocytes from male Sprague-Dawley rats were isolated following a previously reported method (17). Briefly, the portal vein and inferior vena cava of anesthetized animals were cannulated and perfused with 37°C oxygenated perfusion media, pH 7.4, containing 118 mM NaCl, 5.9 mM KCl, 1.2 mM $MgSO_4$, 1.2 mM NaH_2PO_4, 25 mM $NaHCO_3$, 0.2 mM EGTA and 5 mM glucose. After approximately 15 minutes, the liver was excised from the animal and perfused with liver digest medium (Invitrogen, Grand Island NY). Once digested, the liver cells were dispersed in attachment medium (described below) and rinsed four times. Then, cells were plated in attachment medium, consisting of 20 mM glucose DMEM with 30 mg/L proline, 100 mg/L ornithine, 0.544 mg/L $ZnCl_2$, 0.75 mg/L $ZnSO_4$ $7H_2O$, 0.2 mg/L $CuSO_4$ $5H_2O$, 0.25 mg/L $MnSO_4$, 2 g/L bovine serum albumin (Sigma), 5 nM insulin, 100 nM dexamethasone, 100,000 U penicillin, 100,000 U streptomycin, and 2 mM glutamine. Four hours after cells were plated, the attachment medium was removed and replaced with an identical maintenance medium, except the insulin concentration was reduced to 1 nM.

Preparation of fatty acid solutions-

Free fatty acid (FFA) stock solutions were made by dissolving FFA in bovine serum albumin (BSA). A 195 mM stock of palmitate in pure ethanol was added to a 37°C 10% w/w BSA solution to a final concentration of 3 mM. This solution was kept warm until palmitate was fully dissolved and then stored at 4°C. This method yielded a final ratio of palmitate to BSA of 2:1.

Toxicity assays-

Losses in cell viability in response to FFA treatments were assessed using the dead-cell stain propidium iodide (PI). The intercalating dye becomes highly fluorescent when bound to exposed double-stranded DNA of dead cells. Fluorescence was assessed using excitation wavelength of 530 nm and emission wavelength of 645 nm with a BioTek Cytation 3 plate reader.

Caspase activity-

Caspase 3 and 7 activity was measured as a marker of apoptosis using the Apo-ONE Homogenous Caspase 3/7 Assay kit. This kit lyses the cells with the caspase 3/7 specific substrate Z-DEVD-R110, which becomes fluorescent once caspases remove the DEVD peptide. We measured fluorescence at an excitation wavelength of 485 nm and emission wavelength at 530 nm.

Oxygen consumption-

The Oroboros Oxygraph-2K was used to measure oxygen consumption flux as a direct measurement of mitochondrial metabolism. The Oxygraph-2k has two chambers with separate

oxygen probes to allow analysis of oxygen consumption of cells in suspension. The instrument was set to a temperature of 37°C, and the stirring speed for each chamber was 500 rpm. To perform these experiments, H4IIEC3 cells were cultured on 6-cm dishes until 80-90% confluent and subsequently incubated with selected combinations of fatty acids and treatments for 6 hours. Cells were then trypsinized, counted, and resuspended in the same culture medium and injected into the Oxygraph instrument.

Knockdown of Glud1, GOT1, and GOT2-

Small interfering RNA (siRNA) for *Glud1, GOT1, and GOT2* were purchased from Integrated DNA Technologies. Cells were treated with a 25 nmoles of selected siRNA complexed to RNAiMAX (Invitrogen) in antibiotic free DMEM. After 24 hours, complex containing media was replaced with antibiotic free DMEM. Following another 24 hours, experiments were performed. Knockdown efficiency and selection of siRNA targeting sequences are shown in Figure 5.A1.

Polar metabolite extraction and GC-MS analysis of ^{13}C enrichment-

Intracellular metabolites from H4IIEC3 rat hepatomas were extracted as previously described (14). Briefly, intracellular metabolism was quenched with 1 mL of -80°C methanol and cells were scraped into a mixture of 1:1:1 chloroform, methanol, and water. After drying the aqueous phase, samples were derivatized with MBTSTFA + 1% TBDMCS (Pierce). GC-MS ^{13}C isotopic enrichment was then analyzed with an Agilent 6890N/5975B GC-MS equipped with a 30m DB-35ms capillary column.

Metabolic flux analysis-

^{13}C MFA was performed using the INCA software package (18) and initiated with a previously developed model of hepatic metabolism comprising glycolysis, CAC, and anaplerotic pathways (16). This previous model was updated to include the PEPCK mediated conversion of OAA to PEP due to significant labeling found in PEP. Fluxes were estimated a minimum of 50 times starting from random initial values to identify a global best-fit solution. Once this solution was achieved, a chi-square test was used to assess the goodness-of-fit. Additionally, 95% confidence intervals were calculated for all estimated parameters by assessing the sensitivity of the sum-of-squared residuals to parameter variations (19). Comprehensive ^{13}C MFA results and a detailed description of our network model are available in the Appendix.

Statistical Analysis-

Tests for statistical significance were performed using analysis of variance (Model I ANOVA) and Tukey-Kramer methods for multiple comparisons, or Student's t-test for pair-wise comparisons. Plots indicate +/- one standard error of the mean unless otherwise indicated.

Results

Extracellular glutamine enhances palmitate lipotoxicity in hepatic cells in vitro

We have previously shown that glutamine anaplerosis is increased independently of caspase 3/7 activity in palmitate-treated H4IIEC3 cells (16). However, it is unclear whether altered glutamine metabolism would be observed in isolated primary hepatocytes. Furthermore, the effects of glutamine removal or replacement have not been systematically assessed. To test

this, H4IIEC3 hepatic cells or primary hepatocytes were treated with 400 μM palmitate in the presence or absence of 2 mM glutamine. Removal of extracellular glutamine attenuated the lipotoxic cell death associated with 400 μM palmitate treatment by similar amounts in both primary hepatocytes and H4IIEC3 cells (Figure 5.2A). Additionally, this reduction in 24-hour toxicity in H4IIEC3 cells (experiment not performed in primary cells) was associated with a reduction in markers of apoptosis at 12 hours (Figure 5.2B).
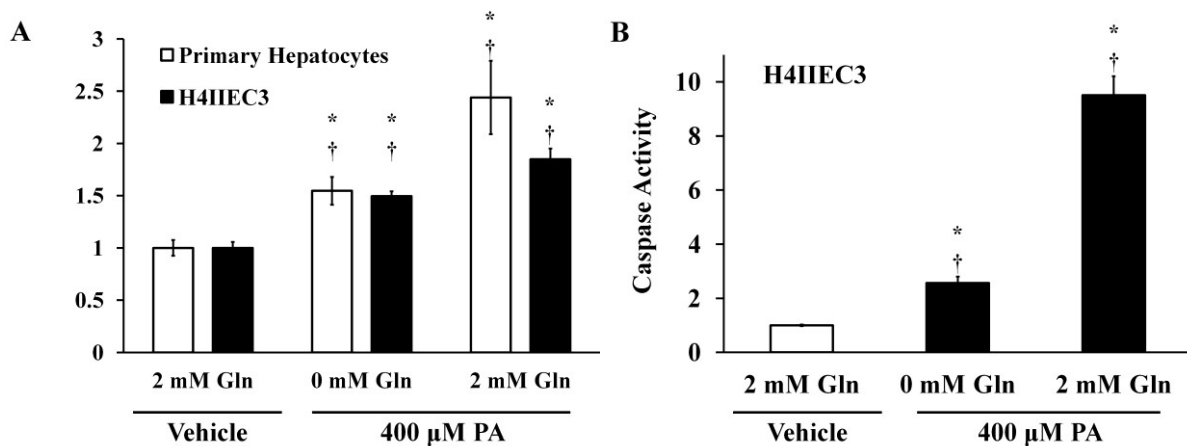
Figure 5.2: Removal of extracellular glutamine attenuates lipotoxicity. Primary hepatocytes and H4IIEC3 hepatic cells were treated with a lipotoxic concentration of palmitate (400 μM) either in the presence (2 mM) or absence of glutamine. (A) 24-hour cell toxicity assessed by PI fluorescence. (B) Caspase activity in H4IIEC3 hepatic cells after 12 hours of palmitate treatment. Data represent mean +/- S.E., n=4; *different from vehicle, $p < 0.05$, † different from treatments in same cell line, $p < 0.05$.

The metabolic products of glutamine and glutamate anaplerosis promote lipotoxic cell death

Glutamine can be metabolized via conversion to glutamate and then to the CAC intermediate α-ketoglutarate (αKG). If glutamine fuels lipotoxicity by providing substrates for mitochondrial anaplerosis, its direct downstream metabolites should also stimulate hepatic cell death in response to elevated doses of palmitate. To test this hypothesis, primary hepatocytes and H4IIEC3 hepatic cells were treated with 400 μM palmitate and incubated with 2 mM

140

glutamine, 2 mM glutamate, or 2 mM α-ketoglutarate (as dimethyl αKG) for 24 hours. H4IIEC3

cells exhibited identical toxicity responses to all media combinations, indicating that these

metabolites act as interchangeable fuels for promoting the mitochondrial lipotoxic phenotype

(Figure 5.3A). Interestingly, primary hepatocytes exhibited increased lipotoxic cell death when

extracellular glutamine was replaced with glutamate or α-ketoglutarate. This increase in cell

death suggests that primary hepatocytes have increased sensitivity to downstream glutamine-

derived anaplerotic substrates than to glutamine itself. This could be due to reduced glutaminase

activity in primary hepatocytes, which is needed to convert glutamine to glutamate. Glutaminase

is located in a very narrow region of the liver. Our primary hepatocyte isolation method

homogenizes the entire liver, producing a mixed population of hepatocytes. This could explain

why glutamate is more synergistic than glutamine in primary hepatocytes (20,21).

Glutamate can produce α-ketoglutarate through direct deamination by glutamate

dehydrogenase (Glud1) or through transamination to produce a non-essential amino acid such as

alanine or aspartate. Of particular interest is the glutamate oxaloacetate transaminase (GOT)

family of enzymes, since they play a key role in the malate aspartate shuttle, a critical redox

shuttle whose activity can be influenced by alterations in intracellular calcium (22,23). GOT

catalyzes the conversion of glutamate to α-ketoglutarate via the transamination of aspartate and

oxaloacetate. Since we have previously observed calcium-dependent anaplerosis in palmitate-

treated hepatic cells (Chapter 4), we hypothesized that GOT metabolism could be the primary

route of anaplerosis that is upregulated in response to palmitate treatment. To test this

hypothesis, hepatic cells were treated with 400 μM palmitate and provided either extracellular

glutamine or a combination of α-ketoglutarate and aspartate. Both primary hepatocytes and

H4IIEC3 cells exhibited enhanced lipotoxic cell death when given the mixture of GOT products

rather than glutamine alone (Figure 5.3B).
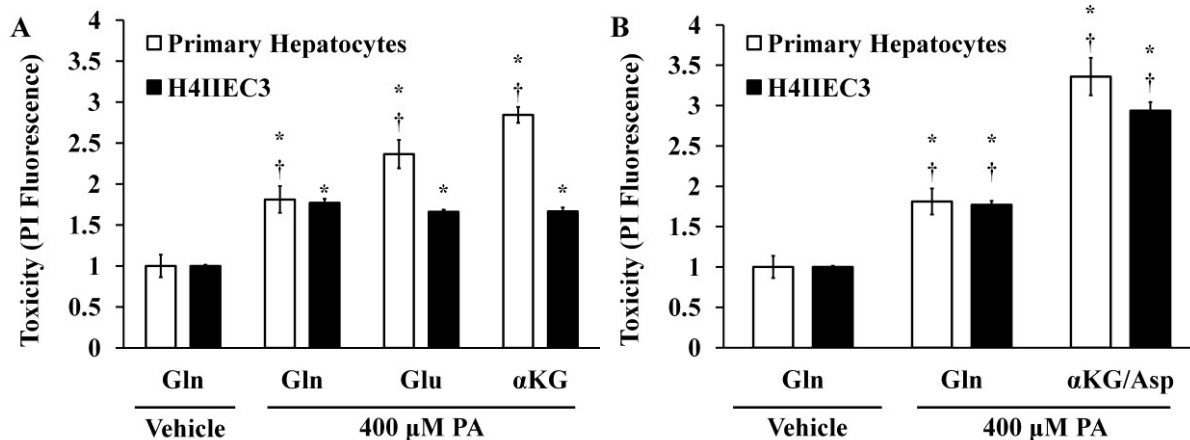
Figure 5.3: Effects of replacing medium glutamine with downstream products of glutamine metabolism. (A) Primary hepatocytes or H4IIEC3 hepatic cells were treated with 400 μM palmitate for 24 hours in the presence of 2 mM glutamine (Gln), glutamate (Glu), or α-ketoglutarate (αKG). Cell death was assessed by PI fluorescence. (B) Relative cell death for primary hepatocytes and H4IIEC3 hepatic cells treated with palmitate in the presence of 2 mM glutamine or a mixture of 1 mM α-ketoglutarate and 1 mM aspartate (αKG/Asp). In both panels, PI fluorescence of palmitate-treated cells is normalized to the response exhibited by vehicle-treated cells (800 μM BSA) provided the same extracellular concentrations of metabolites. Vehicle presented in both cases is for hepatic cells treated with glutamine and vehicle. Other conditions represent a fold change over similar controls. Data represent mean +/- S.E., n=4; *different from vehicle, $p < .05$.

The GOT family of enzymes promotes anaplerosis and lipotoxicity in H4IIEC3 hepatic cells

The observation that products of GOT metabolism enhanced lipotoxicity in both

H4IIEC3 and primary hepatocytes suggests that GOT enzymes play an important role in

providing anaplerotic substrates to fuel CAC activation in response to palmitate treatments.

Thus, we utilized siRNA to selectively modulate glutamate dehydrogenase or GOT metabolic

activities in order to assess these alternative pathways of glutamate anaplerosis. First, we

knocked down mRNA expression of glutamate dehydrogenase using siRNA specific for Glud1.

Knockdown of Glud1 had no effect on palmitate-induced apoptosis, indicating that Glud1 is not a primary metabolic pathway that potentiates lipotoxicity in H4IIEC3 cells (Figure 5.4A). Next, we used siRNA for both the cytosolic and mitochondrial isoforms of GOT, GOT1 and GOT2, respectively. Compared to H4IIEC3 cells treated with a control siRNA (NC1), GOT1 siRNA significantly attenuated caspase activity by approximately 25% after 12 hours of palmitate treatment (Figure 5.4B). Interestingly, GOT2 knockdown attenuated palmitate-induced apoptosis more effectively than GOT1 knockdown (Figure 5.4C). To further confirm these results, we treated H4IIEC3 hepatic cells with the pan-transaminase inhibitor, amino oxyacetic acid (AOA). Co-treatment of H4IIEC3 cells with both 400 μM palmitate and 500 μM AOA resulted in a 50% reduction in palmitate-induced cell death, which was similar to but slightly more effective than GOT2 knockdown (Figure 5.4D).
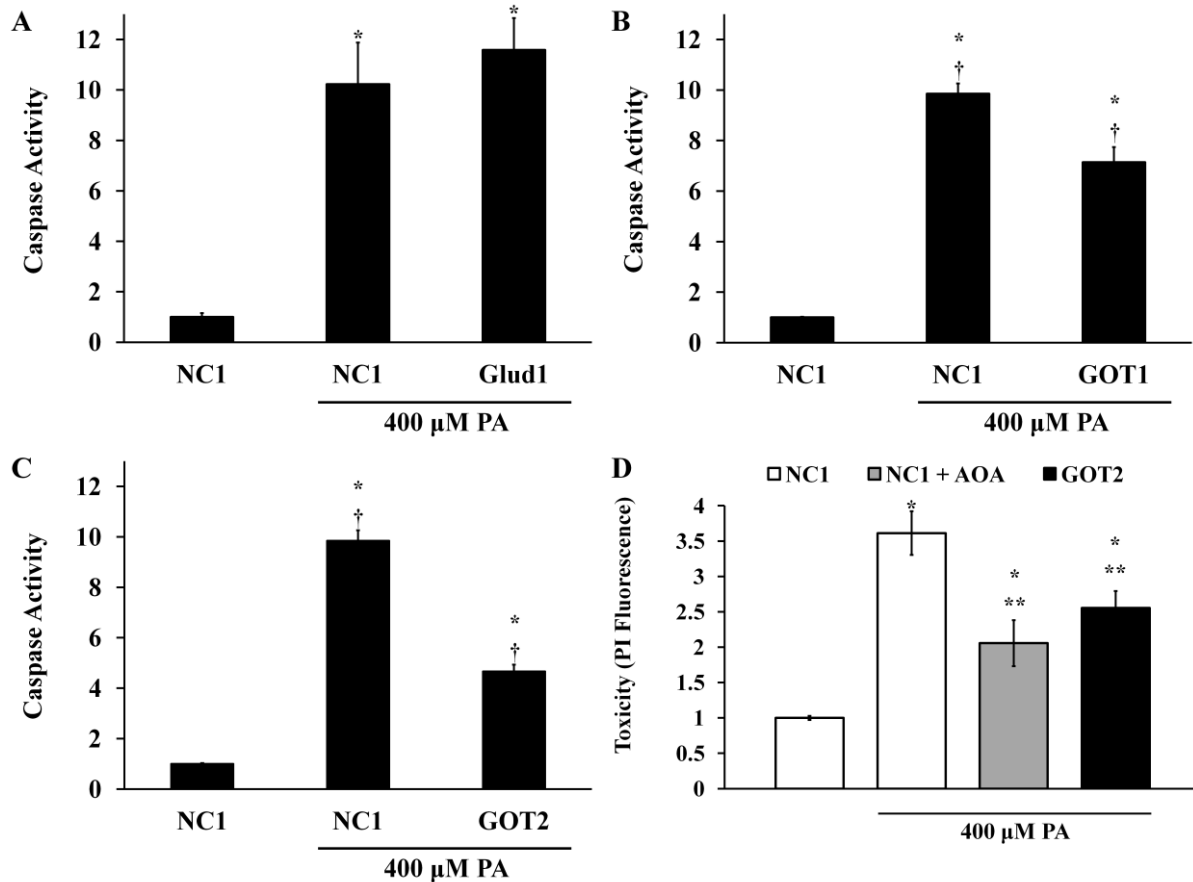
Figure 5.4: GOT metabolism promotes glutamine-dependent palmitate lipotoxicity.
Palmitate-treated H4IIEC3 cells were treated with control siRNA (NC1) or siRNA specific
for (A) Glud1, (B) GOT1, or (C) GOT2 and assayed for markers of apoptosis after 12 hours.
(D) H4IIEC3 cells were treated with 400 μM palmitate in combination with 500 μM of the
transaminase inhibitor AOA and compared to palmitate treated GOT2 knockdown cells. Cell
toxicity was assessed after 24 hours of treatment. All palmitate-treated conditions are
normalized to vehicle-treated cells under the same siRNA conditions. Data represents the
mean +/- S.E., n=4; *different from vehicle, $p < .05$, †different from each other, $p < .05$, **
different from PA, $p < .05$

AOA co-treatment attenuates palmitate-induced oxygen consumption.

Lipotoxic concentrations of palmitate induce metabolic dysfunction characterized by

elevated anaplerosis and oxygen consumption flux in H4IIEC3 hepatic cells (16). To test

whether the lipotoxicity rescue exhibited by GOT inhibition was associated with an overall

decrease in mitochondrial metabolic activity, we measured the oxygen consumption flux of

144

H4IIEC3 cells treated with 400 μM palmitate or a combination of 400 μM palmitate and 500 μM

AOA. Hepatic cells treated with palmitate exhibited a doubling in oxygen consumption flux

compared to vehicle-treated cells. However, co-treatment with AOA attenuated palmitate-

induced oxygen consumption by approximately 30% (Figure 5.5).
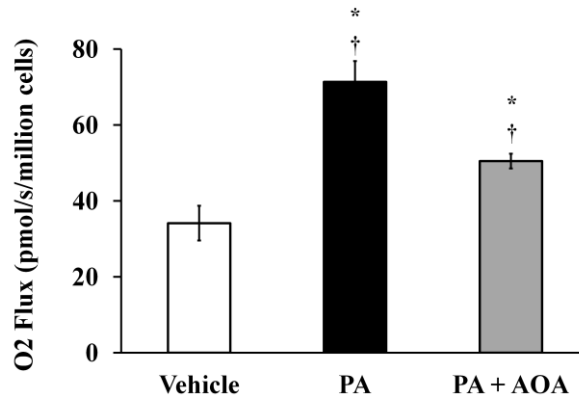
Figure 5.5: AOA reduces palmitate-induced activation of oxidative metabolism. The
oxygen consumption rates of H4IIEC3 cells treated with vehicle (800 μM BSA), 400 μM
palmitate (PA), or a combination of 400 μM palmitate and 500 μM AOA (PA+AOA) were
measured after 6 hours of treatment. Data represent mean +/- S.E., n=3; *different from
vehicle, $p < .05$, †different from each other, $p < .05$.

*AOA transaminase inhibition reduces the magnitude of lipotoxic metabolic deregulation, but
does not reduce the relative CAC/PK flux*

To examine how AOA-inhibition of transaminase activities confers resistance to

palmitate treatments in H4IIEC3 cells, we performed ^{13}C MFA by complete replacement of

medium glutamine with the stable isotope tracer [U-[13]C$_5$]glutamine. We then extracted free

intracellular metabolites and analyzed their isotopic enrichment using GC-MS followed by

correction of the mass isotopomer distributions for natural isotope abundance using the method

of Fernandez et al. (24). Previously, we have observed that palmitate-treated cells incorporate

more [U-^{13}C$_5$]glutamine-derived carbon into CAC intermediates (e.g., malate) relative to vehicle-treated cells, as quantified by their atom percent enrichment (16). The atom percent enrichment (APE) of a metabolite is a measure of its fractional synthesis from the isotopic tracer (i.e., glutamine) versus unlabeled carbon sources (e.g., glucose). Confirming the reported effect of AOA to inhibit transaminase activities, AOA co-treated cells exhibited less isotopic enrichment in the aspartate pool, indicating that GOT activity was effectively blocked (Figure 5.6A). Additionally, compared to palmitate-treated cells, the malate enrichment was significantly lower in cells treated with AOA. Despite these differences, the isotopic enrichment of the glutamate pool was only modestly decreased, suggesting that glutamate synthesis from extracellular glutamine was largely unaffected by AOA co-treatment. Interestingly, co-treating cells with AOA and palmitate increased the APE of both lactate and phosphoenolpyruvate (PEP) compared to cells treated with palmitate alone (Figure 5.6B). This indicates a re-routing of cataplerotic flux leaving the CAC via PEP carboxykinase (PEPCK).
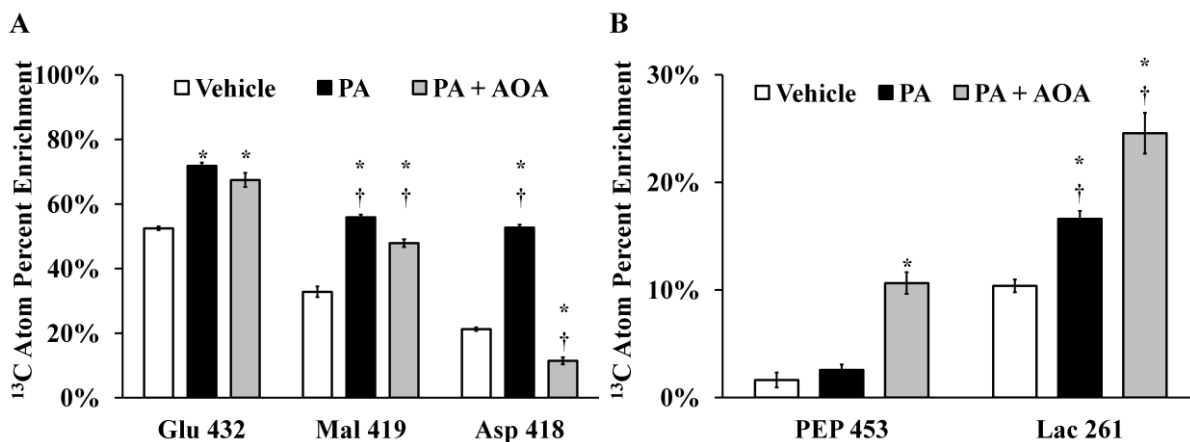
Figure 5.6: Isotopic enrichment of intracellular metabolites indicates flux re-routing in response to AOA treatment. Unlabeled medium glutamine was replaced with [U-$^{13}C_5$]glutamine and used to culture H4IIEC3 cells with vehicle (800 μM BSA), 400 μM palmitate (PA), or a combination of 400 μM palmitate and 500 μM AOA (PA + AOA) added. After extraction and GC-MS analysis of intracellular metabolites, we calculated the atom percent enrichment (APE) of selected metabolites using the formula $APE = 100\% \times \sum_{i=0}^{N} \frac{Mi \times i}{N}$, where N is the number of carbon atoms in the metabolite and Mi is the fractional abundance of the ith mass isotopomer of the metabolite. The fragment ions analyzed for APE were Glu 432, Mal 419, Asp 418, PEP 453, and Lac 261. These ions contain all carbons of the associated parent metabolites (i.e., 5 for glutamate, 4 for malate and aspartate, and 3 for PEP and lactate). Data represent mean +/- S.E., n=3; * different from vehicle, p <.05, †different from each other, p < .05.

Next, we performed ^{13}C metabolic flux analysis by developing a metabolic model consisting of key glycolytic and CAC fluxes and constrained by mass balances on all network metabolites, mass isotopomer balances on all relevant elementary metabolite units (EMUs), and redox balances on NADH and FADH$_2$. Fluxes were estimated by least-squares regression of six mass isotopomer measurements in combination with the measured oxygen uptake rates shown in Figure 5.5 and Figure 5.6. We calculated 14 absolute metabolic fluxes for H4IIEC3 cells treated with vehicle, palmitate, or a combined dose of palmitate and AOA. AOA and palmitate co-treated hepatic cells were characterized by reductions in glutaminase (GLS) and α-ketoglutarate dehydrogenase (ADH) fluxes, although they were still elevated in comparison to vehicle-treated

cells (Figure 5.7A). However, no difference was observed in the citrate synthase flux of cells treated with palmitate alone versus cells co-treated with palmitate and AOA.

Normalizing the intracellular fluxes relative to pyruvate kinase (PK, Figure 5.7B) demonstrates that the mitochondrial alterations associated with lipotoxicity are associated with enhanced glutamine anaplerosis and a decrease in pyruvate carboxylase (PC)-dependent CAC anaplerosis (Figure 5.7C). Interestingly, although AOA co-treatment reduced the absolute calculated, normalization to PK flux reveals that the relative mitochondrial metabolism is still upregulated as marked by increases in the relative GLS/PK, CS/PK, and ADH/PK fluxes compared to both vehicle- and palmitate-treated hepatic cells. That is, in the inhibition of the transaminase pathways using AOA, palmitate-treated cells still prefer to metabolize glutamine for anaplerosis instead of glucose.

Net glutamate anaplerotic flux into the CAC must balance the net cataplerotic flux leaving the cycle (20). In our previous MFA models, glutamine carbon entering the CAC as α-ketoglutarate could leave the CAC through either malic enzyme or CO_2. Here, our updated model includes the PEPCK reaction, which produces PEP and CO_2 from oxaloacetate. Both vehicle-treated and palmitate-treated cells were marked by similar absolute PEPCK fluxes, indicating that this pathway is not the preferred route of cataplerosis in the H4IIEC3 model of lipotoxicity. Instead, flux through malic enzyme was the main mode of cataplerosis. On the other hand, AOA co-treatment was marked by a significant increase in PEPCK flux relative to cells treated with palmitate alone. This is likely required to balance the anaplerotic flux from glutamine in response to the observed reduction in malic enzyme flux. Although the absolute rate of glutamine entry was reduced by AOA treatment, the reduction in malic enzyme flux was even

more dramatic, which apparently precipitates activation of PEPCK in order to maintain carbon

balance at the malate and oxaloacetate nodes (Figure 5.8).
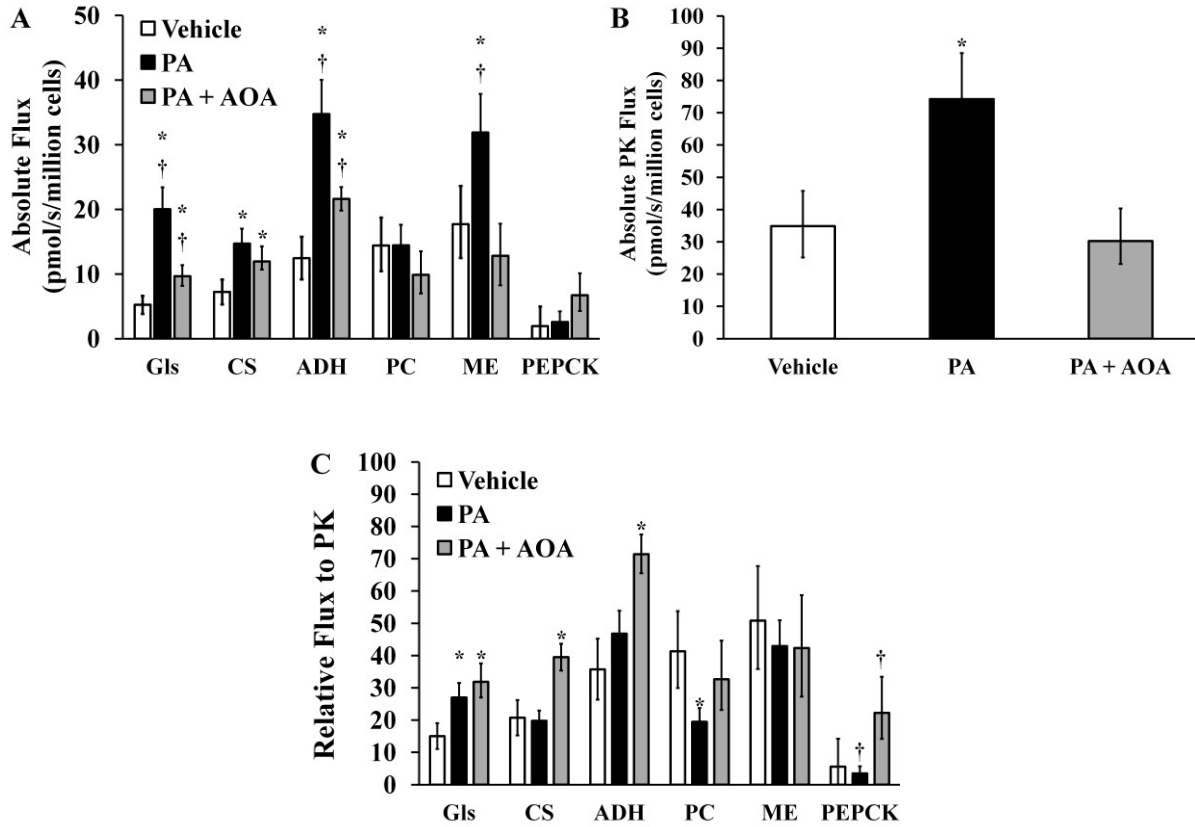
Figure 5.7: **^{13}C MFA reveals that AOA treatment reduces mitochondrial fluxes and re-routes malic enzyme flux in the presence of palmitate.** (A) Absolute intracellular CAC fluxes were calculated as detailed in the Methods section and Appendix for H4IIEC3 cells under the following conditions: vehicle, 400 μM palmitate (PA), or 400 μM palmitate and 500 μM AOA (PA + AOA). (B) Absolute PK flux. (C) Calculated fluxes relative to pyruvate kinase flux (PK) demonstrate that AOA co-treatment is associated with enhanced glutamate anaplerosis, despite a reduction in absolute mitochondrial fluxes. Units are pmol/s/million cells. Error bars indicate 95% confidence intervals; * different from vehicle, $p < .05$, † different from each other, $p < .05$.
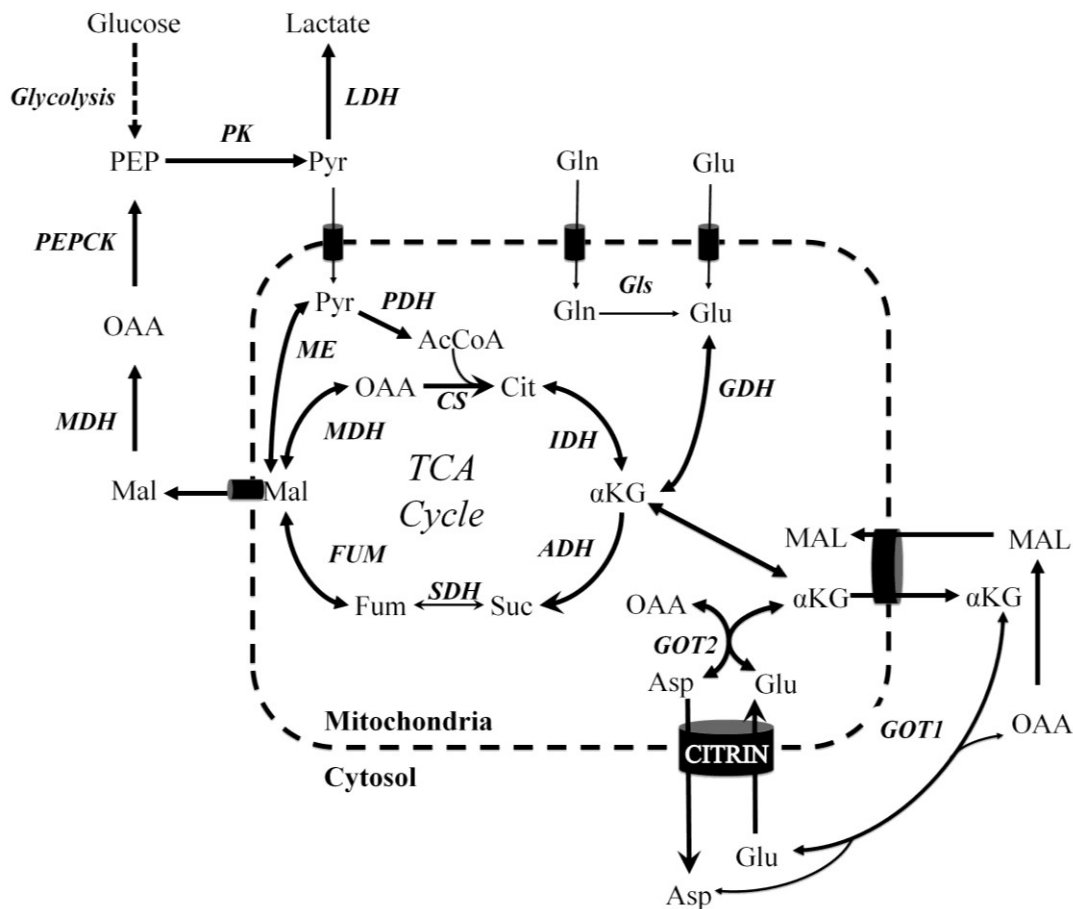
Figure 5.8: Metabolic pathways and putative mechanisms explored in this study. Mechanisms of αKG anaplerosis were inhibited using siRNA and the pharmacological inhibitor AOA. GOT2 metabolism potentiated lipoapoptosis more than other anaplerotic mechanisms. Additionally, simultaneous inhibition of GOT1/GOT2 suppressed lipotoxic dysregulations of mitochondrial metabolism. Combined with Chapter 4, these results suggest a role for the calcium stimulated glutamate/aspartate antiporter citrin, which is known to potentiate mitochondrial metabolism of glutamate.

Discussion

Hepatic lipotoxicity in H4IIEC3 cells is characterized by enhanced CAC anaplerosis fueled by glutamate derived from extracellular glutamine (14,16). However, it is unclear whether this glutamine anaplerosis is mediated solely by the glutamate dehydrogenase or glutamate transaminase enzymes, and whether inhibition of these glutamine-dependent anaplerotic pathways would fully suppress the lipotoxic phenotype. In the current study, we

altered media glutamine concentrations to define a mechanism by which extracellular glutamine controls the rate of palmitate-induced apoptosis in both primary hepatocytes and H4IIEC3 hepatic cells. Replacing the extracellular glutamine with its downstream metabolic products (e.g., glutamate, α-ketoglutarate, etc.) revealed that glutamine exerts its pro-apoptotic effects by enhancing mitochondrial anaplerosis and not simply by the accumulation of other metabolic byproducts. Inhibition of glutamate conversion to α-ketoglutarate using siRNA specific for Glud1, GOT1, or GOT2 indicated that glutamine enhances palmitate lipotoxicity through GOT activity, primarily through GOT2. Pharmacological transaminase inhibition using AOA confirmed these results. Despite a partial rescue in lipotoxic cell death, $[U-^{13}C_5]$glutamine tracer studies demonstrated that AOA co-treatment merely attenuates the overall metabolic dysregulation in lipotoxicity but does not fully restore CAC associated fluxes to basal levels. Overall, these results demonstrate a novel role for GOT enzymes in palmitate lipotoxicity, which depends on their ability to provide substrates for CAC anaplerosis.

Alterations in amino acid metabolism have been linked to obesity, NAFLD, and NASH (8,10). In particular, elevated plasma glutamate/glutamine levels have been reported as a potential risk factor for NAFLD. Additionally, in the methionine-choline deficient (MCD) diet-induced murine NASH model, increases in plasma glutamate and glutamine were paralleled by increases in liver concentrations of these amino acids (8). The authors attributed these elevations to inhibited liver gluconeogenesis and CAC flux in MCD-fed mice. In contrast, a different study demonstrated that mice fed a high-fat diet developed fatty liver and insulin resistance characterized by a high CAC flux (4). Our models of lipotoxicity in the H4IIEC3 hepatic cell line and primary hepatocytes exhibit similarities with these two *in vivo* studies. First, palmitate overload induces mitochondrial dysfunction characterized by elevated CAC flux. Second, the

presence of elevated glutamine or downstream glutamine metabolites (e.g., glutamate, α-ketoglutarate, or α-ketoglutarate combined with aspartate) synergizes with palmitate to enhance lipotoxicity.

It was important to first confirm that glutamine anaplerosis was occurring in primary hepatocytes due to differing reports on the role of glutaminase in primary hepatocytes versus immortalized cell lines (such as the H4IIEC3 hepatic cell line used in our prior studies). *In vivo*, glutaminase is not expressed equally across the liver (25). Therefore, while specific regions of the liver are known to catabolize glutamine in the post-absorptive state, not all cells obtained in our primary hepatocyte isolations would be expected to exhibit identical avidity for glutamine. Despite this, removal of medium glutamine from both H4IIEC3 hepatic cells and primary hepatocytes attenuated palmitate-induced cell death to similar extents, suggesting a common ability of glutamine to stimulate lipotoxicity in both cell types.

Unlike glutamine, glutamate metabolism is not restricted to a small subpopulation of liver cells. Rather, it is involved as a critical intermediate in the metabolism of several different amino acids. It is also an important anaplerotic substrate due to its ease of conversion to the CAC intermediate α-ketoglutarate by glutamate dehydrogenase (GDH) and glutamate oxaloacetate transaminase (GOT). In studies with primary hepatocytes, substituting glutamate for glutamine resulted in an increase in lipotoxic cell death, likely due to higher affinity for glutamate by primary cells. On the other hand, H4IIEC3 cells exhibited equivalent cell death in response to palmitate with either glutamine or glutamate added. Cell immortalization is typically associated with increases in glutamine metabolism and could explain why glutamine and glutamate exert similar effects to promote lipotoxicity in the H4IIEC3 cell line (21,26).

Anaplerosis of α-ketoglutarate into the CAC can occur through Glud1, cytosolic GOT1, and mitochondrial GOT2. To further examine the differences between Glud1 and GOT isoforms, hepatic cells were treated with a combination of α-ketoglutarate and aspartate in the absence of glutamine to mimic the downstream metabolic products of the GOT enzymatic reaction. The combined dose of extracellular α-ketoglutarate and aspartate supplied to palmitate-treated cells was more toxic than glutamine alone, indicating that transaminase metabolism is potentially the primary metabolic route by which extracellular glutamine enhances lipotoxicity. We then applied siRNA for Glud1, GOT1, or GOT2 to specifically inhibit these enzymes in the H4IIEC3 cell line. Although our hepatic cell model expresses all of these enzymes, only knockdown of GOT1 or GOT2 attenuated palmitate-dependent apoptosis. The inability of Glud1 to reduce the toxic effects of palmitate indicates that glutamate dehydrogenase does not play a significant role in glutamate anaplerosis of H4IIEC3 hepatic cells under these conditions.

Both cytosolic GOT1 and mitochondrial GOT2 are reversible reactions which convert an amino acid (glutamate or aspartate) to an α-ketoacid (α-ketoglutarate or oxaloacetate). Additionally both are involved in the malate-aspartate shuttle, which functions to transport cytosolic reducing equivalents (NADH) to the mitochondria to be used for oxidative phosphorylation. In principle, upregulated GOT activity can therefore account for the increased oxygen consumption exhibited by palmitate-treated hepatic cells by providing more α-ketoglutarate for CAC oxidative metabolism and by shuttling more reducing equivalents into the mitochondria via the malate-aspartate shuttle. However, this implies a synergy between both GOT1 and GOT2 that we do not observe in our experiments. While knockdown of either GOT1 or GOT2 is associated with attenuations in hepatic lipotoxicity, GOT2 had a greater effect to reduce markers of apoptosis. This suggests that palmitate overload is able to mechanistically

disrupt GOT2 metabolism prior to GOT1 metabolism. An alternative would be that cytosolic enzymes could compensate for GOT1 that GOT2 inhibition.

In addition to siRNA-mediated knockdowns, we co-treated hepatic cells with the transaminase inhibitor AOA in the presence of a lipotoxic palmitate load. AOA co-treatment attenuated lipotoxicity to a similar extent as GOT2 knockdown in H4IIEC3 cells. ^{13}C MFA studies demonstrated that AOA significantly decreased glutamine anaplerosis, oxygen consumption, and ADH flux, all of which are characteristic of palmitate overload in hepatic cells. Despite the attenuation in mitochondrial fluxes, cells co-treated with AOA and palmitate were still marked by higher relative fluxes (normalized to PK flux) of glutamine anaplerosis, CS flux, and ADH flux in comparison to vehicle-treated cells. This failure to normalize relative glutamine anaplerotic fluxes suggests that an alternate upstream mechanism predisposes the hepatic cells to a glutamine/glutamate avid state in response to palmitate treatment.

Previously, we demonstrated a novel role for intracellular calcium to promote lipotoxicity by inducing metabolic dysfunction and oxidative stress (Chapter 4). In that study, co-treating hepatic cells with palmitate and the intracellular calcium chelator BAPTA decreased mitochondrial metabolism characterized by lower oxygen consumption flux and less glutamine uptake compared to cells treated with palmitate alone. Additionally, the Asp G-parameter calculated for cells treated with BAPTA and palmitate was lower than the G-parameter for cells treated with palmitate alone (Chapter 4 Appendix). These results pointed to a novel, putative role for the glutamate-aspartate antiporter citrin in lipotoxicity (Figure 5.8). The activity of this antiporter is enhanced by elevations in cytosolic calcium, which may increase glutamate entry into the mitochondria in exchange for aspartate (23). Hypothetically, the net result of citrin activation in the context of palmitate lipotoxicity would be an enhancement in oxygen

consumption and glutamate anaplerosis due to GOT2 metabolism. Combined with the observation that the pan-transaminase inhibitor AOA reduced lipotoxic oxygen consumption, aspartate formation, and overall CAC flux, it appears that palmitate overload primarily exerts its lipotoxic effects through a synergism between calcium signaling and GOT2-dependent anaplerosis.

Appendix

RT-PCR confirms knockdown efficiency of siRNA techniques

To choose siRNA targeting sequences, hepatic cells were treated with at least two different siRNA for each metabolic enzyme targeting different sequences.
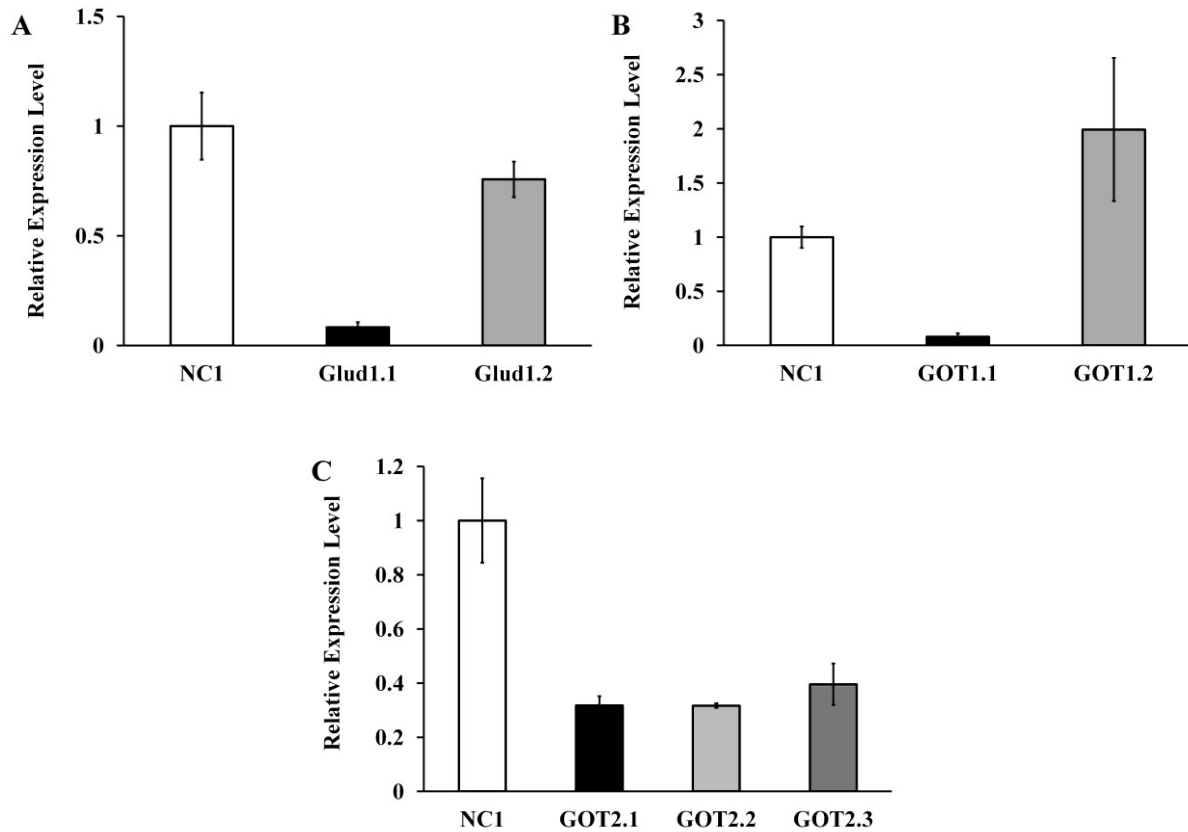
Figure 5.A1: Knockdown efficiency of siRNA targeting sequences on target RNA levels. RT-PCR was used to confirm knockdown efficiency of different targeting siRNA on the targeted RNA. Specifically Glud1.1, GOT1.1, and GOT2.1 targeting sequences were selected for all experiments presented in the main text due to their ability to significantly reduce the relative expression of the targeted sequence in comparison to a scrambled control siRNA. Glud1.2 and GOT1.2 were ineffective at reducing the expression level of their target mRNA.

Metabolic Flux Analysis (MFA) reaction network and modeling assumptions

The following assumptions were used to estimate intracellular fluxes for the reaction network in

Table 5A1 using isotope labeling data for the metabolites in Table 5A2:

1) All measurements were performed at isotopic steady state.

2) Labeled CO_2 produced by CAC oxidation was not reincorporated into central

   metabolism.

3) Metabolite usage for biomass synthesis was negligible.

4) Similarly, due the presence of excess exogenous palmitate and low cell growth, ATP

   citrate lyase activity was assumed to be negligible.

5) We previously found beta-oxidation of palmitate does not contribute significant amount

   of carbon to the CAC (27). Therefore, only carbon entering the CAC derived from

   glucose or glutamine was considered.

6) The oxygen consumption flux was assumed to satisfy the requirements for re-oxidizing

   NADH produced in both the CAC and glycolysis, in order to maintain redox balance.

   Our model cannot discriminate between NADH- and NADPH-dependent isoforms of

   IDH or malic enzyme. Therefore, we have modeled these enzymatic reactions as NADH-

   dependent due to the presence of mitochondrial transhydrogenase that can interconvert

   NADPH and NADH. This assumption will produce the most conservative estimates for

   flux differences between the tested treatments.

7) To account for incomplete isotopic steady state in the measured aspartate pool, we have

   included a *G* parameter. This value represents the fraction of the total aspartate pool that

   was synthesized in the presence of the isotopic tracer (28).

8) Malate and oxaloacetate are assumed to be in complete equilibrium. Since nearly identical enrichment of both malate and aspartate were observed.

9) PEP labeling was added to the model to account for possible PEPCK activity.

Our metabolic model uses ^{13}C enrichment of CAC related metabolites derived from [U-^{13}C$_5$]glutamine. When combined with whole cell oxygen consumption, quantification of absolute carbon fluxes is possible. This method produces conservative estimates of intracellular fluxes and minimizes potential errors associated with models that use only carbon balancing to calculate CAC flux (29,30). Figures 5A2-4 along and Tables 5A3-5 detail modeling results. We report both the degrees of freedom (DOF) and the best-fit sum-of-squared residuals (SSR), which together indicate the goodness-of-fit for each experiment. We define exchange fluxes as

$$v_{exch}^{[0,100]} = 100 \times \frac{v_{exch}}{v_{exch}+v_{ref}},$$ where v_{ref} is the citrate synthase flux value (31).

Table 5A.1: Reactions and atom transitions for metabolic flux analysis of H4IIEC3 rat hepatomas. Dot suffixes denote specific sub-pools of metabolite: .x, extracellular; .t, tracer; .d, dilution.

Pyruvate Metabolism			Reaction Name
½ Glucose (abcdef)	→	½ PEP (cba) + ½ PEP (def) + NADH	Glucose Uptake
PEP (abc)	→	Pyr (abc)	PK
Pyr (abc) + CO_2 (d)	→	Mal (abcd)	PC
Mal (abcd)	→	Pyr (abc) + CO_2 (d) + NADH	ME
Pyr (abc)	→	AcCoA (bc) + CO_2 (a) + NADH	PDH
Pyr (abc) + NADH	→	Lac (abc)	LDH
Mal (abcd)	→	PEP (abc) + NADH + CO_2 (d)	PEPCK
CAC Metabolism			
AcCoA (ab) + Mal (cdef)	→	Cit (fedbac) + NADH	CS
Cit (abcdef)	←→	Akg (abcde) + CO_2 (f) + NADH	IDH
Akg (abcde)	→	Suc (½ bcde + ½ edcb) + CO_2 (a) + NADH	ADH
Suc (½ abcd + ½ dcba)	←→	Fum (½ abcd + ½ dcba) + $FADH_2$	SDH
Fum (½ abcd + ½ dcba)	←→	Mal (abcd)	FUS
Glutamine anaplerosis			
Gln (abcde)	→	Glu (abcde)	GLS
Glu (abcde)	←→	Akg (abcde)	GDH
Oxygen Consumption			
2 NADH + O_2	→	2 H_2O	
2 $FADH_2$ + O_2	→	2 H_2O	
Dilution			
Asp.d (abcd)	→	Asp (abcd)	Asp G parameter

Table 5A.2: GC-MS ions used for metabolic flux analysis. The reported standard error (SEM) is representative of the calculated error amongst n=3 biological replicates.

Metabolite	Mass	Composition	Carbons					SEM (mol%)		
								Veh	PA	PA+ AOA
Gln	431	$C_{19}H_{43}O_3N_2Si_3$	1	2	3	4	5	0.7	0.5	1.6
Glu	432	$C_{19}H_{42}O_4NSi_3$	1	2	3	4	5	0.57	1.0	1.7
Glu	330	$C_{16}H_{36}O_2NSi_2$		2	3	4	5	0.77	1.0	2.0
Mal	419	$C_{18}H_{39}O_5Si_3$	1	2	3	4		1.67	0.88	1.2
Asp	390	$C_{17}H_{40}O_3NSi_3$		2	3	4		1.5	1.3	1.2
Asp	418	$C_{18}H_{40}O_4NSi_3$	1	2	3	4		0.86	0.9	1.1
Lac	233	$C_{10}H_{25}O_2Si_2$		2	3			0.65	0.5	1.8
Lac	261	$C_{11}H_{25}O_3Si_2$	1	2	3			0.6	0.64	1.9
PEP	453	$C_{14}H_{38}O_6Si_3P$	1	2	3			0.7	0.5	1.0

Table 5A.3: Calculated absolute flux parameters and 95% confidence intervals for vehicle cells. Net flux units are pmol/million cells/s. Exchange fluxes and dilution parameters are scaled from 0 to 100%. SSR = 47.1 (36 DOF).

Parameter	Value	95% Confidence Interval	
Net Flux			
Glucose Uptake	32.9	[23.9,	42.8]
PK	34.9	[25.1,	45.8]
PDH	7.2	[5.3,	9.1]
CS	7.2	[5.3,	9.1]
IDH	7.2	[5.3,	9.1]
GLS	5.2	[3.8,	6.6]
GDH	5.2	[3.8,	6.6]
ADH	12.5	[9.2,	15.8]
SDH	12.5	[9.2,	15.8]
FUS	12.5	[9.2,	15.8]
ME	17.7	[12.5,	23.6]
PC	14.4	[10.4	18.7]
LDH	30.9	[22.4,	40.4]
PEPCK	1.9	[0.0	5.0]
O_2 Consumption	34.1	[25.2,	43.1]
Exchange Flux			
IDH	0.2	[0,	100]
SDH	0.0	[0,	100]
FUS	100	[2.5,	100]
GDH	100	[12.0,	100]
Dilution			
Asp G Parameter	76.8	[69.7,	84.2]
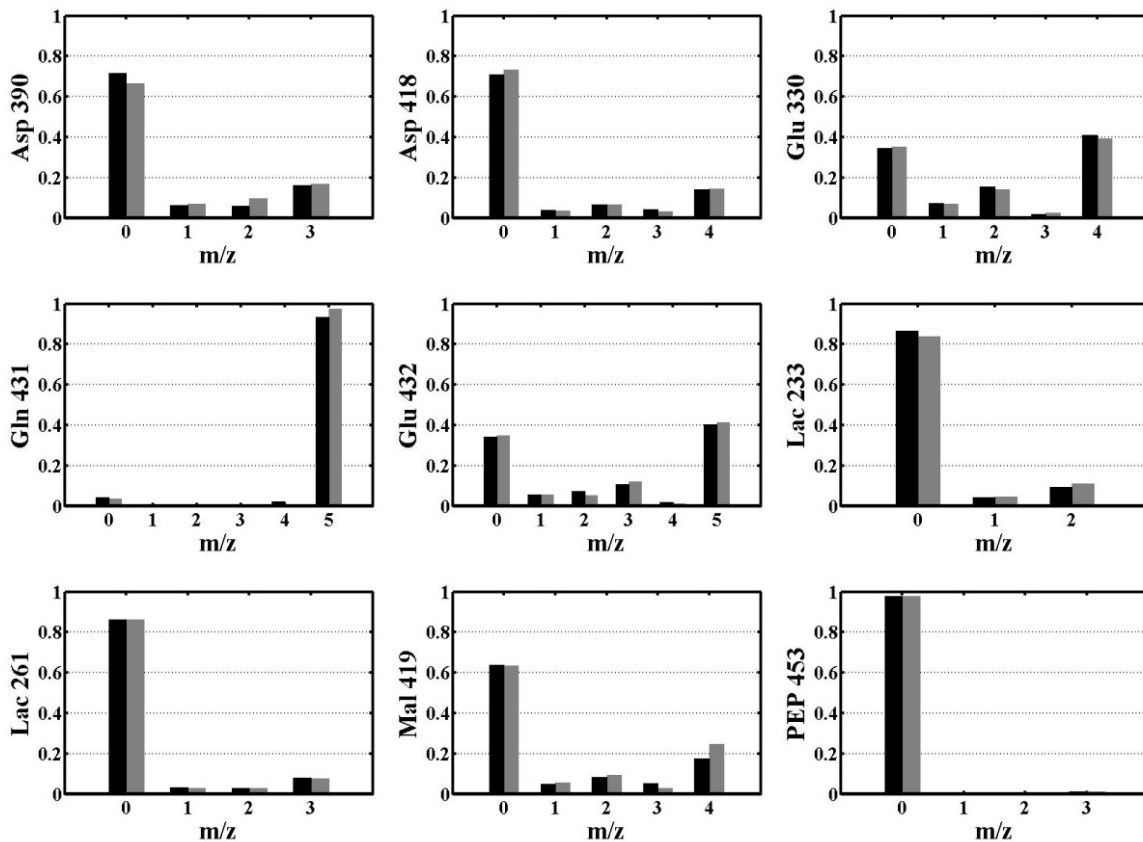
Figure 5A 2. Simulated and measured mass isotopomer distributions for vehicle treated H4IIEC3 hepatic cells. Simulated distributions are shown for best-fit flux estimates. Data are corrected for natural abundance.

162

Table 5A.4: Calculated absolute flux parameters and 95% confidence intervals for palmitate-treated cells. Net flux units are pmol/million cells/s. Exchange fluxes and dilution parameters are scaled from 0 to 100%. SSR = 46.0 (39 DOF).

Parameter	Value	95% Confidence Interval
Net Flux		
Glucose Uptake	71.7	[59.3, 85.3]
PK	74.3	[61.4, 88.5]
PDH	14.7	[12.4, 17.0]
CS	14.7	[12.4, 17.0]
IDH	14.7	[12.4, 17.0]
GLS	20.0	[16.8, 23.4]
GDH	20.0	[16.8, 23.4]
ADH	34.7	[29.5, 40]
SDH	34.7	[29.5, 40]
FUS	34.7	[29.5, 40]
ME	31.9	[26.4, 37.8]
PC	14.4	[11.7, 17.6]
LDH	77.0	[63.2, 92.4]
PEPCK	2.6	[1.1, 4.2]
O_2 Consumption	71.3	[60.6, 80.2]
Exchange Flux		
IDH	0.1	[0, 100]
SDH	0	[0, 100]
FUS	100	[0, 100]
GDH	21.9	[8.1, 100]
Dilution		
Asp G Parameter	97.7	[93.9, 100]
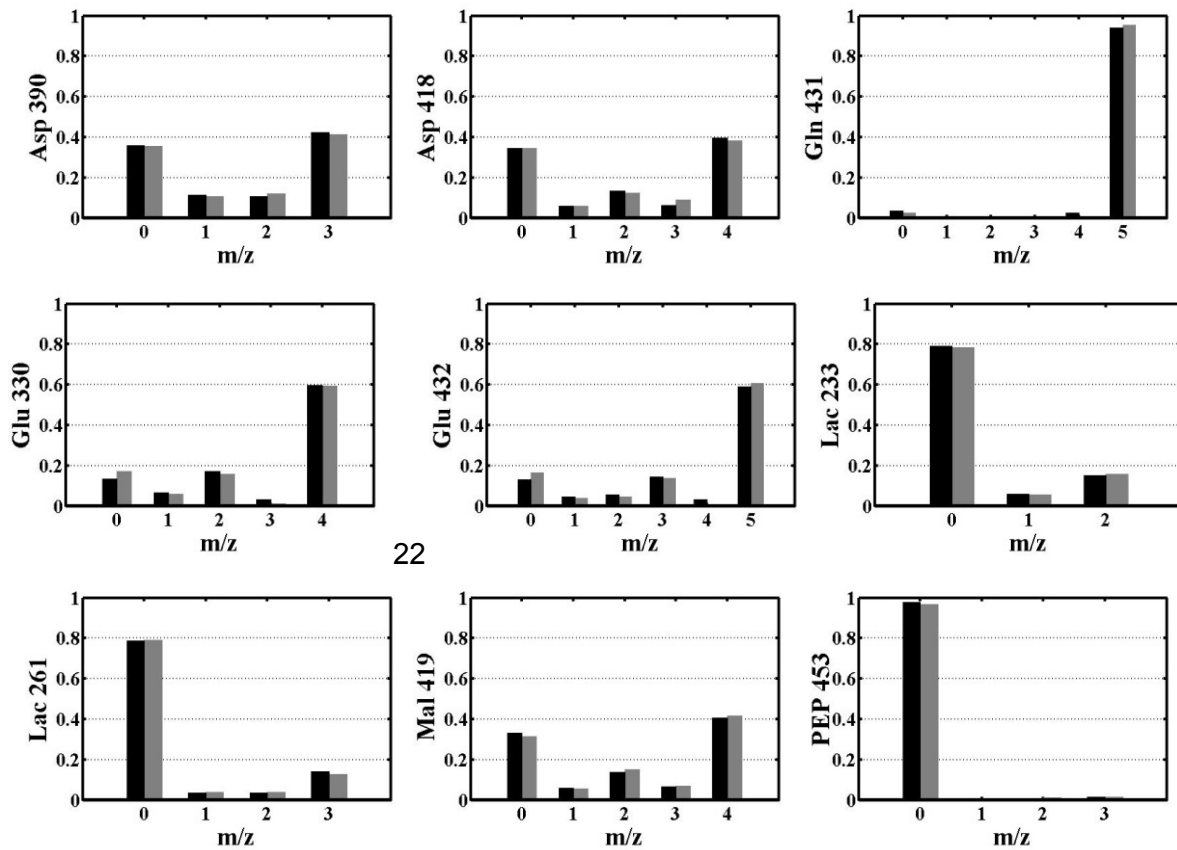
Figure 5A.3: Simulated and measured mass isotopomer distributions for palmitate-treated H4IIEC3 hepatic cells. Simulated distributions are shown for best-fit flux estimates. Data are corrected for natural abundance.

Table 5A.5: Calculated absolute flux parameters and 95% confidence intervals for palmitate and AOA co-treated cells. Net flux units are pmol/million cells/s. Exchange fluxes and dilution parameters are scaled from 0 to 100%. SSR = 19.0 (37 DOF).

| Parameter	Value	95% Confidence Interval
Net Flux		
Glucose Uptake	23.5	[18.5, 31.2]
PK	30.3	[23.2, 40.4]
PDH	12.0	[10.7, 13.2]]
CS	12.0	[10.7, 13.2]]
IDH	12.0	[10.7, 13.2]]
GLS	9.7	[8.2, 11.4]
GDH	9.7	[8.2, 11.4]
ADH	21.6	[19.8, 23.5]
SDH	21.6	[19.8, 23.5]
FUS	21.6	[19.8, 23.5]
ME	12.8	[8.3, 17.8]
PC	9.9	[7.0, 13.5]
LDH	21.2	[14.6, 30.1]
PEPCK	6.7	[4.4, 10.0]
O_2 Consumption	50.5	[46.6, 54.3
Exchange Flux		
IDH	0.4	[0, 100]
SDH	0.0	[0, 100]
FUS	100	[0, 100]
GDH	3.4	[1.6, 15.5]
Dilution		
Asp G Parameter	24.7	[20.1, 29.2]
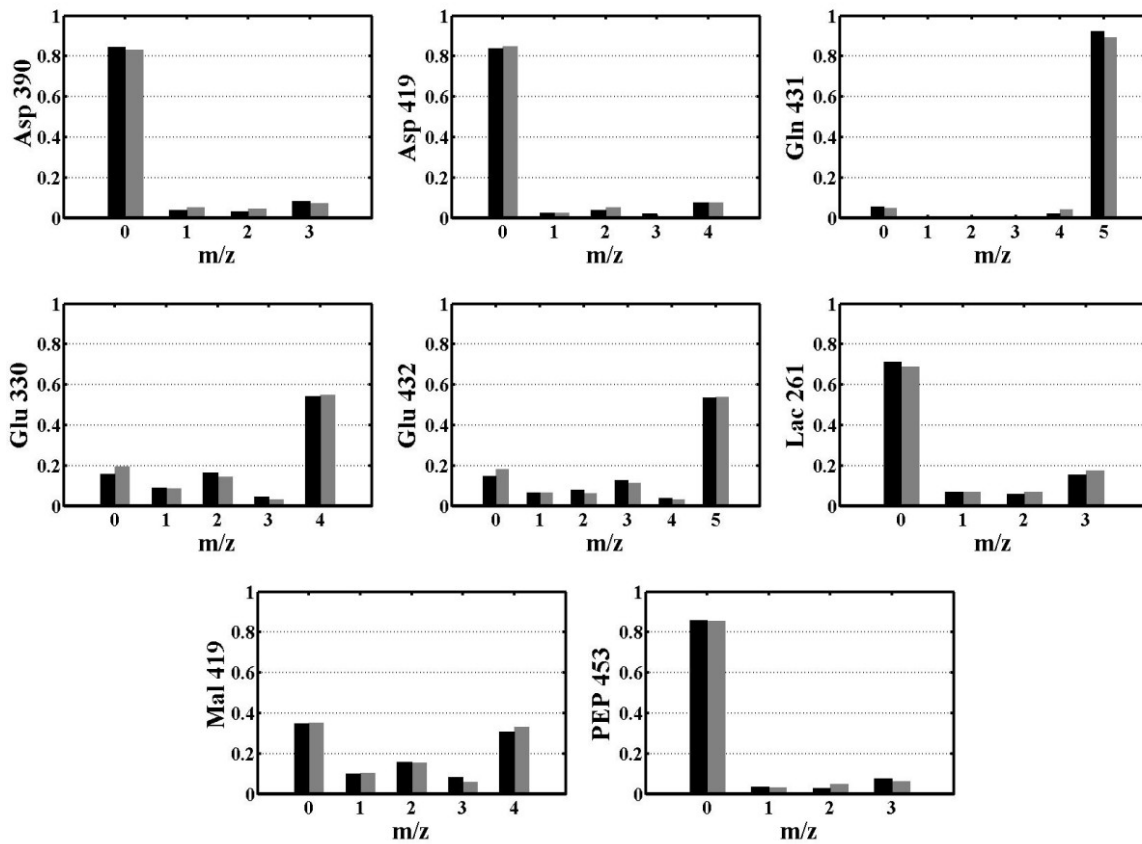
Figure 5A 4: Simulated and measured mass isotopomer distributions for AOA and palmitate co-treated H4IIEC3 hepatic cells. Simulated distributions are shown for best-fit flux estimates. Data are corrected for natural abundance. Lac233 could not be reliable measured in these cells.

References

1. Serviddio, G., Bellanti, F., Tamborra, R., Rollo, T., Romano, A. D., Giudetti, A. M., Capitanio, N., Petrella, A., Vendemiale, G., and Altomare, E. (2008) Alterations of hepatic ATP homeostasis and respiratory chain during development of non-alcoholic steatohepatitis in a rodent model. *European Journal of Clinical Investigation* **38**

2. Perez-Carreras, M., Del Hoyo, P., Martin, M. A., Rubio, J. C., Martin, A., Castellano, G., Colina, F., Arenas, J., and Solis-Herruzo, J. A. (2003) Defective hepatic mitochondrial respiratory chain in patients with nonalcoholic steatohepatitis. *Hepatology* **38**

3. Sanyal, A. J., Campbell-Sargent, C., Mirshahi, F., Rizzo, W. B., Contos, M. J., Sterling, R. K., Luketic, V. A., Shiffman, M. L., and Clore, J. N. (2001) Nonalcoholic steatohepatitis: Association of insulin resistance and mitochondrial abnormalities. *Gastroenterology* **120**, 1183-1192

4. Satapati, S., Sunny, N. E., Kucejova, B., Fu, X. R., He, T. T., Mendez-Lucas, A., Shelton, J. M., Perales, J. C., Browning, J. D., and Burgess, S. C. (2012) Elevated TCA cycle function in the pathology of diet-induced hepatic insulin resistance and fatty liver. *Journal of Lipid Research* **53**, 1080-1092

5. Sunny, N. E., Parks, E. J., Browning, J. D., and Burgess, S. C. (2011) Excessive hepatic mitochondrial TCA cycle and gluconeogenesis in humans with nonalcoholic fatty liver disease. *Cell Metab* **14**, 804-810

6. Li, Z. Z., Berk, M., McIntyre, T. M., and Feldstein, A. E. (2009) Hepatic Lipid Partitioning and Liver Damage in Nonalcoholic Fatty Liver Disease ROLE OF STEAROYL-CoA DESATURASE. *Journal of Biological Chemistry* **284**, 5637-5644

7.   Puri, P., Baillie, R. A., Wiest, M., Mirshahi, F., and Sanyal, A. J. (2006) A lipidomic analysis of non-alcoholic fatty liver disease (NAFLD). *Journal of Hepatology* **44**, S260-S261

8.   Li, H., Wang, L., Yan, X., Liu, Q., Yu, C., Wei, H., Li, Y., Zhang, X., He, F., and Jiang, Y. (2011) A Proton Nuclear Magnetic Resonance Metabonomics Approach for Biomarker Discovery in Nonalcoholic Fatty Liver Disease. *Journal of Proteome Research* **10**, 2797-2806

9.   Boulangé, C. L., Claus, S. P., Chou, C. J., Collino, S., Montoliu, I., Kochhar, S., Holmes, E., Rezzi, S., Nicholson, J. K., Dumas, M. E., and Martin, F.-P. J. (2013) Early Metabolic Adaptation in C57BL/6 Mice Resistant to High Fat Diet Induced Weight Gain Involves an Activation of Mitochondrial Oxidative Pathways. *Journal of Proteome Research* **12**, 1956-1968

10.   Newgard, C. B., An, J., Bain, J. R., Muehlbauer, M. J., Stevens, R. D., Lien, L. F., Haqq, A. M., Shah, S. H., Arlotto, M., Slentz, C. A., Rochon, J., Gallup, D., Ilkayeva, O., Wenner, B. R., Yancy Jr, W. S., Eisenson, H., Musante, G., Surwit, R. S., Millington, D. S., Butler, M. D., and Svetkey, L. P. (2009) A Branched-Chain Amino Acid-Related Metabolic Signature that Differentiates Obese and Lean Humans and Contributes to Insulin Resistance. *Cell Metabolism* **9**, 311-326

11.   Cheng, S., Rhee, E. P., Larson, M. G., Lewis, G. D., McCabe, E. L., Shen, D., Palma, M. J., Roberts, L. D., Dejam, A., Souza, A. L., Deik, A. A., Magnusson, M., Fox, C. S., O'Donnell, C. J., Vasan, R. S., Melander, O., Clish, C. B., Gerszten, R. E., and Wang, T. J. (2012) Metabolite Profiling Identifies Pathways Associated With Metabolic Risk in Humans. *Circulation* **125**, 2222-2231

12. Soga, T., Sugimoto, M., Honma, M., Mori, M., Igarashi, K., Kashikura, K., Ikeda, S., Hirayama, A., Yamamoto, T., Yoshida, H., Otsuka, M., Tsuji, S., Yatomi, Y., Sakuragawa, T., Watanabe, H., Nihei, K., Saito, T., Kawata, S., Suzuki, H., Tomita, M., and Suematsu, M. (2011) Serum metabolomics reveals γ-glutamyl dipeptides as biomarkers for discrimination among different forms of liver disease. *Journal of Hepatology* **55**, 896-905

13. Sookoian, S., and Pirola, C. J. (2012) Alanine and aspartate aminotransferase and glutamine-cycling pathway: Their roles in pathogenesis of metabolic syndrome. *World Journal of Gastroenterology* **18**, 3775-3781

14. Noguchi, Y., Young, J., Aleman, J., Hansen, M., Kelleher, J., and Stephanopoulos, G. (2009) Effect of Anaplerotic Fluxes and Amino Acid Availability on Hepatic Lipoapoptosis. *Journal of Biological Chemistry* **284**, 33425-33436

15. Sunny, N. E., Parks, E. J., Browning, J. D., and Burgess, S. C. (2011) Excessive Hepatic Mitochondrial TCA Cycle and Gluconeogenesis in Humans with Nonalcoholic Fatty Liver Disease. *Cell Metab* **14**, 804-810

16. Egnatchik, R. A., Leamy, A. K., Noguchi, Y., Shiota, M., and Young, J. D. (2013) Palmitate-induced Activation of Mitochondrial Metabolism Promotes Oxidative Stress and Apoptosis in H4IIEC3 Rat Hepatocytes. *Metabolism: clinical and experimental*

17. Shiota, M., Inagami, M., Fujimoto, Y., Moriyama, M., Kimura, K., and Sugano, T. (1995) Cold acclimation induces zonal heterogeneity in gluconeogenic responses to glucagon in rat liver lobule. *American Journal of Physiology* **268**, E1184-E1191

18. Young, J. D. (2014) INCA: A computational platform for isotopically nonstationary metabolic flux analysis. *Bioinformatics*

19. Antoniewicz, M. R., Kelleher, J. K., and Stephanopoulos, G. (2006) Determination of confidence intervals of metabolic fluxes estimated from stable isotope measurements. *Metab Eng* **8**, 324-337

20. Brosnan, M. E., and Brosnan, J. T. (2009) Hepatic glutamate metabolism: a tale of 2 hepatocytes. *The American Journal of Clinical Nutrition* **90**, 857S-861S

21. Matsuno, T., and Goto, I. (1992) Glutaminase and Glutamine Synthetase Activities in Human Cirrhotic Liver and Hepatocellular Carcinoma. *Cancer Research* **52**, 1192-1194

22. Contreras, L., and Satrustegui, J. (2009) Calcium Signaling in Brain Mitochondria INTERPLAY OF MALATE ASPARTATE NADH SHUTTLE AND CALCIUM UNIPORTER/MITOCHONDRIAL DEHYDROGENASE PATHWAYS. *Journal of Biological Chemistry* **284**, 7091-7099

23. Gellerich, F. N., Gizatullina, Z., Trumbeckaite, S., Nguyen, H. P., Pallas, T., Arandarcikaite, O., Vielhaber, S., Seppet, E., and Striggow, F. (2010) The regulation of OXPHOS by extramitochondrial calcium. *Biochimica Et Biophysica Acta-Bioenergetics* **1797**, 1018-1027

24. Fernandez, C. A., Des Rosiers, C., Previs, S. F., David, F., and Brunengraber, H. (1996) Correction of 13C mass isotopomer distributions for natural stable isotope abundance. *J Mass Spectrom* **31**, 255-262

25. Watford, M., Chellaraj, V., Ismat, A., Brown, P., and Raman, P. (2002) Hepatic glutamine metabolism. *Nutrition* **18**, 301-303

26. Gibbons, G. F. (1994) A comparison of in-vitro models to study hepatic lipid and lipoprotein metabolism. *Current Opinion in Lipidology* **5**, 191-199

27.   Egnatchik, R. A., Leamy, A. K., Noguchi, Y., Shiota, M., and Young, J. D. Palmitate-induced Activation of Mitochondrial Metabolism Promotes Oxidative Stress and Apoptosis in H4IIEC3 Rat Hepatocytes. *Metabolism*

28.   Antoniewicz, M. R., Kraynie, D. F., Laffend, L. A., González-Lergier, J., Kelleher, J. K., and Stephanopoulos, G. (2007) Metabolic flux analysis in a nonstationary system: Fed-batch fermentation of a high yielding strain of E. coli producing 1,3-propanediol. *Metabolic Engineering* **9**, 277-292

29.   Altamirano, C., Illanes, A., Becerra, S., Cairo, J. J., and Godia, F. (2006) Considerations on the lactate consumption by CHO cells in the presence of galactose. *Journal of Biotechnology* **125**, 547-556

30.   Ahn, W. S., and Antoniewicz, M. R. (2013) Parallel labeling experiments with [1,2-13C]glucose and [U-13C]glutamine provide new insights into CHO cell metabolism. *Metabolic Engineering* **15**, 34-47

31.   Wiechert, W., Siefke, C., deGraaf, A. A., and Marx, A. (1997) Bidirectional reaction steps in metabolic networks .2. Flux estimation and statistical analysis. *Biotechnology and Bioengineering* **55**, 118-135

CHAPTER 6

^{13}C METABOLIC FLUX ANALYSIS OF AN *IN VITRO* BMPR2 MUTATION DRIVEN
MODEL OF PULMONARY ARTERIAL HYPERTENSION REVEALS AN INCREASE IN
ANAPLEROTIC GLUTAMINE DEMAND

Introduction

Heritable pulmonary arterial hypertension (PAH) is caused by mutations in the bone

morphogenic protein receptor 2 (BMPR2) (1,2). BMPR2 mutations are associated with systemic

metabolic alterations which could represent future targets for therapies or diagnostics. *In vivo*,

the metabolic signature of PAH includes increased glucose intolerance, insulin resistance, and

alterations in oxidative phosphorylation as well as activation of hypoxia inducible factor 1 alpha

(3,4). A recent *in vitro* metabolomic study investigated the effects of expressing two mutant

forms of BMPR2 in human pulmonary vascular endothelial cells (hPMVEC) and found that

mutations in BMPR2 are associated with altered glycolysis and CAC metabolism as

characterized by metabolite levels and enzyme expression (5). For example, it was concluded

that glycolysis was upregulated in BMPR2 mutants since levels of the glycolytic metabolites

starting with glucose and glucose 6-phosphate down through 2-phosphoglycerate were elevated.

Interestingly, although many glycolytic enzymes were overexpressed compared to native

expressing (wild-type) BMPR2 controls, two of the three regulatory enzymes of glycolysis

showed decreased expression. Specifically, hexokinase and phosphofructokinase expression was

lower in BMPR2 mutants while pyruvate kinase was overexpressed. While this thorough study

concluded these alterations in the levels of glycolysis indicated *increased* glycolytic metabolism,

it is possible that increased levels of glycolytic metabolites could indicate a bottleneck in

glycolytic metabolism. While glycolytic intermediates were present in elevated levels, BMPR2 mutants were characterized by elevated levels of the CAC metabolite citrate but decreased levels of the downstream metabolites succinate, fumarate, and malate suggesting CAC impairments. Additionally, intracellular levels of glutamine and glutamate were decreased indicating a role for increased glutamine anaplerosis in BMPR2 mutants to maintain CAC intermediates.

Clearly, BMPR2 mutations are associated with broad metabolic mutations. To further define how mutant BMPR2 reprogram central metabolism, for the first time we have applied stable isotope tracer ^{13}C metabolic flux analysis (MFA) to quantify how BMPR2 mutations alter intracellular metabolic flux. ^{13}C MFA is an integrated approach to studying the movement or flux of the metabolome through biochemical pathways. This approach integrates extracellular uptake and secretion rates with ^{13}C enrichment patterns in downstream metabolites to generate a comprehensive map of the carbon flow though a metabolic network. We hypothesized that using ^{13}C MFA would reveal increased glycolysis in BMPR2 mutants and decreased CAC flux compared to Native expressing (wild type) BMPR2 counterparts. Additionally, we hypothesized glutamine uptake would be a key metabolic feature of BMPR2 mutations as it would provide carbon material for CAC metabolism.

Methods

In vitro models of BMPR2 driven PAH-

Murine pulmonary microvascular endothelial cells (mPMVEC) were engineered to express either a native (wild-type) BMPR2 or a mutant BMPR2 (R899x) identified in patients with heritable PAH. The murine PMVECs are on the Immortomouse background. Cells were

initially grown at 33℃ in Lonza EBM-2 media supplemented with the EGM-2 MV SingleQuot kit (5% FBS, hydrocortisone, rhFGF-B, VEGF, R3 IGF-1, ascorbate, rhEGF, GA-1000) and with 100 u/mL murine interferon-gamma. Prior to any experiments, cells were transitioned to 37℃ and the media was replaced with the above formulation minus interferon-gamma but with 300 ng/mL doxycycline added to activate the BMPR2 transgene.

Extracellular metabolite analysis-

Cell culture media was sampled at indicated 2, 6, and 24 hours after fresh media was added to plates. We used the YSI 2300 Stat Glucose and Lactate Analyzer (Yellow Springs, OH) to determine the concentration of lactate and glucose at each time point. Similarly, amino acids were analyzed using high performance liquid chromatography (HPLC). Prior to HPLC analysis, excess media protein (from cells or serum) was removed using a cold acetone precipitation and norvaline was added as an internal standard. Samples were then injected onto a Zorbax Eclipse Plus C18 column (Agilent) using a two phase chromatography method as previously described (6).

Metabolite extraction and GC-MS analysis of ^{13}C labeling-

To analyze how BMPR2 mutations affected intracellular glutamine metabolism, BMPR2 mutant and native expressing mPMVEC were cultured in media containing 2 mM [U-^{13}C$_5$]glutamine in place of unlabeled glutamine. To analyze the incorporation of labeled glutamine into downstream metabolic products, the intracellular metabolites were extracted from cells quenched with 1 mL of pre-cooled methanol (-80°C). Polar and nonpolar metabolites were separated using a biphasic extraction composed of 2 mL methanol, 2 mL water, and 2 mL

chloroform. After drying the aqueous phase, the polar metabolites were derivatized using MBTSTFA + 1% TBDMCS (Pierce). Lastly, 1 µL of each derivatized sample was injected onto 30m DB-35ms capillary column in an Agilent 6890N/5975B GC-MS.

Metabolic flux analysis-

Replacing unlabeled glutamine with the [U-^{13}C$_5$]glutamine stable isotope tracer resulsted in isotopic enrichment patterns in downstream metabolites dependent on glutamine metabolism. When combined with a metabolic network model and measured extracellular fluxes, it is possible to estimate the intracellular fluxes which would give rise to the observed enrichment patterns by performing a least squares regression to minimize the lack of fit between the measured and simulated isotopomer distributions. Therefore we developed a reaction network model of BMPR2 mutant and native mPMVEC metabolism using the metabolic flux analysis software INCA (7). This software utilizes the elementary metabolite unit (EMU) decomposition to efficiently simulate mass isotopomer distributions dependent on the fluxes and isotope tracer applied (8,9).

The metabolic model for native expressing mPMVEC cells consisted on intracellular labeling data from lactate, alanine, glutamate, citrate, malate, and aspartate. We applied extracellular uptake rates for glucose and glutamine as well as the production rates for alanine and lactate to constrain the network. The model for mutant BMRP2 in mPMVEC used these same parameters. However, when trying to fit for mutant BMPR2 mPMVEC metabolism, we could not reconcile differences between glutamine uptake and CAC labeling. This indicated glutamine was being used for more than just CAC anaplerosis. Glutamate secretion fluxes were added to the model in addition to an anabolic 'sink' to account for this difference.

175

Flux parameters for both models were adjusted iteratively using a Levenberg-Marquardt algorithm. This was repeated until an optimal agreement between simulated and observed measurements was found. This process was initiated with random values and repeated at least 50 times to ensure minimum global fits were achieved. In addition to calculating the magnitude of the fluxes, we assessed goodness-of-fit by subjecting calculations to a chi-square statistical test ($\chi = 0.01$). 95% confidence intervals were calculated for each flux by evaluating the sensitivity of the sum-of-squared residuals to parameter variations (10). Further modeling details can be found in the Appendix.

Results and Discussion

BMPR2 Mutations in an in vitro model of murine pulmonary hypertension are associated with altered extracellular flux.

To determine if BMPR mutations are associated with altered extracellular metabolic flux, media samples were taken across 24 hours for both murine derived native and BMPR2 mutants *in vitro*. We found that mutant and native expressing BMPR2 cells were characterized by similar rates of glucose uptake but the lactate secretion flux was elevated the native expressing cells(Figure 6.1A). Glutamine uptake was greater in BMPR2 mutant expressing cells. Additionally, we found that R899x mutant BMPR2 mPMVEC produced both alanine and glutamate at significant rates compared to their native counterpart (Figure 6.1B). Broadly, the differences in these extracellular fluxes indicate mutations in BMPR2 reprogram mPMVEC metabolism.
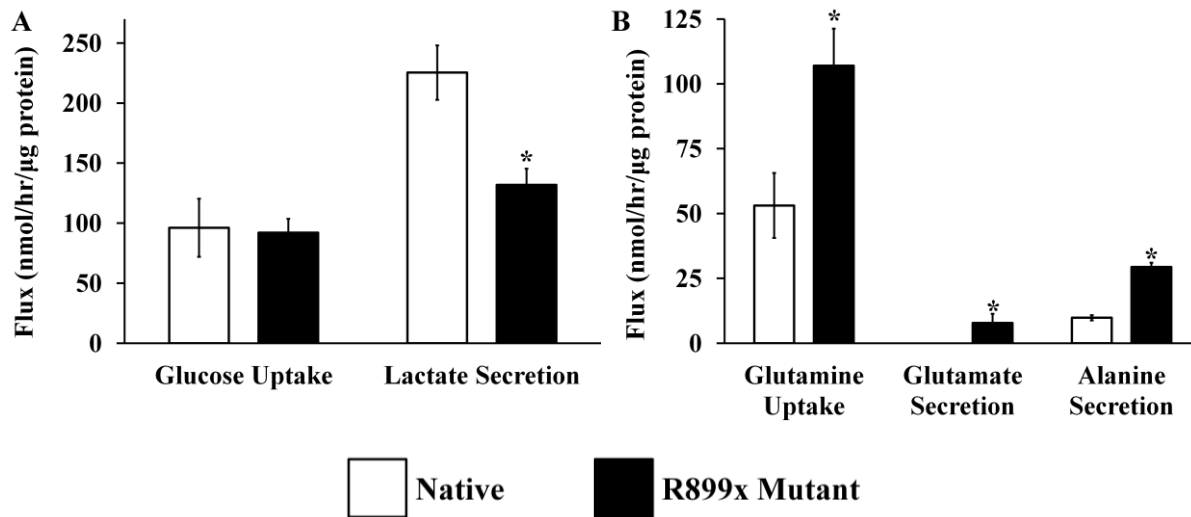
Figure 6.1: Non-glucose extracellular fluxes are dramatically altered in R899x BMPR2 mutant mPMVEC. The extracellular media of mPMVEC expressing native or R899x mutant BMPR2 in culture were sampled over 24 hours. Using the measured metabolites from each timepoint and endpoint protein concentrations, we calculated extracellular uptake and secretion fluxes. (A) Glycolytic fluxes calculated for both cell types. Glucose uptake was nearly identical between both cell types while cells expressing native BMPR2 had increased lactate secretion. (B) Extracellular glutamine uptake, glutamate secretion and alanine secretion were much higher for BMPR2 mutant expressing mPMVEC demonstrating a role for altered amino acid metabolism in these cells. Data represent mean +/- S.E., n=3; * different from vehicle, p <.05.

[13]C tracer analysis reveals BMPR2 mutations are associated with altered glutamine anaplerosis

Since we observed BMPR2 mutation-dependent increases in extracellular amino acid flux, we hypothesized that intracellular amino acid metabolism was greatly altered. It has been shown before that BMPR2 mutations can drive alterations in CAC anaplerosis (5). In particular, it was observed that CD hPMVEC BMPR2 mutants were deficient in intracellular aspartate, glutamate, and glutamine compared to native expressing controls. To test the hypothesis that BMPR2 mutants require excess glutamine to meet anaplerotic needs, R899x BMPR2 mPMVEC mutants were cultured in the presence of 2 mM of the stable isotope tracer [U-$^{13}C_5$]glutamine. After extraction of intracellular metabolites, their isotopic enrichment was analyzed by GC-MS. Next we corrected the measured mass isotopomer distributions for the natural isotope abundance

177

by applying the method of Fernandez et al. (11) and calculated the atom percent isotopic enrichment of the following metabolites: lactate, alanine, glutamate, aspartate, malate, and citrate. The atom percent enrichment of a metabolite pool represents the amount of that metabolite was synthesized from the isotope tracer (i.e. [U-^{13}C$_5$]glutamine) vs. unlabeled sources (i.e. glucose).
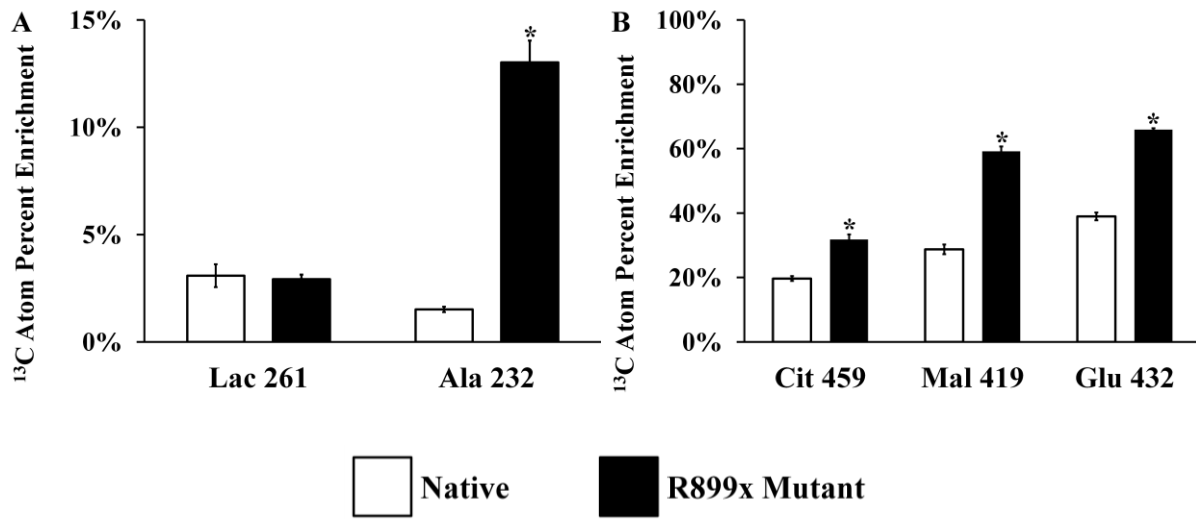
Figure 6.2: Isotopic enrichment of glycolytic and CAC metabolites. [U-^{13}C$_5$]glutamine was fed to mPMVEC expressing either native or R899x mutant BMPR2. We then analyzed the isotopic enrichment of downstream metabolites using GC-MS and calculated the atom percent enrichment. (A) Atom percent enrichment of lactate and alanine. (B) Atom percent enrichment of citrate, malate, and glutamate. ^{13}C atom percent enrichment of intracellular metabolites except for lactate was significantly higher in mutants than native controls. Data represent mean +/- S.E., n=3 for R899x mutant derived metabolites, n=2 for native samples; * different from vehicle, p <.05.

We found that the intracellular lactate pool had only approximately 2% enrichment from labeled glutamine in both the wild type BMPR2 mPMVEC and the R899x mutants.

Interestingly, the labeling of the 2 carbon fragment of alanine 232 from R899x mutants was

approximately 10 fold higher than wild type cells (☐ **Native**   ■ **R899x Mutant**

Figure 6.2A). Next we analyzed the isotopic enrichment of CAC intermediates citrate and

malate as well as glutamate (as a surrogate for alpha-ketoglutarate). Although this data does not

inform us about altered pool sizes, the enrichment in malate, citrate, and glutamate pools from

BMPR2 mutant mPMVECs indicated these cells rely on extracellular glutamine to synthesize

these CAC intermediates (☐ **Native**   ■ **R899x Mutant**

Figure 6.2B). Together, these measurements demonstrate that the R899x BMPR2 mutant is

associated with increased glutamine CAC anaplerosis.

^{13}C metabolic flux analysis reveals BMPR2 mutations drive increased glutamine CAC metabolism relative to glucose uptake

The observation of increased isotope enrichment of CAC intermediates in BMPR2

mutants led us to hypothesize that BMPR2 mutants rely on a shift to glutamine anaplerosis to

maintain intracellular substrate levels for growth and proliferation. To test this hypothesis, we

performed metabolic flux analysis (MFA) to calculate intracellular fluxes associated with

glutamine anaplerosis, CAC metabolism, and pyruvate metabolism along with their 95%

confidence intervals. We found that most CAC fluxes were qualitatively elevated in BMPR2

mutant mPMVEC, but statistical significance could not be attained due to high error in input (i.e.

extracellular flux) measurements which drive errors in the model (Figure 6.3). However, we

179

calculated significantly elevated flux through glutamate dehydrogenase in BMPR2 mutants, which is an intermediate step in the conversion of glutamine to CAC α-ketoglutarate.
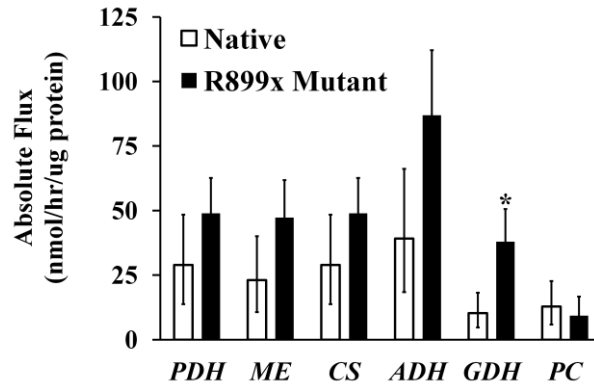
Figure 6.3: **^{13}C flux analysis of CAC metabolism**. We calculated intracellular fluxes associated with CAC anaplerosis and cataplerosis in both native and mutant BMPR2 mPVEC. Qualitatively, R899x mutant BMPR2 was associated with elevated CAC flux fueled by GDH derived alpha-ketoglutarate. Abbreviations: ADH, alpha-ketoglutarate dehydrogenase; CS, citrate synthase; GDH, glutamate dehydrogeanse; ME, malic enzyme; PC, pyruvate carboxylase; PDH, pyruvate dehydrogenase. Error bars indicate 95% confidence intervals; * different from vehicle, p <.05.

Our metabolic model demonstrates that enhanced glutamine uptake in BMPR2 mutants is likely due to enhanced CAC demand for anaplerosis. In building the metabolic network, we were unable to initially fit the CAC demand for glutamine (constrained by isotope labeling) to the measured extracellular glutamine flux since there was excess glutamine entering the cell. To match the incoming glutamine, we added an 'anabolic' pool to the reaction network which allows glutamine carbon to enter non-measured anabolic pathways. These pathways could include glutathione synthesis to combat oxidative stress associated with BMPR2 mutants. It is important to note this step was not required in the modeling of metabolism of the mPMVEC

expressing native BMPR2 demonstrating that the BMPR2 mutation shifts the cell's metabolism to need glutamine for multiple reactions, not solely CAC anaplerosis.

Study limitations

In this study, extracellular fluxes were normalized to protein concentration taken at one time point. BMPR2 mutants are known to have altered growth rates Therefore, future experiments will be performed to determine explicit growth rates for native and BMPR2 mutant endothelial cells grown under the conditions performed in this study. This information will allow for the calculation of more accurate fluxes relative to cell or protein number compared to the current method used.

BMPR2 mutants were cultured in the presence of [U-^{13}C$_5$]glutamine to characterize altered glutamine anaplerosis in PAH models. Besides glutamine anaplerosis, both glycolysis and the pentose phosphate pathway have been shown to be drastically altered by BMPR2 mutations. To further characterize these metabolic pathways in the context of BMPR2 mutation driven PAH, alternate stable isotope tracers must be used.

Conclusions

In these preliminary MFA experiments, we have found that the R899x BMPR2 mutant in mPMVEC is characterized by elevated glutamine uptake that is used to a) fuel CAC flux, and b) provide substrates for non-measured processes, potentially N-acetylaspartylglutamate (5) or glutathione. Future experiments will focus on minimizing error in the extracellular flux, which will allow for better determination of intracellular fluxes. Finally the calculation of growth rates

of BMPR2 mutants will further highlight how BMPR2 mutations reprogram the metabolic phenotype of the cell.

Table 6A.1: Reactions and atom transitions for metabolic flux analysis of mPMVEC expressing native or R899x mutant BMPR2. List of metabolite abbreviations can be found below. Dot suffixes denote specific sub-pools of metabolite: .x, extracellular; .t, tracer; .d, dilution.

Pyruvate Metabolism			Reaction Name
Glucose (abcdef)	→	PEP (cba) + PEP (def)	Glc Uptake
PEP (abc)	→	Pyr (abc)	PK
Pyr (abc)	→	Lac (abc)	LDH
Pyr (abc) + CO_2 (d)	→	Mal (abcd)	PC
Mal (abcd)	→	Pyr (abc) + CO_2 (d)	ME
Pyr (abc)	→	AcCoA (bc) + CO_2 (a) +	PDH
Pyr (abc)	→	Ala (abc)	GPT
CAC Metabolism			
AcCoA (ab) + Mal (cdef)	→	Cit (fedbac)	CS
Cit (abcdef)	←→	Akg (abcde) + CO_2 (f)	IDH
Akg (abcde)	→	Suc (bcde) + CO_2 (a)	ADH
Suc (½ abcd + ½ dcba)	←→	Fum (½ abcd + ½ dcba)	SDH
Fum (½ abcd + ½ dcba)	←→	Mal (abcd)	FDH
Glutamine anaplerosis			
Gln.x (abcde)	→	Gln (abcde)	Gln uptake
Gln (abcde)	→	Glu (abcde)	GLN
Gln (abcde)	→	Anabolism	Anaplerosis
Glu (abcde)	←→	Akg (abcde)	GDH
Glu (abcde)	→	Glu.x (abcde)	Glu secretion
Dilution			
Asp.d (abcd)	→	Asp (abcd)	Asp G parameter

Table 6A.2 Measured Extracellular fluxes and GC-MS ions used for metabolic flux analysis. The reported standard error (SEM) of the GC-MS is representative of the calculated error amongst the listed *n* biological replicates.

Measured Net Fluxes

Metabolite	Flux
Glucose	Glucose → PEP + PEP
Lactate	Lac → Lac.x
Glutamine	Gln.x → Gln
Glutamate	Glu → Glu.x
Alanine	Ala → Ala.x

Measured GC-MS Ions

Metabolite	Mass	Composition	Carbons						SEM (mol%) Native	SEM (mol%) R899x
Glu	432	$C_{19}H_{42}O_4NSi_3$	1	2	3	4	5		0.7	0.7
Glu	330	$C_{16}H_{36}O_2NSi_2$		2	3	4	5		0.7	0.7
Mal	419	$C_{18}H_{39}O_5Si_3$	1	2	3	4			0.9	2.1
Asp	390	$C_{17}H_{40}O_3NSi_3$		2	3	4			0.94	0.85
Asp	418	$C_{18}H_{40}O_4NSi_3$	1	2	3	4			0.53	1.2
Lac	233	$C_{10}H_{25}O_2Si_2$		2	3				0.51	1.1
Lac	261	$C_{11}H_{25}O_3Si_2$	1	2	3				0.5	0.5
Ala	232	$C_{10}H_{26}ONSi_2$		2	3				0.5	0.88
Cit	459	$C20H39O_6Si_3$	1	2	3	4	5	6	0.97	6

Table 6A.3: Calculated fluxes for Native BMPR2 expressing mPMVEC.

Parameter	Value	95% Confidence Interval
Net Flux		
Glucose Uptake	96.1	[48.7, 143.5]
Lactate Secretion	225	[180.9, 269.9]
Glutamine Uptake	53.1	[28.6, 77.6]
Glutamate Secretion	Not detectable via HPLC analysis	
Alanine Secretion	9.8	[7.8, 11.8]
PDH	28.9	[13.7, 48.5]
CS	28.9	[13.7, 48.5]
IDH	28.9	[13.7, 48.5]
GLS	10.2	[4.7, 18.2]
GDH	10.2	[4.7, 18.2]
ADH	39.1	[18.4, 66.2]
SDH	39.1	[18.4, 66.2]
FUS	39.1	[18.4, 66.2]
ME	23.1	[10.6, 40.1]
PC	12.8	[5.8, 22.7]
GPT	9.8	[7.8, 11.8]
Anabolic flux		
'Gln anabolic'	42.9	[17.4, 68.2]
Exchange Flux		
IDH	0.1	[0.0, 0.3]
SDH	0.0	[0.0, 100]
FUS	0.0	[0.0, 100]
GPT	100	[0.0, 100]
GDH	100	[8.1, 100]
Dilution		
Asp G Parameter	100	[96.6, 100]

Table 6A.4: Calculated fluxes for R899x BMPR2 mutant expressing mPMVEC cells.

Parameter	Value	95% Confidence Interval	
Net Flux			
Glucose Uptake	92.2	[69.5,	115]
Lactate Secretion	131	[105.1,	158.5]
Glutamine Uptake	107	[78.9,	135.0]
Glutamate Secretion	7.8	[4.6,	10.9]
Alanine Secretion	29.4	[22.5,	36.3]
PDH	48.5	[37.0,	62.6]
CS	48.5	[37.0,	62.6]
IDH	48.5	[37.0,	62.6]
GLS	45.8	[34.5,	58.7]
GDH	38.0	[27.1,	50.6]
ADH	86.9	[64.8,	112.1]
SDH	86.9	[64.8,	112.1]
FUS	86.9	[64.8,	112.1]
ME	47.3	[34.5,	61.8]
PC	9.3	[0,	16.5]
GPT	29.4	[22.5,	36.3]
Anabolic flux			
'Gln anabolic'	61.2	[30.6,	91.5]
Exchange Flux			
IDH	0.0	[0.0,	0.5]
SDH	100	[0.0,	100]
FUS	100	[0.0,	100]
GPT	43.4	[0.0,	100]
GDH	32.3	[11.3,	100]
Dilution			
Asp G Parameter	97.4	[90.8,	100]

References

1.   Farber, H. W., and Loscalzo, J. (2004) Pulmonary Arterial Hypertension. *New England Journal of Medicine* **351**, 1655-1665

2.   Newman, J. H., Trembath, R. C., Morse, J. A., Grunig, E., Loyd, J. E., Adnot, S., Coccolo, F., Ventura, C., Phillips, I. I. I. J. A., Knowles, J. A., Janssen, B., Eickelberg, O., Eddahibi, S., Herve, P., Nichols, W. C., and Elliott, G. (2004) Genetic basis of pulmonary arterial hypertensionCurrent understanding and future directions. *Journal of the American College of Cardiology* **43**, S33-S39

3.   Archer, S. L., Gomberg-Maitland, M., Maitland, M. L., Rich, S., Garcia, J. G., and Weir, E. K. (2008) Mitochondrial metabolism, redox signaling, and fusion: a mitochondria-ROS-HIF-1alpha-Kv1.5 O2-sensing pathway at the intersection of pulmonary hypertension and cancer. *Am J Physiol Heart Circ Physiol* **294**, H570-578

4.   Fessel, J. P., Flynn, C. R., Robinson, L. J., Penner, N. L., Gladson, S., Kang, C. J., Wasserman, D. H., Hemnes, A. R., and West, J. D. (2013) Hyperoxia Synergizes with Mutant Bone Morphogenic Protein Receptor 2 to Cause Metabolic Stress, Oxidant Injury, and Pulmonary Hypertension. *American Journal of Respiratory Cell and Molecular Biology* **49**, 778-787

5.   Fessel, J. P., Hamid, R., Wittmann, B. M., Robinson, L. J., Blackwell, T., Tada, Y., Tanabe, N., Tatsumi, K., Hemnes, A. R., and West, J. D. (2012) Metabolomic analysis of bone morphogenetic protein receptor type 2 mutations in human pulmonary endothelium reveals widespread metabolic reprogramming. *Pulm Circ* **2**, 201-213

6.   J., G., JW., H., and JP, W. (2009) Rapid and precise determination of cellular amino acid flux rates using HPLC with automated derivatization with absorbance detection., Agilent Technologies

7.   Young, J. D. (2014) INCA: A computational platform for isotopically nonstationary metabolic flux analysis. *Bioinformatics*

8.   Antoniewicz, M. R., Kelleher, J. K., and Stephanopoulos, G. (2007) Elementary metabolite units (EMU): A novel framework for modeling isotopic distributions. *Metabolic Engineering* **9**, 68-86

9.   Young, J., Walther, J., Antoniewicz, M., Yon, H., and Stephanopoulos, G. (2008) An Elementary Metabolite Unit (EMU) based method of isotopically nonstationary flux analysis. *Biotechnology and Bioengineering* **99**, 686-699

10.   Antoniewicz, M. R., Kelleher, J. K., and Stephanopoulos, G. (2006) Determination of confidence intervals of metabolic fluxes estimated from stable isotope measurements. *Metabolic Engineering* **8**, 324-337

11.   Weltman, M. D., Farrell, G. C., Hall, P., Ingelman-Sundberg, M., and Liddle, C. (1998) Hepatic cytochrome p450 2E1 is increased in patients with nonalcoholic steatohepatitis. *Hepatology* **27**, 128-133

CHAPTER 7

CONCLUSIONS AND FUTURE DIRECTIONS

Conclusions

^{13}C metabolic flux analysis (MFA) is invaluable technique to develop an understanding

of how alterations in the complex regulatory network of biological systems (i.e. genetic

mutations, protein-protein interactions, environmental effects) affect the ultimate metabolic

phenotype of the cell. When combined with traditional biochemical techniques of protein

expression, pharmacological inhibition of signaling pathways, and RNAi interference, integrated

molecular mechanisms of pathology can be developed. Armed with the molecular mechanisms

of disease it is therefore possible to identify novel targets for therapies and diagnostics to alter

pathology.

Saturated fatty acid overload disrupts normal hepatic cell function as characterized by

dysregulated CAC anaplerosis, depleted ER calcium, oxidative stress, and apoptosis. The

mechanism by which these alterations occur has not been well characterized. This dissertation

examined the role of aberrant CAC anaplerosis pertaining to *in vitro* models of hepatic

lipotoxicity. Elevated levels of saturated fatty acids redistribute intracellular calcium from the

ER to the mitochondria. This rise in mitochondrial calcium correlates with a rise in CAC flux

and oxidative stress. In particular, α-ketoglutarate, glutamate, and glutamine act as substrates for

lipotoxic dysregulation of CAC anaplerosis.

In Chapter 3, the hypothesis that fatty acid oxidation does not drive mitochondrial

derived oxidative stress was tested. Using ^{13}C MFA, glutamine was demonstrated to provide

carbon for CAC metabolism in the context of lipotoxicity instead of using acetyl-CoA derived

from fatty acid oxidation. Isolating mitochondrial function using a complex I inhibitor reduced lipotoxicity and oxidative stress while simultaneously attenuating metabolic flux. However, reducing oxidative stress with antioxidants prevented lipid-induced cell death without reversing the lipotoxic mitochondrial phenotype. These results defined a role for abnormal anaplerosis in lipotoxicity, which occurs independently of fatty acid oxidation. Therefore, therapies aimed to reduce anaplerosis may alter the course of lipotoxicity. Additionally, antioxidant therapy may attenuate the downstream markers or disease (oxidative stress) but may not alter the upstream signals which precipitate the pathology.

The possible role of intracellular calcium was explored in Chapter 4 since it would represent a functional pro-apoptotic link between the ER and oxidative stress hallmarks of lipotoxicity. Chelation of intracellular calcium in palmitate treated hepatic cells reduced glutamine anaplerosis, which in turn attenuated oxidative stress and lipoapoptosis. This finding is significant because it links ER stress to dysregulated mitochondrial function in hepatic lipotoxicity. Therefore therapies which aim to reduce ER stress could delay mitochondrial dysfunction by increasing ER capacity for calcium.

Since calcium can stimulate CAC metabolism by activating α-ketoglutarate dehydrogenase, it was hypothesized that aberrant anaplerosis which occurs in lipotoxicity is to re-supply α-ketoglutarate to the CAC. In Chapter 5, this hypothesis was tested by replacing the extracellular culture media glutamine with glutamate or α-ketoglutarate and by removing these substrates altogether. Removing glutamine from culture media attenuated lipotoxicity presumably by reducing the amount of anaplerotic substrate available to fuel the aberrant calcium stimulated metabolism. Targeted and pharmacologic inhibition of the glutamate oxaloacetate pathways revealed that these pathways provided the α-ketoglutarate to fuel lipotoxic

anaplerosis. These results are particularly interesting because in humans obesity is associated

not just with increased fat uptake, but also net uptake of all macromolecules (carbohydrates and

protein). From a nutritional standpoint, these results indicate that the net uptake of non-lipid

substrate can greatly alter disease progression. Together Chapters 3,4, and 5 have characterized

the metabolic determinants of hepatic lipotoxicity (Figure 7.1).
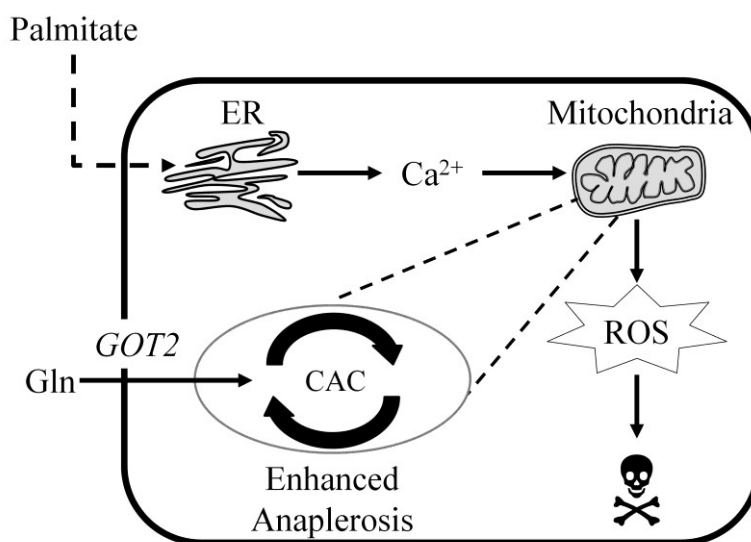
Figure 7.1 Metabolic determinants of hepatic lipotoxicity. Elevated saturated fatty acids
(palmitate) induce oxidative stress-dependent apoptosis. Increased mitochondrial calium
enhances anaplerosis and metabolic flux through CAC pathways primarily relying on
glutamine carbon. Based on this mechanism, therapies can delay lipotoxicity at several
nodes. In particular, therapies which target the ER are most attractice since they would target
the most upstream node in the disease mechanism.

Lastly, Chapter 6 examined anaplerosis by applying ^{13}C MFA to an *in vitro* model of

BMPR2 mutation-driven pulmonary arterial hypertension. BMPR2 mutants have an increased

dependence on glutamine to maintain the level of CAC intermediates. It was previously

hypothesized that the decreased levels of CAC intermediates would result in decreased CAC flux

in BMPR2 mutants. However, it was found that BMPR2 mutants relied on glutamine

anaplerosis to maintain a similar or higher CAC flux compared to the native BMPR2 expressing cells. Understanding how BMPR2 mutations reprogram metabolism will assist in both in the diagnosis of disease as well as development of novel treatments.

Suggestions for Future Work

The majority of the work in this dissertation tested hypotheses in immortalized hepatic cells *in vitro* using ^{13}C MFA. Although several key experiments were repeated in isolated primary hepatocytes, future work should aim to translate the experiments and hypotheses generated by this dissertation to *in vivo* models of NASH.

Prior to *in vivo* flux studies, optimal tracers will need to be selected. In Chapter 5, primary hepatocytes were labeled using [U-^{13}C$_5$]glutamine. Although our *in vitro* experiments with isolated primary hepatocytes metabolize this tracer, it is possible that alternative tracers may be more ideal for future studies. One limitation to using [U-^{13}C$_5$]glutamine to study hepatocyte metabolism is that liver glutaminase, which catalyzes the conversion of glutamine to glutamate, is not expressed equally across the liver. Unlike glutaminase, hepatocytes express glutamate dehydrogenase and glutamate dependent transaminases fairly equally across the liver (1,2). Additionally in Chapter 5, it was observed that lipotoxicity was enhanced when hepatocytes were cultured in glutamate instead of glutamine. Therefore, both future *in vitro* and *in vivo* experiments should consider using a [U-^{13}C$_5$]glutamate in addition to the [U-^{13}C$_5$]glutamine tracer, although costs may limit [U-^{13}C$_5$]glutamine *in vivo*. An alternative to glutamine/glutamate tracers is [U-^{13}C$_3$] propionate, a tracer traditionally used to estimate hepatic gluconeogenesis relative to CAC flux *in vivo* (3). These methods currently in development in the Young Lab.

There are many diet induced and genetically altered animal models of fatty liver and NASH (see Chapter 2). However, several of the mechanisms proposed in this dissertation may be difficult to directly test *in vivo*. For example, blocking mitochondrial calcium uptake *in vivo* could have numerous, deleterious side effects. Alternatively, overexpression of sarco-endoplasmic reticulum calcium ATPase 2b (SERCA2b) in the livers of NASH or fatty liver animals could be utilized to test the hypothesis that elevated hepatic lipid results in decreased ER calcium stores and net mitochondrial calcium uptake. The function of this protein *in vivo* is to facilitate ER calcium reuptake, which in turn reduces ER stress. Additionally, obesity is associated with decreased ER calcium due to SERCA inhibition (4). Interestingly, SERCA2b overexpression can restore glucose tolerance suggesting an overarching mechanism connecting obesity and glucose intolerance with calcium maintenance. Additionally, in control animals, SERCA2b overexpression had no effect on metabolic markers. Based on the mechanisms explored in this dissertation, lipid-altered calcium flux could stimulate CAC anaplerosis which could account for the mitochondrial alterations reported in humans and mice with elevated intra-hepatic lipids (5,6). When combined with the proper cocktail of isotope tracers, a very similar mechanism tested in this dissertation could be tested *in vivo*. Broadly, as a powerful tool of metabolic engineering, ^{13}C MFA can assist in translational research by developing molecular mechanisms of disease which provide unique therapeutic targets to test *in vivo*.

References

1.   Watford, M., Chellaraj, V., Ismat, A., Brown, P., and Raman, P. (2002) Hepatic glutamine metabolism. *Nutrition* **18**, 301-303

2.   Brosnan, M. E., and Brosnan, J. T. (2009) Hepatic glutamate metabolism: a tale of 2 hepatocytes. *The American Journal of Clinical Nutrition* **90**, 857S-861S

3.   Landau, B. R., Schumann, W. C., Chandramouli, V., Magnusson, I., Kumaran, K., and Wahren, J. (1993) 14C-labeled propionate metabolism in vivo and estimates of hepatic gluconeogenesis relative to Krebs cycle flux. *Am J Physiol* **265**, E636-647

4.   Fu, S., Yang, L., Li, P., Hofmann, O., Dicker, L., Hide, W., Lin, X., Watkins, S. M., Ivanov, A. R., and Hotamisligil, G. S. (2011) Aberrant lipid metabolism disrupts calcium homeostasis causing liver endoplasmic reticulum stress in obesity. *Nature* **473**, 528-531

5.   Satapati, S., Sunny, N. E., Kucejova, B., Fu, X. R., He, T. T., Mendez-Lucas, A., Shelton, J. M., Perales, J. C., Browning, J. D., and Burgess, S. C. (2012) Elevated TCA cycle function in the pathology of diet-induced hepatic insulin resistance and fatty liver. *Journal of Lipid Research* **53**, 1080-1092

6.   Sunny, N. E., Parks, E. J., Browning, J. D., and Burgess, S. C. (2011) Excessive Hepatic Mitochondrial TCA Cycle and Gluconeogenesis in Humans with Nonalcoholic Fatty Liver Disease. *Cell Metab* **14**, 804-810

APPENDIX OF DETAILED PROTOCOLS

Cell Titer Blue Viability Assay

Purpose:

To measure the viable population of H4IIEC3 cells in response to various treatments in 96 well plates.
This protocol is specific for adherent cells.

Mechanism:

The active reagent in the Cell Titer Blue Cell Viability Kit is the nonfluorescent resazurin which is reduced to fluorescent resorfin when in the presence of NAD(P)H. Live cells continuously recycle NAD(P)H through metabolic activity making resazurin a useful dye for measuring viability. This is most useful at long time points where the metabolism of all viable populations (regardless of treatment) is approximately equal. Increased dye fluorescence is therefore a function of population viability. However, if inhibitors are used which decrease the metabolic activity without killing the cell population (i.e. Complex I inhibitors), population viability will be underestimated.

Materials:

- Cell Titer Blue Concentrated stock (Promega Catalog No. G8081)
- HBSS buffer
- Low glucose DMEM (Media w/out phenol red)
- 96 well plate- opaque, clear bottom.
- Plate reader

Prior to experiment:

- 48 hrs before assay, seed 2x10^4 cells per well in a 96 well plate (black, clear bottom)

Procedure:

- *30 minutes prior to adding Cell Titer Blue dye- add Hydrogen Peroxide controls. Normally we use .5-1 mM concentration (final).*
- Remove media from cells.
- Wash 2x with HBSS.
- Add 100 uL of Low glucose DMEM (or other media) that **does not** contain phenol red. This will react with the dye and result in measurement errors.
- Add 20 uL of Cell Titer Blue Reagent.
- Incubate for a minimum of 4 hours.
- Read fluorescent signal at an ex/em of 560/590. If reader can shake plate, do so for ~5 seconds prior to fluorescent measurement.

Propidium Iodide Toxicity Assay

Purpose:

To measure the nonviable population of cells in response to various treatments in 96 well plates.
This protocol is specific for adherent cells.

Mechanism:

Propidium iodide (PI) is an intercalating dye and will only bind to double stranded DNA longer than 4-5 base pairs. Since PI cannot cross the cell membrane, it is useful when trying to discriminate dead from live cells in a population.

Materials:

- Propidium Iodide powder stock (Invitrogen Catalog No. P1304MP)
- HBSS buffer
- Low glucose DMEM (Media w/out phenol red)
- 96 well plate- opaque, clear bottom.

Prior to experiment:

- 48 hrs before assay, seed 2×10^4 cells per well in a 96 well plate (black, clear bottom)

Procedure:

- Dye preparation- dissolve PI in HBSS to make a stock solution of 1 mg/mL (1.5 mM)
- *1 hour prior to adding PI dye- add 70% ethanol solution to appropriate wells for a positive control.*
- Remove media from cells.
- Do not wash, doing so could wash out dead cells
- Add 100 uL of Low glucose DMEM (or other media) that ***does not*** contain phenol red. This will react with the dye and result in measurement errors.
- Make stock of 5 uM PI by adding 33.3 uL of PI stock to 10 mL of DMEM
- Incubate for a minimum of 1 hr. Remove dye and replace with phenol red free media.
- Measure fluorescence
  - Ex 535, Em 617
  - For FL 600 use ex: 530, em: 645, bottom read, sensitivity: 100

Apo-ONE Caspase 3/7 Reagent Apoptosis Detection

Purpose:

To measure apoptosis in H4IIEC3 cells by detecting the activities of caspase-3 and -7. *This protocol is specific for adherent cells.*

Mechanism

The Apo-ONE kit is used to measure apoptosis in cells by measuring caspase activity. The kit contains a lysis buffer which permeabilizes the cell population to facilitate dye introduction to caspases 3/7. When the nonfluorescent dye comes in contact with the caspases, quenching groups are removed from the dye and return it to its fluorescent rhodamine state. T

Materials:

- Apo-ONE Caspase 3/7 Kit (Promega Catalog No. G7791)
- 96 well plate (opaque, clear bottom)
- Low Glucose DMEM
- Staurosporine can be used as a positive control.

Prior to experiment:

- 48 hrs before assay, seed 2x10^4 cells per well in a 96 well plate (black, clear bottom)

Procedure:

- Dye preparation- add 100 uL Substrate into 9900 uL Buffer provided in the kit- good for 24-48 hrs. Additionally, smaller volumes of the reactive mixture can be made at a time if the substrate and buffer ratio is kept constant.
- Remove media from cells.
- Wash 2x with HBSS carefully to not dislodge dying cells.
- Add 100 uL of Low glucose DMEM (or other media) that ***does not*** contain phenol red. This will react with the dye and result in measurement errors.
- Add 100 uL of Apo ONE stock.
- Incubate for a minimum of 1 hour.
- Wavelengths- excitation 499, emission 521
    - For FL-600 plate reader
    - Use 485 filter for excitation and 5
    - Bottom Read
    - Set Sensitivity to 125, if "overflow" is returned by the instrument, reduce sensitivity and retake measurement.

Reactive Oxygen Species (ROS) Assay

Purpose:

To measure the levels of reactive oxygen species (ROS) in H4IIEC3 cells using H_2DCFA in 96 well plates.
This protocol is specific for adherent cells.

Mechanism:

Non-fluorescent H_2DCFA is converted to fluorescent DCF in the presence of intracellular ROS species (most sensitive to H_2O_2).

Materials:

- H_2DCFA (Invitrogen Catalog No. D-399)
- DMSO
- HBSS buffer
- 96 well plate- opaque, clear bottom.

Prior to experiment:

- 48 hrs before assay, seed 2x10^4 cells per well in a 96 well plate (black, clear bottom)

Procedure:

- *30 minutes prior to adding H2DCFA dye- add Hydrogen Peroxide controls. Normally we use .5-1 mM concentration (final).*
- To make H_2DCFA stock solution- dissolve H_2DCFA powder in DMSO to make 10 mM solution.
- Dilute H_2DCFA in HBSS to make 10 uM working solution. H_2DCFA is light sensitive and the tube should be wrapped in tin foil to prevent any degradation due to light.
- Vortex for 30 seconds.
- Remove media from cells.
- Wash 2x with HBSS.
- Add 100 uL of H_2DCFA mixture to cells.
- Incubate for 30-45 minutes.
- To measure ROS- H_2DCFA fluorescence, set excitation wavelength to 485 nm and emission wavelength to 530 nm. Set sensitivity of reader to 150. *– specific FL-600 plate reader*

Rhod-2 Calcium Indicator

Purpose:

To measure the relative level of calcium in the mitochondria of H4IIEC3 rat hepatomas. *This protocol is specific for adherent cells.*

Mechanism:

Potential driven uptake allows for selective staining of mitochondria with Rhod-2. Increases in calcium increase emitted fluorescent signal.

Materials:

- Rhod-2 fluorescent dye in 50 ug aliquots (Invitrogen catalogue R1245MP)
- DMSO
- Media
- 96 well plate- opaque, clear bottom.

Prior to experiment:

- 48 hrs before assay, seed 2x10^4 cells per well in a 96 well plate (black, clear bottom)

Procedure:

- Add 8.9 uL DMSO to vial to make 5 mM stock
- Final treatment concentration is 10 uM for 1 hr
- Make secondary stock of 110 uM depending on how many wells we will treat
    - Final volume per well is 220 uL. Add 20 uL of secondary stock per well
- Incubate for 1 hour.
- Remove media from cells.
- Rinse cells 3 times with PBS
- Measure fluorescence- Must use core plate reader or DRTC reader- use monochromator
    - Ex 552, Em 581
- Ionomycin can be used as a positive control

JC-1 Analysis of Mitochondrial Potential

Purpose:

To identify mitochondrial impairments as a function of mitochondrial potential.
This protocol is specific for adherent cells

Mechanism:

The JC-1 dye accumulates in mitochondria in monomeric (green) form. The increase in mitochondrial potential causes the dye to form aggregates characterized by a shift from green to red fluorescence. Therefore a ratio of red to green fluorescent emissions (using the same excitation) indicates the relative mitochondrial potential.

Materials:

- JC-1 Dye (Invitrogen T-3168)
- 96 well plate, black, clear bottom
- Plate reader
- Ethanol
- Media

Prior to experiment:

- 48 hrs before assay, seed $2x10^4$ cells per well in a 96 well plate (black, clear bottom)
- Stock solution is 5 mg in 1 mL of ethanol (5mg/mL concentration)

Dye loading:

- Treatment final concentration is **10 ug/mL**
- Make secondary stock concentration of **110 ug/mL**
- Calculate total volume needed. For a 96 well plate you will need **1950 uL – 2000 uL**.
- For **2000 uL** add **44 uL of 5 mg/mL stock to 1956 uL DMEM** in a small tube.
- VORTEX VIGOROUSLY. JC-1 is tough to dissolve. Pre-warm media ahead of time.
- Add 20 uL of 110 ug/ml of secondary stock directly on top of 200 uL media with treatments.
- Incubate for 1 hour
- Rinse 3 times with PBS
- Add **100 uL** DMEM back to wells
- Excite dye at 485 nm and measure fluorescence at 530 nm (green) and 590 nm (red)

Data Analysis:

Ratio Red/Green signals, increase in this ratio indicates higher relative mitochondrial potential.

Protocol for siRNA transfection of attached cells

Purpose:

Silence native gene expression using siRNA.

Mechanism:

Antisense RNA is added to cells using transfection reagent (lipofectamine). After a series of processing steps inside the cell (Dicer/RISC complex), a strand of the added RNAi can then bind native RNA and reduce native gene expression.

Materials:

- Transfection reagent (RNAiMAX)
- Antisense RNA (i.e. IDT Trifecta kit)
- Opti-MEM
- Antibiotic free media with serum and glutamine
- Cells in culture

Prior to transfection:

Seed cells at approximately 250,000 cells/mL in a 6 well plate, 1.25 million cells per 96 well plate 24 hours before transfection. Make sure media is antibiotic free but contains regular amounts of serum and glutamine.

Transfection (makes 2 mL aliquots per antisense RNA):

- Dilute concentrated siRNA stocks to a concentration of 2 μM with DNA-, RNA-, and nuclease-free water.
- Couple siRNA and Lipofectamine by preparing two vials. In the first vial add 25 μL of 2 μM siRNA to 125 μL Opti-MEM. In the second vial add 12 μL RNAiMAX to 138 μL Opti-MEM.
- Let each vial sit at room temperature for 5 minutes.
- Add contents of each vial together (300 μL total) and allow to complex for 20 minutes at room temperature.
- Add 300 μL of complexed siRNA to 1.7 mL of antibiotic free media (normally use DMEM for H4IIEC3 experiments)
- Add 2 mL per well for 6 well plate. Add 20 μL per well for 96 well plate.
- Incubate for 24 hours
- Remove siRNA media and replace with fresh, anti-biotic free media with serum and glutamine.
- Incubate an additional 24 hours prior to experiments.
- Perform experiments or extract RNA using Qiagen RNeasy kit to assess knockdown efficiency.

- Extraction of RNA using Qiagen RNeasy (follow manufacturer's protocol) provides RNA of a known concentration. From the RNA, one can synthesize cDNA by using the iScript cDNA synthesis kit (Bio-Rad 170-8891). Quantitative polymer chain reaction (qPCR) can then be performed using the iQ SYBR Green Super kit (Bio-Rad 170-8882) with primers for target of choice.

Whole cell oxygen uptake measurements

Purpose:

Assess mitochondrial activity as a function of whole cell oxygen uptake.

Mechanism:

Media oxygen is consumed as a cells oxygen to water as part of electron transport chain activity. We measure media oxygen depletion as a function of the number of cells and treatments.

Materials:

- Oxygraph 2K
- Fresh media

Prior to performing oxygen uptake measurement:

Seed cells at desired density along with any treatments designed to alter mitochondrial metabolic capacity.

Oxygraph 2K Protocol:

General Operation of Oroboros Oxygraph 2K
- First, turn on instrument. The switch is on the back.
- Open instrument software- DatLab
- A window will pop up asking you to set temperature. Click Connect to Oxygraph
- Set name or initials after experiment name -> save
- Instrument will likely have ethanol in it from previous user. Remove and rinse ethanol using the aspirator set up near instrument. The 'On' button is on the face of the aspirator. Add H_2O to rinse. Do this 3x making sure stir bars are on (should be set to 750 rpm). Keys F11 and F12 should toggle stir bars in chamber A, B respectively.
- <u>Don't Forget to Rinse Stoppers</u>. These are used to seal cells in the chamber to perform uptake measurements. Residual ethanol can result in extra noise in the data.
- At least an hour before you are ready to make uptake measurements, close chambers with stoppers. Use plastic tool to close the chamber just enough so there is oxygen in the chamber. This allows you to stabilize the probe in gas phase.
- Set up oxygen, let oxygen level stabilize, flux should approach zero
- Once the oxygen level stabilizes and the flux is stabilized at zero, you are ready to begin your experiments.
- Remove stoppers, remove 1 mL of media, replace with 1 mL of media with cells (make sure you know the concentration of the cells).
- Place stoppers back and allow flux to stabilize again.
- Click **F4** to set a note on the graph that you have placed the cells in the chambers.
- Change Layout to flux per volume corrected on 'plots' tab

- Hit F7 to stop recording
- Click save file and disconnect
- Press shift to select regions to use for calculations
- Click number of region that I highlighted to name
- Click marks/stats to get data

Cell Culture Prep for Oxygraph Experiments
- Culture cells on 10 cm dish (can also use 3 or 6 cm dish).
- If effects of treatments are to be studied, treat cells for designated amount of time.
- Remove media- ***Save for later!***
- Wash 2x with PBS
- Trypsinize with 1 mL of Tryple.
- Once trypsinized, resuspend cells in old culture media that you removed in previous step.
- Count cells. Spin down and remove media so final concentration of cells is 2 million per mL
- Add 1 mL of this cell solution to Oxygraph.

Measurement of cytoplasmic calcium as a function of ER calcium release

Purpose:

Assess impairments in ER calcium capacity indirectly using the cytoplasmic calcium indicator Fura-2.

Mechanism:

ER calcium reuptake will be inhibited using the SERCA inhibitor thapsigargin. This causes a rise in cytoplasmic calcium which can be measured using the ratiometric dye Fura-2. Using a perfusion setup, thapsigargin can be added to the plates in a controlled manner.

Materials:

- Fura-2, AM (Invitrogen No. F1201) in 1 mM stock dissolved in DMSO
- Mattek 3 cm dish with glass coverslip center
- Thapsigargin (Invitrogen T-7458)
- PBS

Prior to assay:

24 hours prior to experiment, seed cells at 500,000 cells per plate. It is important to ensure the cells are not too dense during the assay. Total dish volume should be 1.5 mL

Protocol: This experiment is performed in the David Jacobson Lab.

- Load cells with 3 μM Fura for 30 minutes at 37 °C. Dye concentration and loading time should be optimized.
- Rinse cells three times with PBS
- Replace media with solution containing (compound, mM): NaCl, 119; $CaCl_2 \cdot [(H_2O)_6]$, 2.5; KCl, 4.7; Hepes, 10; $MgSO_4$, 1.2; KH_2PO_4, 1.2; glucose, 2.   With a final pH of 7.35.
- Place cell dish on imaging platform. Focus microscope on cells as perfusion buffer (above) flows across cells continuosly at 2 mL/min.
- Using the controlling software, select individual cells as regions of interest to monitor fluorescence over time.
- Program a continuous assay using the Nikon TE2000-U microscope to perform excitations of 340 and 380 nm every 5 seconds.
- When a stable baseline is attained after approximately 5 minutes, add thapsigargin to stimulate net ER calcium release. This involves switching the perfusion line to use a stock of 1 μM thapsigargin.
- Record response curve.
- Export data to excel sheet.

Data Processing

- Exporting experimental data to an excel sheet will yield the change in the fluorescence ratio per cell with respect to time.
- Each cell response should be normalized to a point designated F_0. This is normally the point where thapsigargin increases in fluorescence begin. The normalization occurs using the equation:

$$R = (F(t) - F_0)/F_0$$

Where R is the normalized response, $F(t)$ is the time dependent fluorescent signal, and F_0 is the normalization fluorescence.

- Using this for each cell response, one can calculate the average relative ER calcium load in response to thapsigargin inhibition or ER reuptake. Treatments designed to inhibit ER calcium stores will result in less dynamic ER calcium release curves (longer time to peak, lower area under the curve, etc.) compared to healthy cells.

Protocol adapted from:

Jacobson, D.A., Weber, C.R., Bao, S., Turk, J., and Philipson, L.H. (2007). Modulation of the pancreatic islet beta-cell-delayed rectifier potassium channel Kv2.1 by the polyunsaturated fatty acid arachidonate. J Biol Chem 282, 7442-7449.

" Fluorescence imaging was performed using a Nikon Eclipse TE2000-U microscope equipped with an epifluorescent illuminator (Sutter instruments, Novato, CA), a CoolSNAP HQ2 camera (Photometrics, Tucson, AZ) and Nikon Elements software (Nikon, Japan). The $[Ca^{2+}]_i$ ratios of emitted fluorescence intensities at excitation wavelengths of 340 and 380 nm ($F340/F380$) were determined every 5 s with background subtraction. Cells were perifused at 37 °C at a flow of 2 mL/min; the solutions utilized during the experiments are the loading solution with various glucose concentrations and VU0071063 as indicated. "

Extraction of intracellular metabolites

Purpose:

This protocol describes the extraction of intracellular metabolites from cultured animal cells. This is a biphasic extraction protocol, with non-polar metabolites partitioning into a chloroform phase and polar metabolites partitioning into a methanol/water phase.

Required Materials and Equipment:

- Cells plated on a 100 mm dish
- Ice cold water
- Methanol pre-cooled to -80ºC and stored on dry ice (2 mL)
- Chloroform pre-cooled to -20ºC (4 mL)
- Cell scraper
- 15 mL centrifuge tube
- Internal standard norvaline (8 mM stock)
- Benchtop centrifuge (Forma 5678 with model 815 fixed angle rotor)
- Eppendorf tubes
- Evaporator
- Vortexer with attachment to hold 15 mL tubes, placed inside -20ºC freezer

Protocol per dish:

- Add 2 mL pre-cooled chloroform to 15 mL centrifuge tube
- Add 2 mL of ice-cold water to same centrifuge tube
- Remove media from culture dish, save for further analysis
- Wash cells twice with ice-cold PBS
- Add 1 mL pre-cooled methanol to dish
- Add 12.5 uL of 8 mM Norvaline internal standard
- Place dish in dry ice container for 1 min
- Scrape cells into 15 mL centrifuge tube using cell scraper
- Add 1 mL pre-cooled methanol to dish
- Remove remaining cells from dish into the same 15 mL tube
- Vortex tube for 30 min at -20ºC
- Centrifuge at 3,000 rpm (~1,000g) for 20 min at 0ºC
- Collect aqueous (upper) phase in two 2 mL Eppendorf tubes (label the tubes!)
- Collect organic (lower) phase in two 2 mL Eppendorf tubes (label the tubes!)
- Evaporate all extracts to dryness using air dryer at room temperature
- Store samples at -80ºC

MOX-TBDMS derivatization of metabolite extracts

Purpose

This protocol describes the preparation of intracellular metabolites for subsequent GC-MS analysis.

Mechanism

Dried metabolites from extraction protocol are made volatile by the addition of functional groups to allow for the analysis by GC-MS.

Required Materials and Equipment

- MOX reagent (Pierce Biotechnology, product# 45950)
- TBDMS: MTBSTFA + 10% TBDMCS, 1 mL ampules (Pierce Biotechnology, Catalog No. 48927)
- 2 mL amber glass injection vial
- 150 uL insert for injection vial
- Evaporator (Pierce Reacti-Vap)
- Sonicator
- Heating block

Sample preparation prior to derivitization

Dry frozen sample under air flow at room temperature (approximately 60 min)

MOX derivatization protocol

- Dissolve dried sample in 50 uL MOX reagent
- Place in sonication bath for 30 min. at room temperature
- Incubate for 90 min. at 40ºC on a heating block

TBDMS derivatization protocol

- Add 70 uL of MTBSTFA +1 % TBDMCS
- Incubate for 30 min. at 70 degC on a heating block
- Remove from heating block and incubate overnight at room temperature

Preparation for GC/MS:

- Centrifuge for 5 min at 14,000 rpm to remove solid debris
- Transfer liquid to injection vial containing a 150 uL microvolume insert

GC-MS Protocol for analysis of amino acids and free organic acids

Purpose:

Separate organic and amino acids to analysis isotopic enrichment using GC-MS, injection volume and purge flow should be optimized depending sample concentration

Materials

- GC-MS
- HP-5MS column
- Prepared samples in amber vial with insert

Injection Protocol

- Syringe Size-10 µL
- Injection Volume-1 µL
- Injection Repetitions-1
- Solvent A Washes (PreInj)-3
- Solvent A Washes (PostInj)-3
- Solvent A Volume-8 µL
- Solvent B Washes (PreInj)-1
- Solvent B Washes (PostInj)-1
- Solvent B Volume-8 µL
- Sample Washes-1
- Sample Wash Volume -2 µL
- Sample Pumps-4

Where Solvent A and B are both methanol.

Oven Temperature Program

- Begin at 80 °C for 5 min
- Then 20 °C/min to 140 °C for 0 min
- Then 4 °C/min to 234 °C for 5 min
- Then 20 °C/min to 315 °C for 5 min
- Total Run Time   45.55 min